Chemical Shock Tube Studies

of

Mechanisms of Grain Dust Ignition

by

Gary Walter Breipohl

B.S., Kansas State University, 1978

A Master's Thesis

submitted in partial fulfillment of the
requirements for the degree

MASTER OF SCIENCE

Department of Nuclear Engineering

Kansas State University
Manhattan, Kansas

1979

Approved by:

Thomas W. Porter
Major Professor

Table of Contents

List of Figures

List of Figures

List of Tables

List of Tables - continued

1.0 INTRODUCTION

1.1 Origin of the Problem

The effects of explosions occurring in atmospheres laden with grain dust have plagued mankind for nearly two centuries. The first recorded explosion, specifically attributed to the ignition of an agricultural dust, took place in Turin, Italy in 1785[1]. Unfortunately, immeasurable technological advances since this initial incident have not resulted in adequate methods of preventing these devastating explosions. Dust explosions continue to occur more frequently as evidenced by the fact that eight grain dust elevator explosions per year occurred during the period between 1958 and 1975, while during the preceding 17 year period the annual average was 6.7[1].

The need for research pertaining to agricultural dust explosions was first recognized in the United States in 1917 when the Bureau of Chemistry and Solids, Department of Agriculture was directed to conduct such investigations[2]. Six decades later, safety and financial considerations dictate that additional research concerned with the prevention of grain dust explosions be conducted. The research contained herein is directed towards an understanding of the fundamental mechanisms occurring during the ignition of a suspended dust cloud. It is hoped that such an understanding will eventually result in the implementation of practical techniques for preventing explosions in commercial grain handling facilities.

The foremost problems associated with investigating either ignition or devolatilization phenomena in grain dust clouds are dispersing the dust to form a reasonably homogeneous dust suspension within the appropriate atmosphere and supplying the energy necessary to induce the chemical and physical phenomena of interest. Many different experimental techniques have been employed to achieve these ends, and these will be discussed later in this chapter. The appropriate investigative method depends heavily upon the type of information which one desires to obtain. The research described herein is not concerned with the manner in which the cloud is initially dispersed, nor with the phenomena that produce ignition, whether it be a match, a cigarette, a hot bearing, or a spark. Rather it concerns itself with the chemical mechanisms by which the dust ignites and burns once in suspension.

A single pulse shock tube (SPST) is particularly well-suited to explore the ignition and devolatilization kinetics of suspended dust. The incident shock disperses the dust sample, which is subsequently heated by the reflected shock wave at a rate generally greater than 10^6 K/sec. The peripheral diagnostics associated with the SPST as employed in this study permitted calculation of the reaction temperature and pressure as well as the effective reaction time. The utilization of optical techniques facilitated examination of sample dispersion, the onset of ignition, and particle temperature. Gas chromatographic analysis of the stable devolatilization products provided an additional means of examining the mechanics of ignition and devolatilization resulting when

a suspended dust cloud undergoes rapid heating.

The United States Department of Agriculture Grain Marketing Research Laboratory, Manhattan, Kansas, provided the corn, milo, soybean, and wheat dust samples in addition to the cow cockle starch used in this investigation. These dust samples, originating from dust collection facilities in commercial grain elevators, were ball-milled to the desired size and were subsequently characterized in terms of: 1) size distribution, 2) elemental composition, and 3) proximate analysis.

The experimental strategy consisted of first determining the temperature dependence of the ignition of the four grain dusts when suspended in an oxidizing environment. Insofar as analysis of these data revealed that the release of volatile gases probably plays an integral role in the ignition process, the second and complimentary portion of experimentation was directed at quantitative analysis of the lower molecular weight hydrocarbons and oxides of carbon produced prior to ignition when dust clouds were subjected to rapid heating.

Inasmuch as there has been very little research concerned with either the devolatilization of grain dust under rapid heating conditions or the mechanism of its ignition, this research is pioneering to such an extent that the existing literature cannot be used for direct comparison. Therefore, in the following literature review, the pertinent studies of the pyrolysis of materials with similar chemical structure are included in addition to those utilizing grain dust. Similarly, a general review of solid particle ignition and a description

of the ignition mechanism hypothesized for materials similar to grain dust are also included. In the remaining chapters the experimental apparatus, the results, and conclusions are discussed.

1.2 Previous Work

Significant advances have been made in recent years towards a better understanding of the ignition process occurring in solid particles suspended within a gaseous medium. However, this understanding generally remains somewhat inadequate and our knowledge concerning the ignition of grain dust is even more deficient. The intent of this review is to unfold the ideas central to the development of a description of the grain dust ignition process. It begins by a characterization of the grain dust employed in this study and is followed by a summary of the available results concerned with the pyrolysis of grain dust or structurally similar materials. The review is concluded with a discussion of studies relevant to this investigation.

1.2.1 Grain Dust Structure

Grain dust may be characterized in many different ways. For example, Martin[3] has characterized the physical properties of grain dust on the basis of size, density, heat of combustion, and surface area. In addition, the chemical properties of grain dust, based upon the results of a proximate analysis, are useful for predicting global combustion behavior. A proximate analysis yields a measure of the moisture, protein, and ash content of a substance as determined from a series of standardized tests specified by the American Association

of Official Analytical Chemists[5]. The weight percentage of starch is then determined by difference from the total percentage of the six constituents mentioned above. The results of Martin's proximate analysis of agricultural dusts are presented in Table 1.

From the point of view of a study of combustion, a more useful form of the data presented in Table 1 can be obtained using the mean values in each classification range. The percentage combustibles, defined as the sum of the weight percentages of protein, fat, fiber, and starch present in corn, milo, soybean, and wheat dusts, are, respectively, 81.6, 71.3, 63.2, and 75.0 percentage by weight. Subtraction of the weight percentage ash and moisture from 100% and renormalization of the data in Table 1 provides a proximate analysis of the combustibles on a moisture and ash free basis. This dry and ash free tabulation is presented in Table 2.

The relative percentages of the various constituents, essentially equivalent for the various dust types, do not provide a measure of relative ignition characteristics (for instance, relative ignition temperature, minimum explosive concentration, or activation energy for ignition.) Rather these data provide a basis for modelling the overall mechanisms of devolatilization and ignition by hypothesizing the role of each constituent in the global processes. To this end, a discussion of the type of organic structure contained within the broad classifications of protein, fat, fiber, and starch follows.

Proteins are polymers composed of amino acids linked together by peptide bonds. A generalized structure of a protein molecule composed

Table 1. Range of Proximate Analysis Results Obtained using Grain Dust (from Martin[3]) in percentage by weight.

Grain Dust	Moisture Content	Protein	Ash	Fat	Fiber	Starch
Corn	11.7-13.5	6.1- 8.7	4.1- 9.2	1.2-3.6	5.0-10.0	60.9-67.6
Wheat	6.5-12.8	7.9-12.2	7.9-25.8	1.6-2.8	15.0-17.2	39.8-55.8
Milo	8.0-12.0	5.3- 7.8	8.2-32.2	4.0-4.6	9.2-17.3	38.0-61.5
Soybean	9.2-11.8	5.9-13.0	12.1-40.5	1.9-2.3	8.8-11.8	33.6-57.7

Table 2. Dry and Ash Free Proximate Analysis of Data from Martin[3] in percentage by weight.

Grain Dust	Protein	Fat	Fiber	Starch
Corn	9.1	2.9	9.2	78.8
Wheat	13.3	2.9	21.1	62.7
Milo	9.0	5.8	17.4	67.8
Soybean	13.0	3.1	15.3	76.6

of n amino acids is represented in Fig. 1-A. In this diagram the R groups represent the side chain or remaining portion of any of the twenty naturally occurring amino acids[6], i.e., the R_1 group would be a CH_3 if the first amino acid forming the chain was alanine.

Fats, also called fatty acids or lipids, generally contain an even number of carbon atoms (4-30) linked together in a straight chain terminated by a carboxyl group[6]. Some fats are unsaturated, containing up to six double bonds, generally of the cis configuration, within the linear hydrocarbon chain. The structure of oleic acid, which may be considered representative of a fatty acid, is presented in Fig. 1-B.

Starch, the storage polysaccharide of higher plants, consists of two components, amylose and amylopectin[6]. Amylose, a linear polymer composed of up to 3000 D-glucose residues joined together by α-1,4 glycosidic links, is represented in Fig. 1-C. Amylopectin is a branched polysaccharide in which the linear portion contains D-glucose units joined together by α-1,4 glycosidic linkages. The branching from the linear chain distinguishes the structure of amylopectin from amylose. A representation of the α-1,6 link forming this branch is given in Fig. 1-D. The amount of branching within a starch compound varies greatly and is dependent upon its biological origin.

Fiber, composed primarily of cellulose, differs from amylose in that the glucose residues are joined together by β-1,4 glycosidic links rather than α-1,4 links[6]. The structure of cellulose is shown in Fig. 1-E.

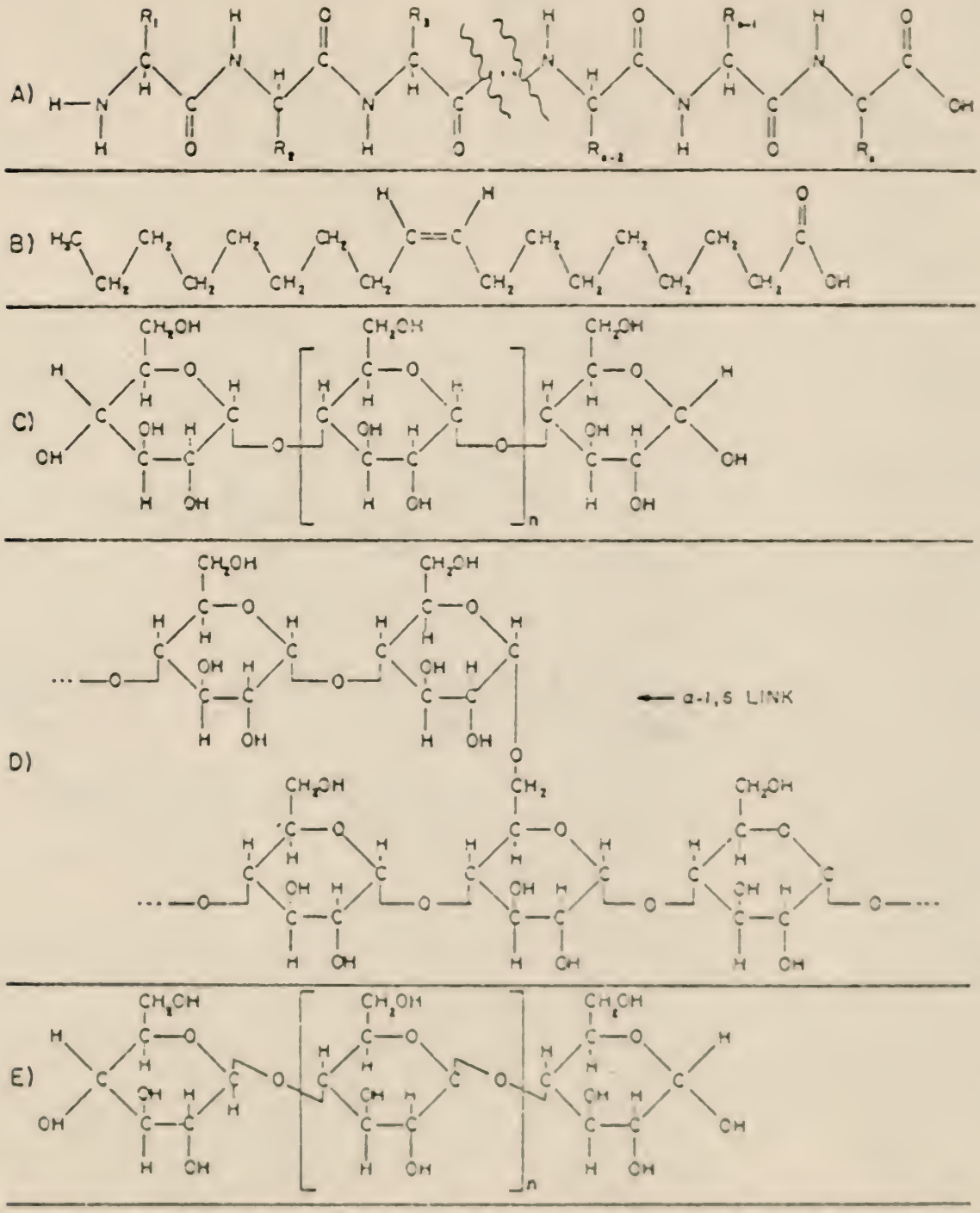

FIGURE 1 DIAGRAMS REPRESENTING THE STRUCTURAL COMPONENTS FOUND IN GRAIN DUSTS (FROM(6)).

A) STRUCTURE OF A GENERALIZED PROTEIN IN WHICH R DENOTES THE REMAINING SIDE CHAIN OF AMINO ACID
B) REPRESENTATION OF OLEIC ACID
C) DIAGRAM OF AMYLOSE
D) DIAGRAM OF AMYLOPECTIN SHOWING THE α-1,6 LINK.
E) DIAGRAM OF CELLULOSE

1.2.2 Pyrolytic Behavior of Grain Dusts and Related Materials

Pyrolysis can be defined as the thermal degradation of a substance in an inert environment*. The addition of heat to a solid particle sets in motion a series of chemical reactions, leading to the release of a variety of gaseous compounds at these elevated temperatures and a change in the physical structure of the parent material. Numerous devolatilization studies have been conducted with grain dusts, but for reasons which will be discussed later, their applicability to ignition and combustion in suspension is questionable because they were carried out only at relatively low heating rates and low temperatures. Thus, this review includes a discussion of the current state of knowledge and beliefs concerning pyrolysis of coal and cellulose. Relatively more is known about coal because of its historical place as an important fossil fuel while cellulose has been studied extensively with respect to fire spread.

Coal is a high molecular weight organic structure composed of non-crystalline building blocks, a substantial percentage of which possess an aromatic character. Numerous investigations[7-10], utilizing scanning electron microscopy (SEM) to explore the structural changes occurring within pyrolyzed coal, have reported similar findings despite the variety of experimental apparatus used to heat the coal. General descriptions of the SEM photographs include the fact that many coals, having undergone pyrolysis, exhibit fissures and/or sur-

---

*The word "pyrolysis" means death due to heat or more idiomatically "thermal decomposition".

face blistering. Cenospheres, essentially hollow particles possessing surface holes or larger blow holes, are also described to be thin-walled lacy baloons with evident blow holes. SEM photographs, shown in Fig. 2, of high volatile bituminous coal shock heated here at Kansas State University depict the physical changes accompanying pyrolysis.

Coal devolatilization experiments over the last two decades have produced an unexpected discrepancy between the weight percent of the original coal sample released as volatiles as determined by the standard ASTM procedure[11] and investigations employing heating rates in excess of the prescribed value of approximately 5 K/min. For example, Anthony and Howard[12], reviewing coal devolatilization studies, reported twenty-five instances when more volatile matter was obtained using a higher heating rate than was determined for these same coals using the ASTM procedure. They attributed this additional release of volatiles partially to an unidentified process which converted fixed carbon, as determined by ASTM analysis, into volatiles. The authors also felt that part of the enhanced volatile yields may have resulted from the techniques used to achieve a higher heating rate. This last explanation has more credence as evidenced by Suuberg, et al.[13] who concluded, based upon their experimentation, that the heating rate has a negligible effect on total yields and product distributions from pyrolysis of bituminous and lignite coals. Thus, the experimental procedure must remain an important consideration in discussions of the devolatilization phenomena.

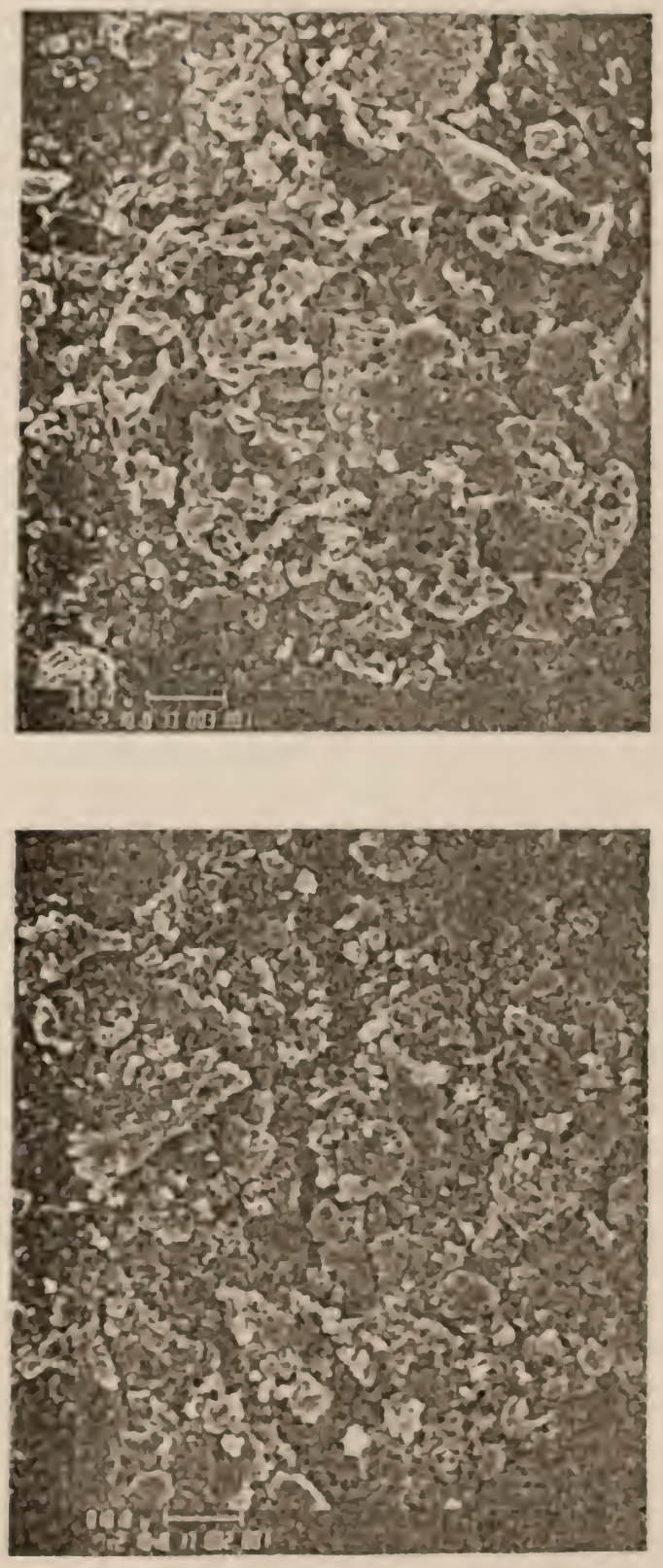

Fig. 2. Scanning electron micrographs of Pittsburgh seam coal subjected to high temperatures, high pressures and a short residence time. The scale at the lower left of each micrograph indicates 10 um.

The pyrolysis of cellulose has been the subject of numerous investigations utilizing a wide variety of experimental techniques. Once again, the effect of the heating rate on volatile yields as it has been addressed in the literature, merits discussion. Min[14] reported that the amount of residue present after pyrolysis of a cellulose sample decreased with increasing heating rates, which of course implies increasing volatile yields with increasing heating rates. In this study filter paper (essentially cellulose), was pressed against a stainless steel wire screen contained inside a test section, the temperature of which could be increased linearly at the rate of 3-30 K/min. The pyrolyzate was swept out of the test section with nitrogen and was subsequently analyzed with a combustible gas detector. The author reported (without explanation) that 16 weight percentage of the original sample remained as residue at the 3 K/min while only 12 weight percentage remained after subjecting the sample to a heating rate of 30 K/min.

Martin[16] investigated the pyrolysis of cellulose containing 2 weight percentage carbon black. The cellulose samples, which were mounted in a helium atmosphere beind a quartz window, were heated by radiation emitted from a carbon arc and focused on the sample by a parabolic mirror. Helium circulated through the sample chamber and into a gas chromatograph, where it served as the carrier gas. The identity of each pyrolytic product was confirmed by mass-spectrometric analysis. At the lower of the two irradiation levels employed, 20-35 weight per-

centage of the decomposed cellulose was determined to be char while at the higher level less than 4 weight percentage remained as char. The author believed this trend of decreased char yield with higher heating rates indicated that there were two fundamental ways in which cellulose decomposes. In the low temperature regime (<523 K) H_2O, CO and CO_2 are released, while at higher temperatures hydrocarbons are released.

Among other salient points presented by Martin are that a signifi-cant portion (approximately 50 weight percentage) of the decomposed cellulose formed high molecular weight tars which had an infrared-absorption spectrum nearly identical to that of levoglucosan, the structure of which is given later in Fig. 3. Additionally it was reported that gaseous volatiles, measured using chromatographic techniques, comprise roughly 20-50 weight percentage of the decomposed cellulose. The bulk of the chromatographically determined substances consisted of water and oxides of carbon. Finally, and somewhat surprisingly when considering the amount of oxygen present in cellulose (roughly 50 weight percentage), acids, esters, acetals, and formaldehyde were missing in the chromatograms.

Martin's description of the evolution of gaseous products during pyrolysis of cellulose is very similar to the description of the release of gaseous products during pyrolysis of lignite coal offered by Suuberg et al.[13] In an analogous manner, both authors contend that water and carbon dioxide are released at temperatures lower than those at which

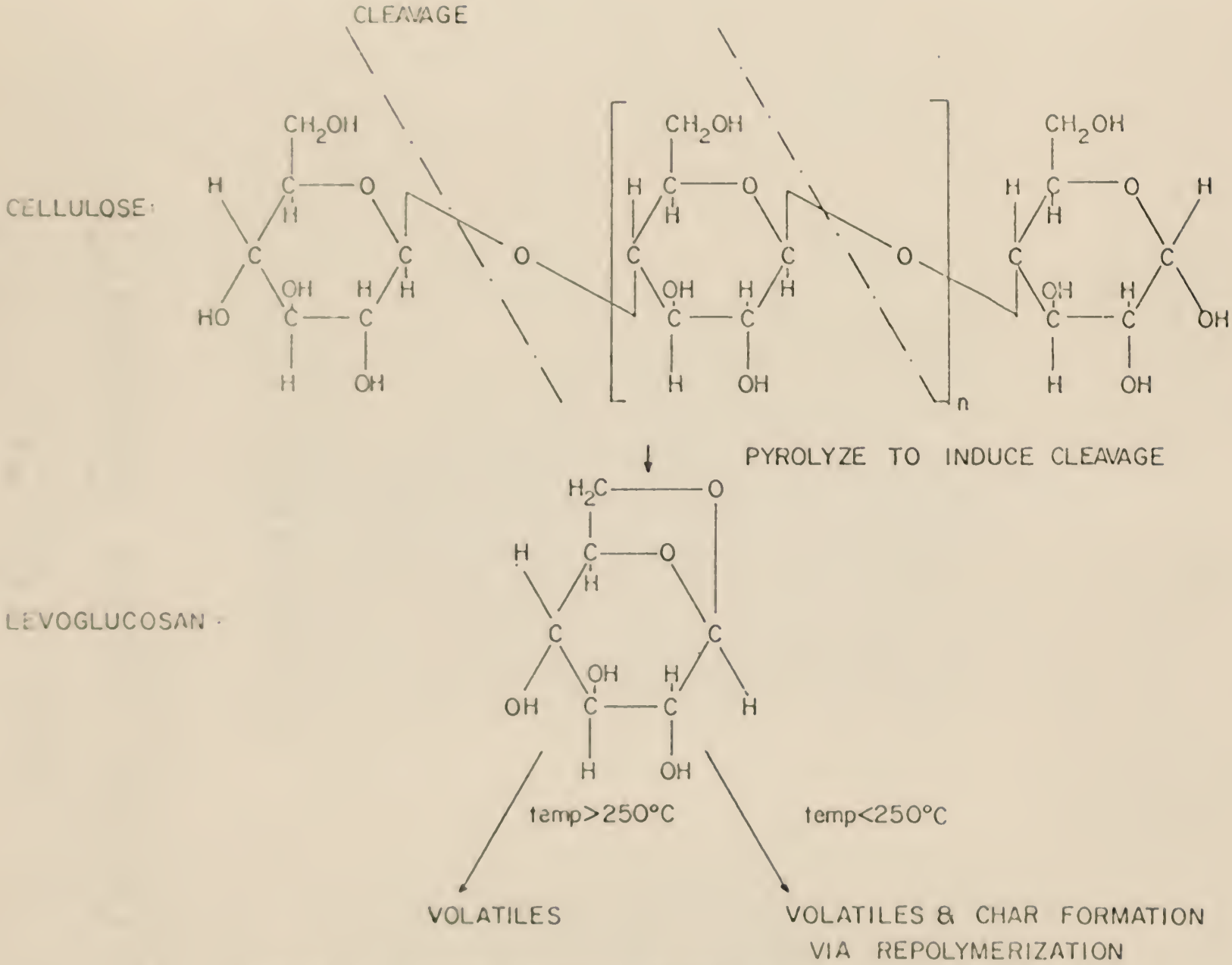

Figure 3. Proposed pyrolytic pathway for cellulose (from 17).

hydrocarbon evolution is observed. The similarity of these evolution sequences is somewhat surprising considering the differences in the sample materials and the data from which the conclusions were derived. Martin deduced his temperature dependent evolution scenario based upon the level of radiant exposure to the cellulose samples while Suuberg and co-workers based their findings upon the temperature measurements obtained between the wire mesh heating elements containing the coal sample. The similarity of the initially produced pyrolytic products leads to the conclusion that water and carbon oxides may be released first during the rapid pyrolysis of grain dust.

Shafizadeh[16], in his review of pyrolysis and ignition of cellulosic materials, contends that there are two fundamental modes of thermal decomposition. At temperatures lower than 523 K, the author concludes that thermal degradation results in decomposition to the oxides of carbon, water and carboxyl compounds in addition to the production of char. At higher temperatures, the decomposition was portrayed as a rapid devolatilization accompanied by the formation of levoglucosan. Both of these observations are consistent with Martin's experimental findings.

Lewellen, et al.[17] provided an explanation which seems to explain the effect of heating rate on char yield and the role of levoglucosan in this process. The experimentation consisted of pyrolyzing filter paper supported inside a wire mesh heating element which in turn was contained in a chamber filled with helium. (This was the same apparatus

used to determine that the volatile yield was not a function of the heating rates in the previously mentioned coal study.) The percent conversion to volatiles, measured by weighing the original sample and residual char after heating, was investigated as a function of final temperature (523-1273 K), heating rate (4×10^2 - 10^4 K/sec), and ambient pressure (0.0005-1 atm). The authors concluded that over the range of heating rates employed all of the cellulose was converted to volatiles with the exception of the runs maintained at 523 K for one hour or longer in which 2 weight percentage of the original sample remained as char. The authors explained this char formation by maintaining that if levoglucosan was formed, as in their postulated mechanism, then the levoglucosan would repolymerize to form char since it would be 20 K below its sublimation temperature of 543 K. A graphic illustration of this explanation is shown in Fig. 3. Thus, it can be inferred that at any temperature above 543 K, the heating rate has no effect upon char yield since all of the cellulose will be converted to volatiles. Inasmuch as this author's experimentation occurs at temperatures much greater than 523 K, pyrolytic products produced in the high temperature regime are more germane to the ignition of grain dust.

The direct pyrolysis of cellulose in the solid probe of a mass spectrometer equipped with a gas chromatograph-mass spectrometer (GCMS) data system was performed by Franklin[18]. The experimental procedure consisted of placing 35 ug of cotton into a capillary tube which was then positioned in the sample chamber of the solid probe.

A linear temperature programmer permitted heating of the sample chamber at the rate of 4 K/min. The rapid scanning capabilities of the GCMS permitted an ion pyrogram to be generated at intervals corresponding to a temperature increase of 0.7 K. The ultimate advantage of a system capable of such rapid characterization of the volatiles is that qualitative information depicting whether the observed products are released simultaneously or in a sequential manner may be obtained. From the ion pyrogram the author concluded that all of the products of cellulose pyrolysis are formed almost simultaneously. Thus, the pyrolyzate observed by Franklin are the primary products evolved when cellulose is pyrolyzed. These observed products are shown in Table 3.

Roberts[19], reviewing the pyrolysis of wood and related substances, presents evidence showing that the activation energy for the pyrolysis of cellulose varies from approximately 30 to 56 kcal/mole. The author explains this variation on the basis of the purity of the cellulose sample. Under ideal conditions with carefully purified cellulose, pyrolysis may proceed entirely by a reaction with an activation energy equal to 56 kcal/mol. The presence of trace impurities, namely inorganic salts, catalyze alternate reaction pathways having an activation energy of about 30 kcal/mol. This explanation is an outgrowth of numerous investigations concerned with the effects of flame retardants upon the ignition of cellulosic materials. The foremost of these investigations was performed by Tang[20], who examined the

PRODUCT	STRUCTURE	W/o OF INITIAL MASS
LEVOGLUCOSAN	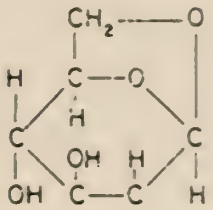	30
1,6-ANHYDRO-B-D-GLUCOFURANOSE	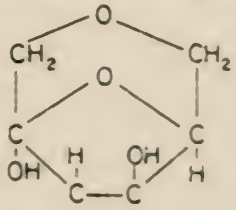	8
5-HYDROXYMETHYL-2-FURFURAL	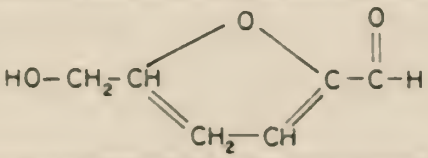	9
2-FURYL-HYDROXYMETHYL KETONE	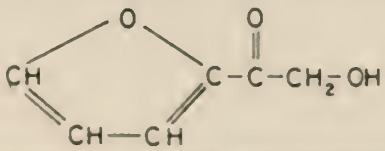	6
2-FURFURAL	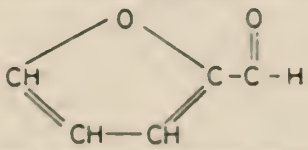	TRACE
CARBON DIOXIDE	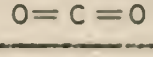	4
CARBON MONOXIDE		10
WATER	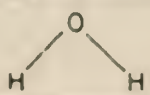	7
UNIDENTIFIED		

TABLE 3 PYROLYSIS PRODUCTS OF CELLULOSE. (AFTER(18)).

effect of soaking α-cellulose in 2% solutions of various inorganic salts upon the observed pyrolytic behavior. This analysis was based upon standard thermogravimetric analysis (TGA) and differential thermogravimetric analysis (DTA) which provide, respectively, plots of the rate of weight loss versus temperature and the differential temperature between an inert reference and the cellulose sample versus temperature. The author reported that the effect of these absorbed inorganic salts was to consistently lower the activation energy of pyrolysis from the value of approximately 54 kcal/mol obtained with pure cellulose to a minimum value of 38.2 kcal/mol obtained after treatment of the cellulose sample with a 2% $KHCO_3$ solution. The results of these two studies seem particularly important since grain dust has a significantly large ash fraction which could conceivably affect the kinetics of devolatilization in a similar manner.

Numerous studies, aimed at maximizing the yield of levoglucosan from starch, have been conducted inasmuch as levoglucosan has potential use in the chemical industries for the manufacture of plastics, surfactants, explosives, propellants, and as a sweetner[21]. The conditions employed by Wolff, et al.[22] to produce a maximum yield of approximately 35% included pressures of 1-20 torr and temperatures of 693-763 K. The significance of these findings is that levoglucosan is formed during the pyrolysis of starch; therefore, the spatial orientation of a glycosidic link does not prohibit levoglucosan formation from starch, and the thermal degradation mechanisms postulated for cellulose may be extrapolated with some confidence to starch.

The pyrolysis of starch, cellobiose, and simple sugars was performed by Puddington[23] at temperatures less than or equal to 483 K in 1948. Inasmuch as its application to this investigation seems questionable, a summary of the main findings is included for the sake of completeness. Water, carbon monoxide, and carbon dioxide were reported as the pyrolytic products of potato starch, and the author hypothesizes that after the evolution of water, rearrangements occur within the starch molecule which lead to the release of CO and considerably less CO_2. It is interesting to note that the order of volatile evolution is similar to that found by Martin[16] using cellulose.

Bryce and Greenwood[24] pyrolyzed starch in a furnace at 573 K in a stream of nitrogen. The results of the qualitative analysis performed on the pyrolyzate using chromatographic techniques is presented in Table 4. It is unfortunate that the authors gave no indication as to what fraction of the starch was converted to volatiles or of the relative concentration of the identified species because comparisons cannot be made with quantitative studies. The authors made the interesting observation that the majority of the detected components were combustible.

Chiotti and Morris[25] investigated the low temperature pyrolysis of grain dust. The objective of this study was to identify the volatile pyrolytic products in light of the fact that detection of their presence on a dust elevator could conceivably function as an early warning system to indicate when flammable gas concentrations become hazardous. The predominant products from pyrolysis of grain dust were reported to be water, carbon dioxide, and carbon monoxide.

COMPOUND	STRUCTURAL REPRESENTATION
CARBON DIOXIDE	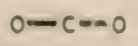
CARBON MONOXIDE	
METHANE	
ETHANAL	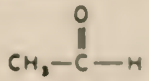
FURAN	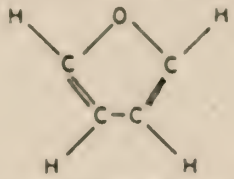
PROPANAL	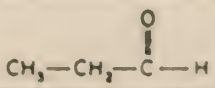
ACETONE	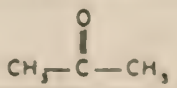
ACROLEIN	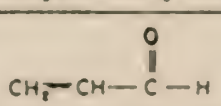
2-METHYL FURAN	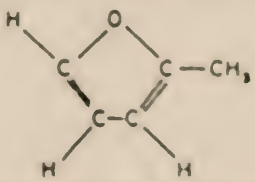
BUTANAL	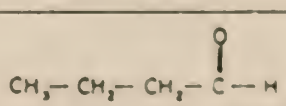
METHYLETHYL KETONE	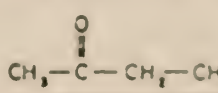
2,5-DIMETHYL FURAN	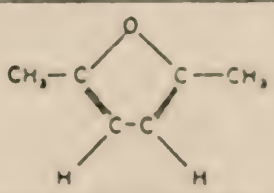
PENTANAL	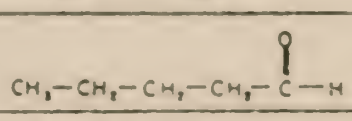

TABLE 4: PYROLYSIS PRODUCTS OF STARCH. (FROM [24]).

In summary, most recent discussions name levoglucosan as one of the most important intermediates in the pyrolysis of cellulose. The primary reactions, are thought to produce principally levoglucosan from the cellulose polymer. Levoglucosan is then believed to react further via either a sequence of cracking reactions to produce volatiles or to undergo repolymerization leading eventually to char formation. Starch also produces levoglucosan upon pyrolysis. In light of the similarity in the low temperature evolution of pyrolytic products from cellulose, starch, and grain dust, as well as the fraction of cellulose and starch contained within grain dust, it can be concluded that proposed cellulose thermal degradation mechanisms may be consistent with those exhibited by grain dusts.

1.2.3 Ignition of Grain Dust and Related Materials

Combustion of grain dust in suspension may lead to either a deflagration or a detonation. A deflagration is a subsonic combustion wave sustained by a chemical reaction and is characterized by isobaric behavior[26]. In a closed vessel, a series of deflagrations may accelerate into preceeding ones resulting in the formation of a detonation. A detonation is a violent process resulting in propogation velocities greater than the local speed of sound and the formation of a shock wave producing an almost instantaneous rise in pressure. A detonation, which is driven by a series of deflagrations, causes ignition by compression of the unreacted mixture rather than by diffusion of heat and reactive species ahead of the wave as in a deflagration. Aldis and Lai[2] specu-

late that the primary reaction in a grain elevator can be considered a deflagration. They contend that if a detonation were to occur in an elevator, it would originate in a mixture composed of dust and flammable gases generated in the primary explosion. Inasmuch as Palmer[27] reports the generation of pressures up to 10 atm in dust explosions, it is likely that detonations may occur in the more severe grain dust explosions.

The vast majority of the research concerned with the combustion of grain dust has been directed at characterizing the physical parameters necessary to sustain an explosion in a grain dust cloud. Led by the efforts of the Bureau of Mines, U.S. Department of Agriculture researchers designed experiments which would provide the data necessary to determine an explosibility index for grain dusts. The explosibility index E, as defined by the Bureau of Mines is given below as[2]:

$$E = \left(\frac{T_{min,c}}{T_{min,d}}\right)\left(\frac{C_{min,c}}{C_{min,d}}\right)\left(\frac{P_{max,d}}{P_{max,c}}\right)\left(\frac{\dot{P}_{max,d}}{\dot{P}_{max,c}}\right) \qquad (1)$$

where T_{min}, C_{min}, P_{max}, $\dot{P}_{max}$, are, respectively, the relative ignition temperature, the minimum explosive concentration, maximum explosion pressure, and maximum rate of pressure rise in an explosion. Additionally the subscripts d and c refer to, respectively, the test dust and reference coal dust. The outcome of such experimentation is the determination of an arbitrary index relating the explosibility of a grain dust cloud to that of the coal dust. Obviously, such experiments do not provide much basic understanding of the dust ignition process.

The Hartmann apparatus, which was developed by the Bureau of Mines over 30 years ago[27], is used to measure the pressure transients resulting from an explosion. The standard experiment is initiated by forcing a jet of air into the closed bomb causing dispersion of a dust sample. The suspended dust then passes by an ignition source, typically spark electrodes, an ignition coil, or exploding fuse heads, causing an explosion. Pressure transducers are used to monitor the pressure behavior during the explosion. Analysis of the output signal provides the maximum pressure obtained, P_{max}, and the maximum rate of change of pressure with respect to time, $\dot{P}_{max}$. The parameter $\dot{P}_{max}$ can be substituted into the "cube law" which states that in an explosion of a given mixture in a closed vessel the product of $\dot{P}_{max}$ and the cube root of the vessel volume is a constant[28]. If this relationship holds on a larger scale, then this parameter has important ramifications since prevention of the devastating effects of dust explosions may be designed for with the use of venting tactics. Eckhoff[28], in a paper citing the importance of the Hartmann bomb, states that a strong positive correlation exists between $\dot{P}_{max}$ and the combined content of starch and cellulose in various dusts. This implies that the starch and/or cellulose may play a dominant role in the explosion process. Enomoto[29], utilizing the Hartmann bomb, concludes that P_{max} increases with the volatile matter content of grain dusts. Experimentally reported values of P_{max}, $\dot{P}_{max}$, and other significant parameters are presented in Table 5.

Table 5. Significant ignition parameters of agricultural dusts, corn starch, coal, and cellulose. Sources are noted with individual entries.

Dust	Minimum Ignition Temperature (K)	Minimum Explosion Concentration (g/m^3)	Maximum Explosion Pressure (psi)	Maximum Rate of Pressure Rise (psi/sec)
Wheat	693[27]	55[30]	103[30]	3,600[30]
Milo	--	--	100[29]	3,550[29]
Soybean	823[27]	35[30]	99[30]	6,500[30]
Corn	663[27]	45[30]	95[30]	6,000[30]
Corn Starch	663[27]	40[27]	145[27]	9,500[27]
Coal	758[27]	55[31]	83[31]	2,300[31]
Cellulose	683[27]	45[27]	117[27]	8,000[27]

The Hartmann bomb can also be utilized to determine the minimum dust cloud concentration required to sustain an explosion. The only modification of the procedure described for obtaining pressure data is the removal of the top of the bomb, making it an open vessel[27]. Eckhoff[28] reports, contrary to intuitive expectations, that the dust giving the largest value of P_{max} upon ignition does not produce the most rapid rate of pressure increase, $\dot{P}_{max}$.

There are two commonly employed methods of obtaining the minimum relative ignition temperature. The horizontal tube apparatus[27], constructed of glass, is 1.38 meters long with an internal diameter of 7.6 cm. A metered blast of air, made turbulent by a flow channeler at the point of dust entry, carries the dust cloud past an ignition coil maintained at a predetermined temperature. Ignition is determined by the presence of a flame in the dust cloud. The minimum coil temperature that causes ignition is defined as the minimum ignition temperature. A Godbert-Greenwald furnace apparatus is another method of measuring minimum ignition temperature[27]. Again a jet of air disperses the contents of a dust holder, whereupon the resulting dust suspension travels through an open tube into a thermostatically controlled furnace. The minimum ignition temperature is defined as the lowest furnace temperature at which ignition is observed.

Essenhigh[32] contends that the term relative ignition temperature is the proper terminology for the results obtained using the aforementioned apparatus. He substantiates this claim by plotting the minimum

ignition temperature obtained utilizing the Godbert-Greenwald furnace against the values obtained with the horizontal tube apparatus from identical dust samples as shown in Fig. 4. From this plot, Essenhigh concludes that the lack of correlation is self-evident. Thus, the experimental techniques employed to disperse and ignite the dust give rise to widely differing values of ignition temperature. Obviously, physical effects attendent with dust dispersion and ignition must play an important but elusive role in these types of experiments.

The utility of performing these "standardized" tests on a number of explosive dusts lies in the ability to correlate the explosion severity (as measured by standardized tests) with the physical and chemical properties of the dusts. Eckhoff[28], using the Hartmann apparatus, examined the explosibility parameters of 12 grain dusts. The most important points of his conclusions can be summarized as: 1) The Hartmann apparatus gave consistently reproducable values for P_{max} and $\dot{P}_{max}$ (under a given set of conditions as performed by different researchers), 2) a correlation does not exist between gross calorific value and either P_{max} or $\dot{P}_{max}$, 3) A reasonably good correlation exists between $\dot{P}_{max}$ and the combined starch and cellulose content of the dust, 4) a simple empirical relationship exists between the specific surface area of the dust, (as calculated from particle size distributions assuming impervious, spherical particles) and $\dot{P}_{max}$, and 5) a simple empirical relationship is evident between $\dot{P}_{max}$ and the moisture content of the dust.

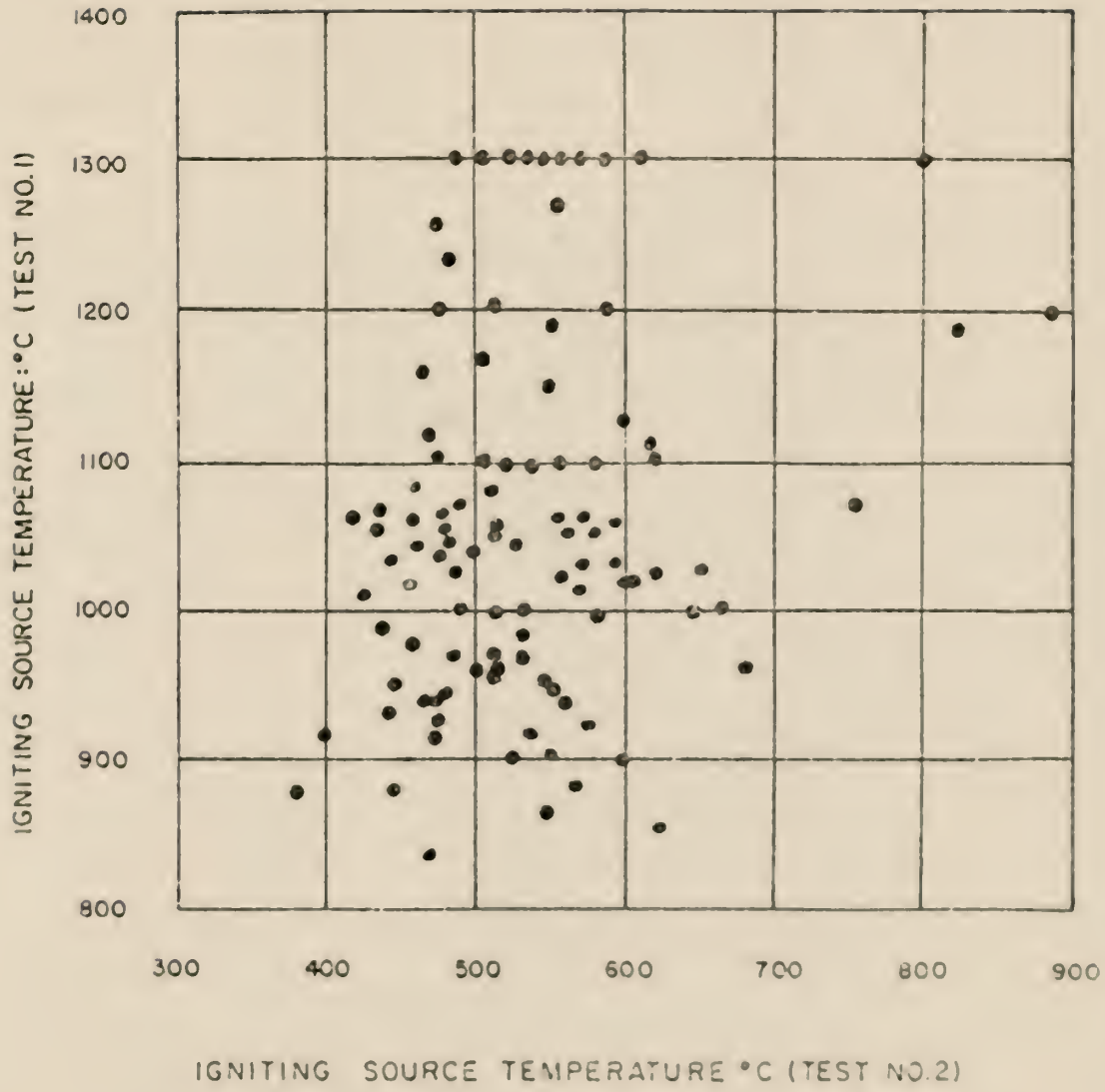

Figure 4. Comparison of relative minimum ignition temperatures obtained using horizontal tube apparatus (Test No. 1) and Godbert-Greenwald Furnace (Test No. 2) (From (32)).

Despite this impressive sounding list of accomplishments, the experimentation described above is severely limited. What do these test results really reveal? Is it not that very small, dry dust particles ignite more easily and release their energy more rapidly than a dispersion of larger dust particles containing a significant quantity of moisture? Investigations of this type are not aimed at the identification of the underlying chemical and physical phenomena, but towards the identification of some dust property, which if controlled, could be used in certain instances to reduce explosion severity. This is contrary to the more basic approach to research which involves investigating the fundamental phenomena, in this case ignition, and subsequently applying the knowledge gained from these investigations towards the solution of the practical problem of interest, in this case grain dust explosions. Essenhigh[32], in his concluding remarks to the 1977 International Symposium on Grain Dust Explosions, stated "The essential conclusions are that advances in the control of dust explosions must rely increasingly on a better understanding of both the phenomena and mechanics of ignition and propogation involved." He contends the problem is difficult but not insuperable as evidenced by the considerable advances which have been made towards understanding the combustion behavior of coal suspensions during the last decade. Following this line of reasoning, a review of the theory of solid particle ignition is presented and is followed by a discussion of the experimentation directed at determining the ignition mechanism in cellulose and grain dusts.

Theoretical considerations of a non-adiabatic oxidation process lead to a reasonable definition of ignition as the lowest temperature at which the rate of heat loss is overbalanced by the rate of heat generation[26]. Ignition can occur by either a homogeneous or heterogeneous process. Homogeneous ignition is believed to occur in the gas phase after the solid particle has devolatilized in accordance with the traditional "Faraday" mechanism. Heterogeneous ignition reverses the order of ignition and devolatilization such that ignition occurs on the particle surface generating the heat necessary for concurrent release of volatiles that burn in the gas phase.

Over the past two decades there has been considerable disagreement among researchers as to which of these conflicting ignition theories best describes the combustion of coal particles. In support of the Faraday mechanism is the famous deGrey data[33] which demonstrated that the maximum observable flame speed increases with the volatile matter of the coal. This indicates that the volatile matter content, in some obscure manner, controls the propagation mechanism which is intimately linked with the ignition process. Anson's[34] photographic examination of burning particles provides corroborating evidence since he observed an ejection of volatiles prior to ignition.

There exists considerably more evidence favoring heterogeneous ignition of coal and consequently it is currently thought that coal ignition is a surface phenomenon. The most satisfying evidence was presented by Nettleton and Sterling[35] in an investigation directed at

determining the effect of gas phase inhibitors upon measured ignition delays of heated coal. Inasmuch as these inhibitors, specifically chosen to influence only gas phase oxidation, had little effect upon ignition delays, the heterogeneous process appears much more plausible under conditions characteristic of dust cloud explosions. In direct conflict with Anson[34], Thomas and co-workers[36] heated a single captive particle, 1 mm in diameter, of brown coal and reported that a sequence of high speed photographs of the burning revealed a post-ignition (presumably heterogeneous) flashing of volatiles.

The results of a theoretical study of the ignition of coal particles performed by Annalamalai and Durbetaki[37] provides insight into the effect that particle size has upon the process of ignition. The authors determined, by invoking the adiabatic ignition criterion, the functional dependence of the gas ignition temperature (in a homogeneous process) upon the particle size using the kinetic data of Anthony et al.[38] Additionally, the relationship between heterogeneous ignition temperature and particle size was calculated by applying steady state thermal ignition theory to the assumed kinetic data of Bandyopadhyah and Bhaduri[39]. The important general conclusion gleaned from a comparison of these results, obtained for a partially pyrolyzing particle, is that smaller particles ignite in a heterogeneous process while larger particles tend to undergo a homogeneous ignition process. Seeker[7] substantiates this analysis with his experimental findings which indicate that the transition from heterogeneous to

homogeneous ignition of bituminous coal under rapid heating conditions occurs within a particle diameter range of 5-15 μm.

The ignition of cellulosic materials has been believed commonly to originate in the gas phase. Welker[40], in a review of the pyrolysis and ignition of cellulosic materials, states simply in his abstract that pyrolysis must precede ignition. Correspondingly, the author defines ignition as the appearance of a flame in the volatile stream evolved from a material undergoing pyrolysis. He contends that ignition may be classified as either spontaneous if no external ignition source, such as an open flame or an igniting coil, is required or piloted if such an external source is necessary. Furthermore, the author states that spontaneous ignition can be initiated at the solid surface if it is heated to the point where it ignites the volatiles or alternately, ignition can result from heating the gases alone to the ignition temperatures. Weatherford et al.[41], investigating the thermal processes in the heating of slabs of cellulosic materials, prefer to define the criteria for ignition as a perceptably more rapid increase in the surface temperature than would be predicted from heat transfer calculations in which chemical heat generation is neglected. This practical definition, based upon thermal ignition theory, merits consideration in the experimental investigation described below.

Martin[15] embedded thermocouples between thin layers of α-cellulose sheets subjected to intense radiation from a carbon arc source. The surface exposed to the irradiation was observed to undergo an abrupt temperature

rise upon the onset of flaming ignition and appeared well-charred prior to ignition. The author hypothesized that the charred surface was a site for secondary reactions leading to the production of H_2, CH_4, C_2H_4, and C_2H_6. Measurements (in an inert atmosphere) of the volatile products showed a maximum rate of evolution at a time close to the instant of ignition (in air). However, the author maintained that any attempt to draw a cause and effect relationship between the rate of volatile evolution and the onset of ignition is unjustified since the rate of volatile production is directly related to the radiant flux incident upon the sample. In any event, the author reports that the role of the surface in the ignition process is as a site for secondary reactions rather than as the site of oxidation as would be expected if the process were heterogeneous.

Kuwata and co-workers[42], investigated the weight loss resulting when paper spheres, ranging in diameter from 0.8 to 4.5 cm, attached to a continuous read-out balance were burned in air. The spheres were suspended by a wire into a 7.62 cm diameter combustion tube possessing glass windows through which visual observation and high speed photography of the oxidation process was conducted. The velocity of the air or oxygen enriched air flowing through the tube ranged from 0 to 160 cm/sec. The paper spheres were initially ignited by a gas flame which was extinguished after the onset of ignition. The authors observed that after ignition, volatile combustion was evident. At higher air stream velocities the flame appeared downstream of the burning spheres.

Following the release of volatiles, the remaining char burnt out on the upstream side in a reducing diameter process in contrast to a devolatilization which occurred via a constant diameter and changing density process.

The most significant conclusion deduced by the authors was that pyrolysis and char-combustion were independent (except for competition for oxygen) and yet they proceeded simultaneously. The basis for this conclusion, numerically illustrated in Table 6, was that one half of the available char (approximately 10% of the original sample) burned along with the volatile matter present in the paper spheres during four-tenths of the total burning time. During the remaining six-tenths time char burnout proceeded to completion. The authors stated that the 80% loss attributed to loss of the volatile components was not due to heterogeneous combustion, rather the loss resulted from pyrolysis of the paper spheres. Consequently, if the majority of the weight loss does not result via heterogeneous ignition, then homogeneous ignition of the devolatilized material produced from the cellulose must occur.

Only one paper could be located which addresses the subject of whether grain dust ignition proceeds via a heterogeneous or homogeneous process. Nagy et al.[43], concluded (somewhat questionably) that grain dust ignited by a heterogeneous ignition mechanism. The logic behind this deduction begins with the observation that grain particles ignited when heated in an oxidizing environment using the Godbert-Greenwald furnace. In addition, the authors reported that, in pyrolytic studies performed on coal dust using the same apparatus,

Table 6. Approximate composition of paper spheres at various times during combustion (from (42)).

Fraction of Burning Time	Weight percentage of original sample	
	Volatiles	Char
0.0	80	20
0.4	0	10
1.0	0	0

little devolatilization occurred. In the opinion of the authors this implies that grain dust would not pyrolyze. The conclusion is also based on the observations that ignition of metals can occur without significant quantities of vapor present, surface specific catalysts increase the oxidative reaction rate of carbon black particles and carbonaceous dusts ignite at temperatures at which the released volatiles could not ignite. The authors' reasoning is so convoluted and experimental details so sketchy that it is impossible to place much importance in their findings.

In conclusion, significant material discussed in the literature surveyed may be summarized as follows. Grain dusts contain a relatively large fraction of volatile material as determined by standard testing procedures. Cellulose, a major component of grain dust, yields relatively small quantities of char residue after pyrolysis at temperatures commensurate with those encountered during ignition. This is based on the fact that no char formation is observed at sufficiently high temperatures implying that all of the cellulose has been converted (presumably) to volatile components. Pyrolysis of cellulose is believed to proceed through a levoglucosan intermediate, but the devolatilization to a variety of fragments (including levoglucosan) occurs extremely fast. Explosibility parameters $\dot{P}_{max}$, P_{max}, and relative minimum ignition temperatures have been well characterized for grain dust, and a particularly significant finding is that the parameter $\dot{P}_{max}$ is directly related to the combined starch plus cellulose content of the dust sample. Solid particles have been observed to ignite in either a

homogeneous or heterogeneous fashion. However, most data have been compiled at unrealistic conditions insofar as explosions are concerned; therefore, the role of volatiles in the ignition process of grain dusts remains unexplored at heating rates and temperatures characteristic of explosions.

2.0 EXPERIMENTAL APPARATUS

2.1 Shock Tube Gas Dynamics

In the simplest terms, a single pulse shock tube, SPST, can be thought of as a means of very rapidly generating high temperatures and pressures for a short, yet controlled time. These transformations result from the step-changes in pressure and temperature associated with the propagation of a shock wave through a gas. The SPST at Kansas State University, designed and constructed by Seeker[44], is illustrated in Fig. 5. A dump tank, the purpose of which is to prevent repeated shock reflections, distinguishes the SPST from a conventional shock tube. Specifically, only an incident shock wave, which disperses the dust sample and heats the test gas and particles to a temperature of 600 to 800 K, and the reflected shock, which further heats the particle suspension to the final reaction temperature, are permitted. The propagation of any unwanted shock waves is precluded by trapping the shock wave reflected from the test section end wall in the dump tank.

An experiment is initiated by bursting a diaphragm separating the low pressure gas in the test section from the high pressure gas in the driver section. The resulting behavior of the waves generated by the diaphragm rupture, as predicted from the Rankine-Hugoniot equations[45] can best be explained using the x-t diagram shown in Fig. 6. Upon breaking the diaphragm at time equals zero, the incident shock forms from a succession of pressure pulses and propagates down the tube at supersonic velocities until it encounters the test section

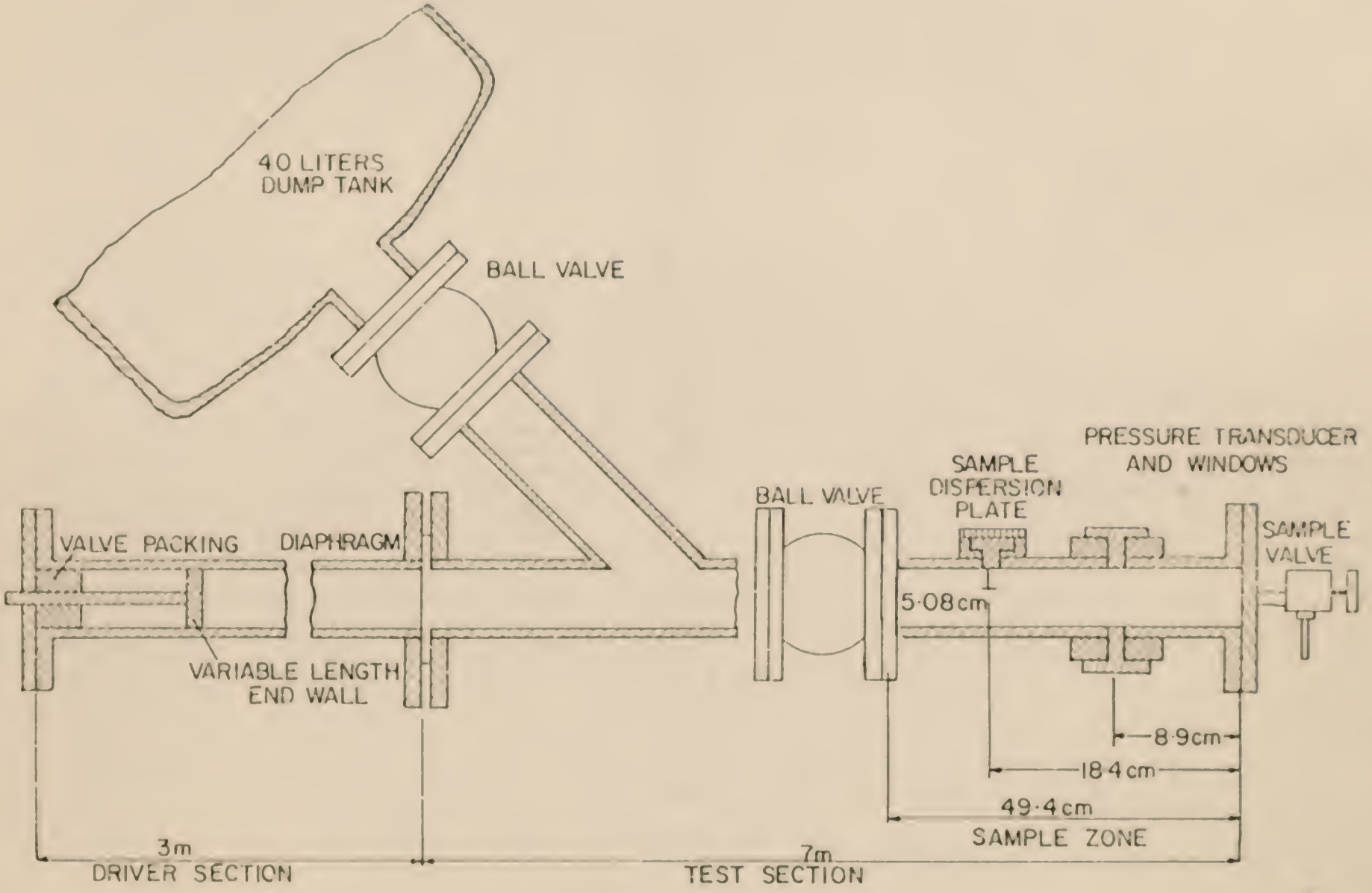

Fig. 3. Single Pulse Shock Tube Diagram.

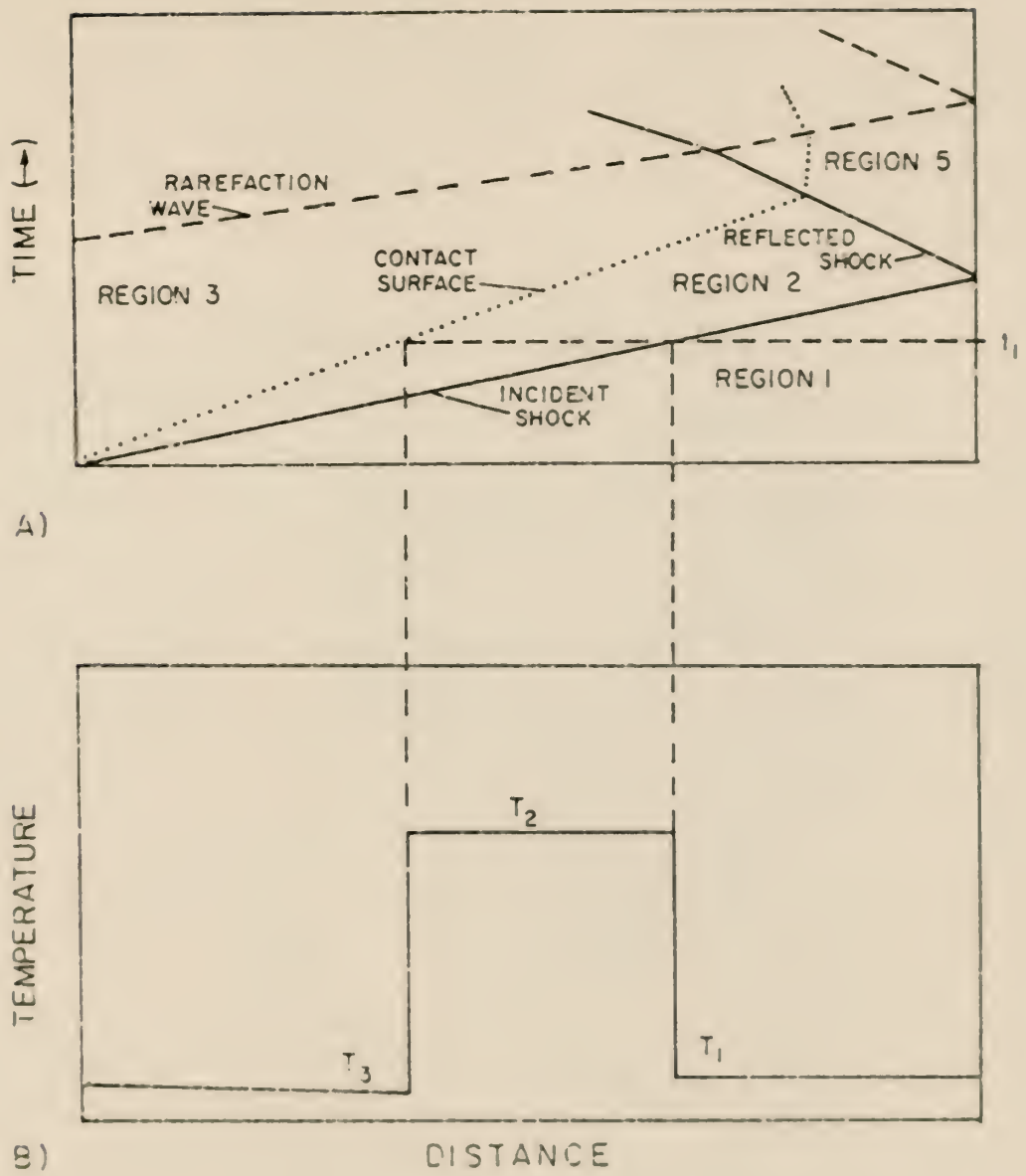

Fig. 6. A) an x-t diagram showing relative behavior incident shock, the reflected shock, the rarefaction wave, and the contact surface. The various regions associated with the shock tube are also distinguished. This wave diagram is incomplete in that it only shows the wave interactions from the diaphragm to the test section end-wall.

B) The temperature distribution at time t_1.

end wall, at which point it reflects back into itself. The nearly instantaneous temperature increase commensurate with the passage of the incident shock is shown in Fig. 6. The incident shock also disperses the dust sample from the dispersion plate (located 19 cm from the test section end wall) to form a particle suspension which is carried towards the test section end wall by the propagation of the heated gas behind the incident shock.

The reflected shock wave produces an additional heating of the particle/test gas suspension to the reaction temperature, T_5. The region behind the reflected shock, shown as region 5 in Fig. 6, is comprised of an essentially stagnant particle/test gas suspension at elevated temperatures and pressures of T_5 and P_5, respectively. It is in this region that the dust particles experience a combination of temperatures high enough and dwell times sufficiently long such that ignition and pyrolysis can occur.

The reaction conditions behind the reflected shock may be calculated from the velocity of the incident shock via the gas dynamic relations[46]

$$\frac{T_5}{T_1} = \frac{[2(\gamma-1)M_I^2 + (3-\gamma)][(3\gamma-1)M_I^2 - 2(\gamma-1)]}{(\gamma+1)^2 M_I^2}, \tag{2}$$

$$\frac{P_5}{P_1} = \left[\frac{2\gamma M_I^2 - (\gamma-1)}{\gamma+1}\right]\left[\frac{(3\gamma-1)M_I^2 - 2(\gamma-1)}{(\gamma-1)M_I^2 + 2}\right], \tag{3}$$

where T_5 and T_1 are the temperatures behind the reflected shock and of the gas initially in the tube, respectively, P_5 and P_1 are the

corresponding pressures; γ is the specific heat ratio of the test gas and M_I is the Mach number of the incident shock. The latter quantity is defined as the ratio of the shock velocity to the local speed of sound of the test gas. Equations (2) and (3) are based on the assumption of a perfect frozen gas (i.e., the gas is ideal, undergoes no dissociation or ionization, has no vibrational or rotational vibration energy modes excited), and a perfect reflection (conservation of momentum). If the vibrational and rotational degrees of freedom to participate in the energy storage, then both the specific heat at constant pressure, C_p, and the specific heat at constant volume, C_v, increase. Effectively, this lowers the specific heat ratio, γ, causing an overprediction of the reflected shock gas temperature as calculated by Eq. (2) when a diatomic test gas (N_2) is employed.

A discussion of the wave behavior associated with quenching the chemical reaction again requires reference to Fig. 6. Immediately behind the incident shock the contact surface, ideally represented as the plane of contact between the driver and test gases, travels down the test section until it interacts with the reflected shock wave. Additionally at the instant at which the diaphragm is burst, an expansion fan propagates into the driver section and is reflected back from the end wall into the test section. This rarefaction wave moves at a nearly constant velocity, $v_3 + a_3$, where v_3 is the velocity of the gas in region 3 relative to the tube and a_3 is the local speed of sound in that gas. Because the speed of the rarefaction head, $v_3 + a_3$,

is greater than that of the contact surface traveling at v_3, the reflected rarefaction can be made, if the relative lengths of the driver and test sections are designed properly, to overtake the contact surface during its propagation down the tube.

If the rarefaction overtakes the contact surface before the latter reaches the end of the shock tube, then the contact surface actually reverses its direction and moves back towards the driver section. In this instance, no mixing of the test gas with the cool driver gas is observed. If the contact surface is not overtaken by the rarefaction wave, then undesirable mixing of the dust/test gas suspension occurs prior to the arrival of the rarefaction wave.

In either event, quenching occurs when the rarefaction wave comes in contact with the dust/test gas suspension. The cooling occurs via an isentropic expansion which cools the stagnant suspension at a rate in excess of 10^5 K/sec.

The presence of the dump tank insures that the reflected shock wave does reach the driver section end wall; at which point it would be reflected back towards the test section to induce further reactions though an additional increase in temperature. Because of the oblique angle of the dump tank with the direction of the incident shock, only a very weak shock propagates into the low pressure gas in the dump tank. The main shock travels down the tube, reflects off the test section end wall, and proceeds back towards the driver section until it encounters the junction leading to the dump tank. At that point, the reflected shock preferentially moves into the lower pressure gas in the dump tank

where it is trapped into oblivion. Experimental evidence documenting the effectiveness of the dump tank in suppressing shock waves is provided by Seeker[7].

In summary, the wave behavior associated with suddenly bursting a diaphragm separating a high pressure gas from a low pressure gas can be calculated through the conservation equations. The test gas temperature and pressure behind both the incident and reflected shock waves can be computed from only a knowledge of the incident shock velocity, test gas properties, and the initial conditions. The principle benefits of studying chemical phenomena behind the reflected shock wave are that high temperatures and pressures can be obtained with more modest driver gas pressures than behind the incident shock and the heated test gas/dust suspension behind the reflected shock is stationary. The latter allows relatively simple methods to be utilized in the sampling of the product gases. A discussion of the experimentation performed to verify that the temperatures predicted by Eq. (2) are reasonable is contained in the next section of this chapter. Additionally, the details of SPST operation and associated diagnostics are also included.

2.2 Shock Tube Operation and Associated Diagnostics

The details of the construction of the single pulse shock tube employed in this study are addressed by Seeker[44]. The insertion of a 5.1 cm inside diameter ball valve, which is used to isolate the last 49.4 cm of the test section from the remainder of the tube, is the only major modification to the SPST configuration since its original con-

struction. The variable length driver section was fully extended to 3 m during all experiments. The preparation of the SPST for an experimental run required a lengthy and detailed procedure in order to assure reproducible and reliable data. A comprehensive list of the individual steps required during the course of a single experimental run is tabulated in Appendix A.

Two thicknesses (76.2 and 127.0 μm) of mylar diaphragms were used to separate the test section from the driver section. A manually operated plunger was employed to burst the diaphragms. Consistently reproducible shocks were generated when the driver gas pressure was slightly less than the spontaneous bursting pressure of the mylar diaphragms as documented by Seeker[44].

Helium was used as the driver gas for all runs in this study. Test gases, nitrogen and moisture-free air, were used for pyrolysis and oxidation runs, respectively. These gases were of high purity, 99.9995% for N_2 and 99.9995% for the air, and no additional purification was performed. Inasmuch as a gas chromatograph is capable of detecting impurities at these levels, gas samples were taken from a blank experimental run in which the dust sample was absent. Chromatographic analysis revealed the presence of hydrocarbon impurities, but at such a location in the chromatogram as to not affect the lower order hydrocarbon analysis performed in this study.

Four agricultural dusts, corn, milo, soybean, and wheat, were used in this study. In addition, cow cockle starch was used as a

standard in devolatilization studies. The results of a proximate analysis (performed by Martin[47]) of the dusts used in this study are given in Table 7.

Dust samples were inserted into the tube on a small plate (approximately 1.5 cm in diameter) suspended from the top of the tube and located 19.0 cm from the test section end wall. The samples were stored in a vacuum desiccator to prevent the adsorption of moisture; therefore, all experimentation in this study was conducted with moisture free dusts in test gases containing zero percent moisture.

The incident shock wave was used to disperse the positioned sample into a fluidized cloud flowing towards the test section end wall. Subsequent arrival of the reflected shock dispersed the cloud further, and brought it to an approximately stagnant condition. Seeker[7] demonstrated that this method of dispersion was satisfactory for particles less than 10 μm in diameter. Originally it was intended to obtain a sufficiently small size distribution by sieving the dust through a U.S. standard 400 mesh screen (< 38μm); however, research personnel at the Grain Marketing Research Center felt that this technique was not appropriate inasmuch as the previously characterized chemical composition of the dusts would be altered upon sieving. Thus, the grain dust samples used in this study were ball-milled until sufficiently small size distributions were obtained. The size distributions of the ball-milled dust samples, as determined by Particle Data Laboratory[48] using a Coulter counter, are given in Appendix B. Size histograms characterizing each dust sample

were calculated from these data and are presented in Figs. 7 and 8.

Individual dust samples were massed to 20.0 ± 0.2 mg on an analytical balance before each pyrolysis run. A sample of this size resulted in the production of detectable quantities of pyrolytic products while keeping the heat capacity of the dust low (less than 10%) in comparison with the heat capacity of the nitrogen in which the sample was dispersed. The heat capacity of a 20 mg dust sample, typically possessing a specific heat of 2.00 J/g[49], is approximately 4×10^{-2} J. Assuming a dust sample is dispersed over 12 cm of the tube as observed for similarly sized coal particles[7], the heat capacity of the nitrogen surrounding the dust dispersion at a pressure of 7.5 atm and temperature of 1200 K is approximately 5.75×10^{-1} J. The results of this approximate calculation show that about 7% of the heat capacity available in the gas surrounding the dust dispersion was utilized to heat the dust.

For ignition runs, the dust samples were somewhat smaller at 15.0, 8.0 8.0, and 6.0 ± 0.2 mg, for corn, milo, soybean, and wheat dust samples, respectively. The sample size was reduced to avoid complete extinction of the laser beam that was utilized in the analysis of the duration of ignition delay.

Three on-line diagnostic techniques were available at the observation port, located 8.9 cm from the test section end wall. Three quartz windows were installed in the same transverse plane as a Kistler pressure transducer (Model 603A), which was mounted flush to the inner wall of the fourth port (see Fig. 9). The continuum emission from the

Table 7. Results of proximate analyses performed by Martin[47] and an elemental analysis performed by Howell[57] on the dusts used in this study.

Dust	Moisture (w/o)	Protein (w/o)	Ash (w/o)	C (w/o)	H (w/o)	O (w/o)†	N (w/o)	Inerts (w/o)
Milo	10.9	6.8	10.9	41.0	6.1	39.1	1.27	12.5
Wheat	8.9	8.9	10.6	42.0	5.8	38.2	2.01	11.94
Soybean	7.7	13.5	19.7	-	-	-	-	-
Corn	11.1	5.3	2.0	-	-	-	-	-

†By difference.

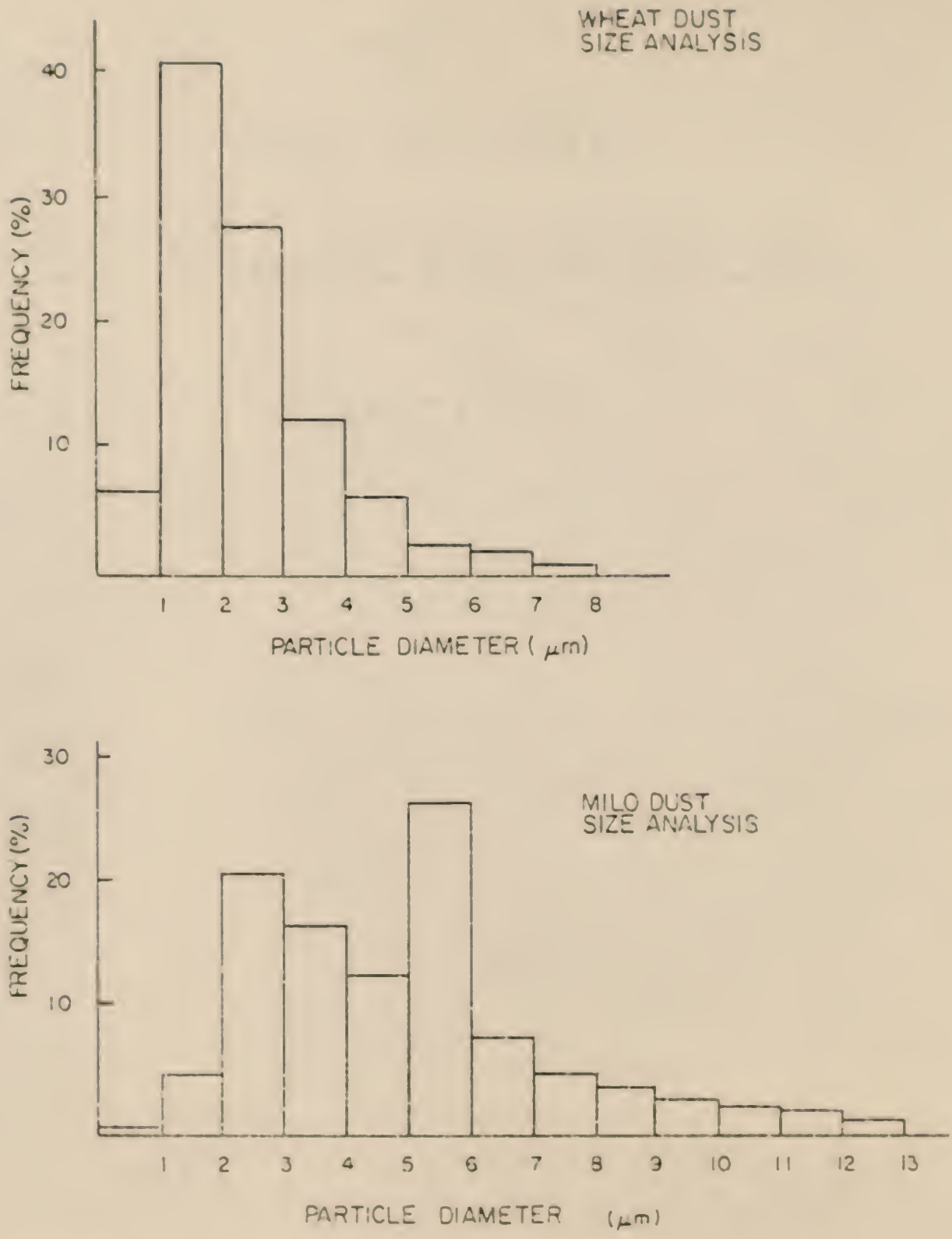

Fig. 7. Size histograms of wheat dust and milo dust (from (48)).

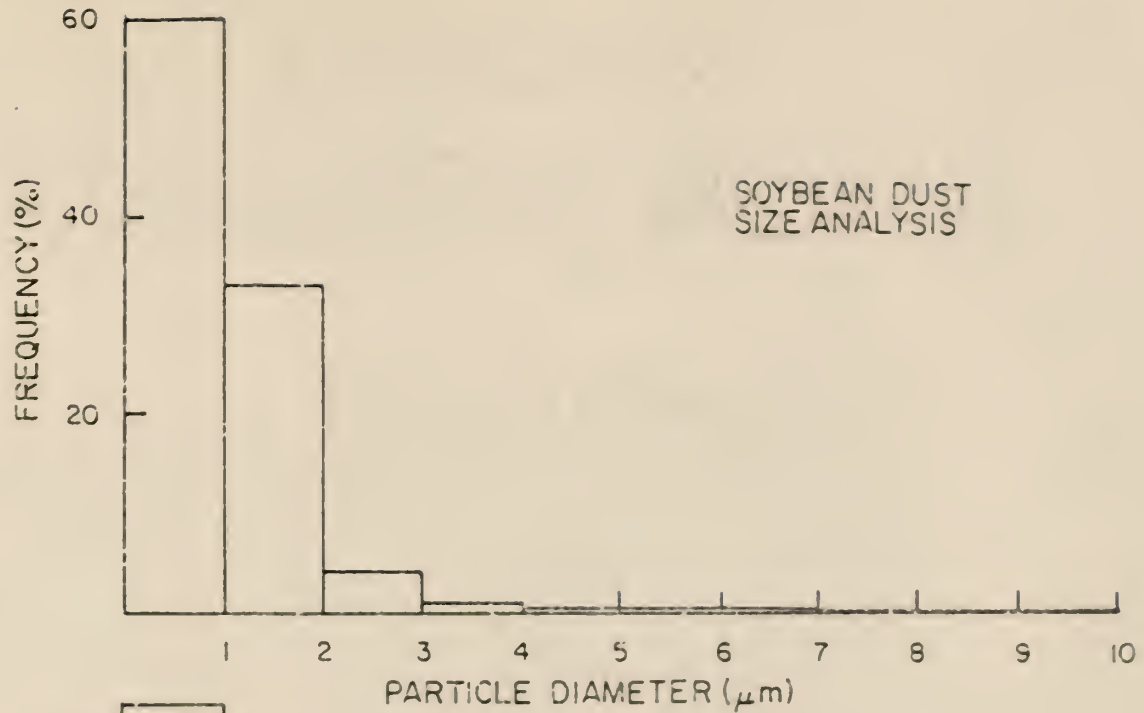

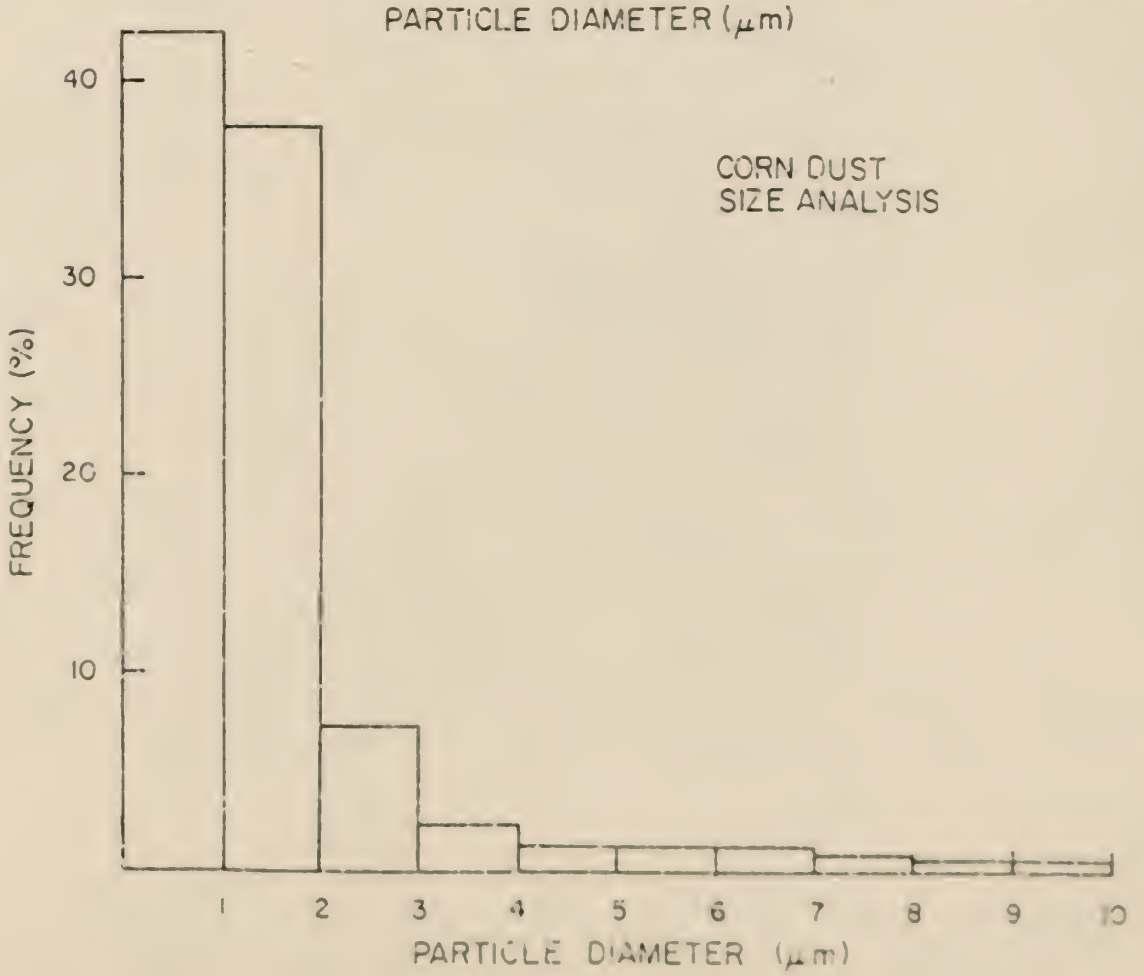

Fig. 3. Size histograms of corn and soybean dust (from (41)).

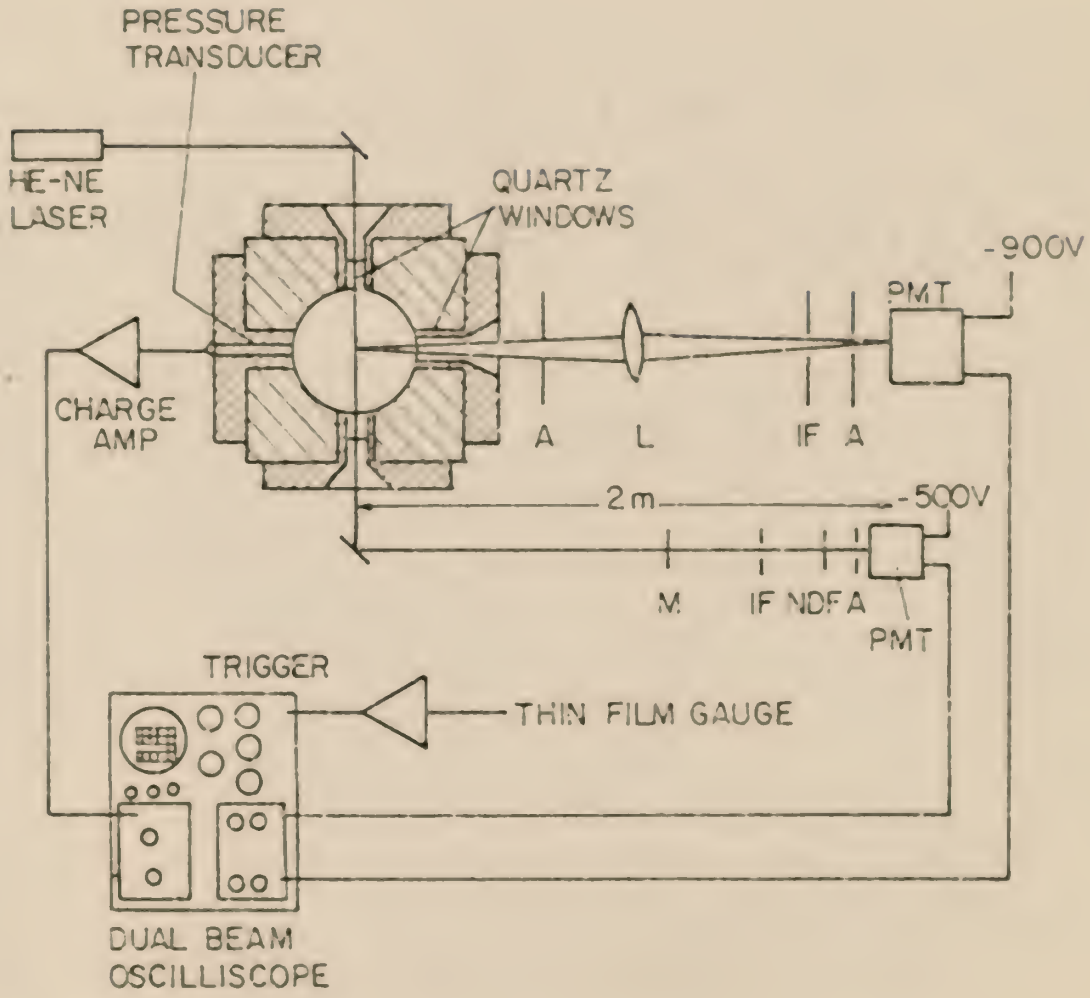

Fig. 9. A cross-sectional view of the diagnostics at the four port observation station where: A-aperture, L-lens, IF-interference filter, M-mylar screen, NDF-neutral density filter, and PMT-photomultiplier tube.

incandescent grain dust particles was monitored through one of the observation windows. The emergent radiation passed through a line filter (589.3 nm, full width at half maximum (FWHM) = 11.1 nm) and was focused on a photomultiplier tube (RCA 1P28). This line emission was used to determine the onset of ignition using the techniques described in the next chapter. A beam of monochromatic radiation generated by a 1 mW helium-neon laser (Metrologic Model ML620) at a wavelength of 632.8 nm was passed vertically through the remaining two quartz windows. The emergent beam was directed through a series of apertures, a mylar diffusing screen, and a narrow band pass filter (632.8 nm, at(FWHM) = 11.5 nm) to obtain the desired beam intensity and to eliminate the unwanted continuum emission prior to striking a photomultiplier tube (RCA 1P28). The extinction of this beam was a measure of the concentration of the dust suspension behavior during an experimental run.

The output currents of the photomultiplier tubes were directed into a load resistor, and the resulting voltages were fed into a Tektronix Model 551 dual beam oscilloscope. Additionally, the pressure transducer output was converted into a voltage signal by a charge amplifier (Kistler, Model 504A) for transmission to the oscilloscope. The behavior of these three input signals during an experimental run was photographically recorded from the oscilloscope. An explanation of the information portrayed on these oscillograms is provided in the next chapter.

The fourth on-line diagnostic associated with the shock tube was two thin film platinum resistance gauges positioned flush against the

inner tube wall at distances of 77.2 and 99.7 cm from the test section end wall. The temperature and, correspondingly, the resistance of the thin platinum films are increased by the passage of the incident shock. The resulting voltage pulses were shaped and amplified with a wide band preamplifier and a linear amplifier (Ortec, Model 410). The processed signal from the leading thin film gauge was used to start a time interval counter (Fluke, Model 1952B). The processed pulse from the second thin film gauge was used both to stop the time interval counter and to trigger a single sweep of the oscilloscope. The speed of the incident shock was thus calculated using the time required to travel the known distance between the two thin film gauges.

The temperature and pressure behind the reflected shock were calculated originally using the frozen gas equations, Eqs. (2) and (3) and the specific heat ratio γ, evaluated at 298 K. However, there are two questionable assumptions implicit in the use of these equations. First, as alluded to previously, the assumption that the specific heat ratio of the test gas is not a function of temperature results in an over prediction of the temperature behind the reflected shock. In fact the specific heat ratio of nitrogen decreases from 1.400 at 300 K to less than 1.300 at 1900 K[46]. Second, the presence of the dispersion plate may alter the structure of the incident shock to such an extent that ideal reflection will not occur as demanded in the derivation of the frozen gas equations.

Vaughn[50] devised and performed an experiment which permits calculation of T_5 from the basic conservation equations without any assumption re-

garding the specific heat ratio or ideality of the shock wave reflection. The experiment requires that both the incident shock and the reflected shock velocities be measured. Towards this end, the sweep speed of the oscilloscope was increased enough to permit accurate determination of the time between passage of the incident shock and the reflected shock past the pressure transducer as evidenced by the resulting pressure jumps on the oscillogram. Hence, assuming that the speed of the incident shock, v_I, as determined from the thin film gauges does not change significantly, the speed of the reflected shock, v_R, can be readily calculated from the equation,

$$t = \frac{d}{v_I} + \frac{d}{v_R} , \qquad (4)$$

in which t is the time interval between the passage of the incident and reflected shock wave past the pressure transducer located a distance d from the test section end wall. The temperature behind the reflected shock may then be calculated from gas dynamic equations based upon the conditions behind the incident shock.

The experiments conducted without the dispersion plate revealed that the shock wave reflection was far from ideal. The runs conducted with the dispersion plate in place indicated that a further degradation of the shock structure had occurred. The temperatures predicted by the ideal shock equations with a constant γ were compared to those obtained from the more rigorous approach. The result of a least square fit of the temperatures from both procedures is[50]:

$$T_{5C} = 0.8696\ T_5 + 43.3 , \qquad (5)$$

where, T_5 and T_{5C} are the temperatures behind the reflected shock as calculated using the ideal shock equations and the conservation equations respectively.

This experimentally derived correction agrees quite well with the values obtained using an averaged value of the specific heat ratio at 300 K and the originally calculated T_5. Additional justification for calculating T_5 in this manner is presented by Lester, et al.[51]. In the remainder of the text, the reported T_5 actually represents the T_{5C} obtained using Eq. (5) in which the subscript C was dropped for the sake of simplicity.

2.3 Gas Chromatographic Analysis and Gas Sampling Technique

After the pyrolytic reactions occurring in the heated dust suspension were quenched, gas samples were obtained and analyzed using gas chromatography. The gas sampling system, shown in Fig. 10, is connected to the tube end wall by a 3-way valve which functions to isolate the gas sampling system from the shock tube, vent the tube to a laboratory hood, and direct the pyrolyzate to 75 cm^3 stainless steel sample bottles. In route to the sample bottles the gases pass through a 15 micron filter which prohibits particles larger than 15 μm in diameter from reaching the sample bottles and eventually contaminating the chromatographic columns. A Hamilton Model CR-700-200 gas syringe was used to inject the samples withdrawn from the sample bottles into the injection port of the chromatograph.

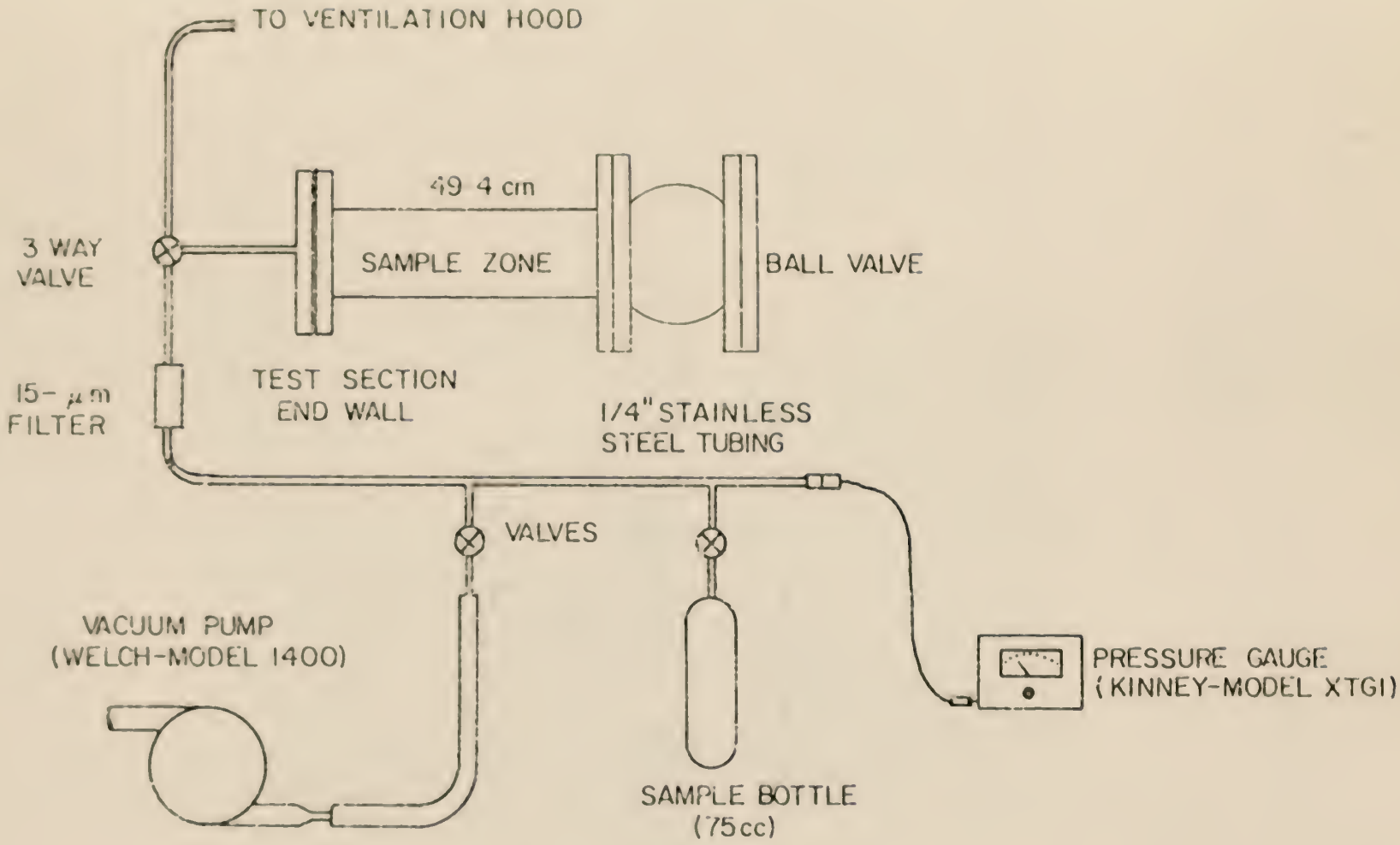

Fig. 10. Gas Sampling System.

Gas chromatographic analysis was performed using two gas chromatographs. A F and M Model 700 gas chromatograph with a thermal conductivity detector was employed to detect the concentration of carbon monoxide and carbon dioxide in the sample gases. A pair of matched 6' x 1/8" stainless steel columns with Carbosieve S packing were maintained at a constant oven temperature of 323 K for carbon monoxide and 423 K for carbon dioxide. A comprehensive listing of the conditions used during the detection of these compounds is given in Table 8. The sensitivity of this detector assembly was somewhat reduced by oxidation of the filaments to such an extent that CO and CO_2 concentrations below 180 and 100 ppm, respectively, were impossible to detect.

A Tracor Model 560 gas chromatograph, equipped with a pair of flame ionization detectors, was used to detect hydrocarbons; namely, methane, ethane, ethene, ethyne, propene, propyne, and an unidentified unsaturated compound containing four carbon atoms. During the normal operation of this chromatograph, samples were injected into a 6' x 1/4" glass column packed with Poropak Q. All of the previously listed species were detected and separated during normal operation with the exception of the ethene and ethyne which eluted simultaneously. Separation of these compounds was accomplished using an identical glass column packed with Carbosieve B. The chromatographic conditions used in both operating modes are presented in Table 9.

Originally the gas sampling procedure developed by Wegener[52] was employed to collect the gaseous pyrolytic products. However, instead

Table 8. Operating conditions of the chromatograph used to detect oxides of carbon.

Parameter	Operating Conditions	Operating Conditions
Species Detected	CO	CO_2
Column Packing	Carbosieve S	Carbosieve S
Carrier Gas	H_2	H_2
Flow Rate	55 ml/min	55 ml/min
Filament Current	200 mA	200 mA
Column Temp.	50 C	145 C
Recorder Speed	1"/min	1"/min

Note: Units correspond to those of the chromatographic system.

Table 9. Conditions used to detect C_1-C_4 hydrocarbons and separate C_2H_2 from C_2H_4 on flame ionization chromatograph.

Parameter	Normal Operation	Specialized Operation
Species Detected	(C_1-C_4 hydrocarbons)	($\frac{C_2H_2}{C_2H_4}$ ratio)
Column Packing	Poropak Q	Carbosieve B
Carrier Gas	N_2	N_2
Flow Rate	35 ml/min	45 ml/min
Flow Rate H_2	400 ml/min	400 ml/min
Flow Rate Air	0.80 scfh	0.80 scfh
FID Temperature	200 C	200 C
Inlet Temperature	125 C	125 C
Recorder Speed	1"/min	1"/min
Programmed	yes	no
Initial Temperature	125 C	125 C
Final Temperature	125 C	125 C
Prog. Rate	25 °C/min	
Initial Hold	3 min	
Final Hold	7 min	

Note: Units correspond to those on instrument.

of using 500 cm^3 sample bottles as specified by Wegener, 75 cm^3 sample bottles were utilized. With this modification, the results obtained using the prescribed procedure were invalid inasmuch as preliminary measurements of the pyrolytic yield indicated that more than 100 w/o of the charged sample was devolatilized to lower order hydrocarbons! As a result, a new sampling technique was developed which eliminates the need for the sample dilution multiplication factor (SDMF) as prescribed by Wegener.

The recent addition of a ball valve between the sample zone (the last 49.9 cm of the test section) and the remainder of the test section facilitated the development of a new sampling technique. Approximately two seconds after bursting the diaphragm, the ball valve is closed, confining the pyrolytic products within the sample zone. These trapped gases are allowed to disperse throughout the sample zone until a nearly homogeneous mixture is obtained. In the strictest sense, a true homogeneous mixture will never be obtained in times consistent with experimental work; however, a test was devised to show how long is required to achieve an acceptably homogeneous mixture.

The reason for the error in the original sampling technique is that immediately after the reaction is quenched, the concentration of the product gases is greatest in the region in which the reaction occurred (roughly the last 15 cm of the sample zone). If such a concentration gradient exists within the sample zone, then immediate sampling of this region through the end-wall will result in "product rich" samples. This

hypothesis was confirmed by simultaneously drawing samples from the isolated sample zone at two locations, one through the end-wall and another 39.4 cm from the end-wall, five minutes after an experimental run. Chromatographic analysis of these samples revealed that the concentration of products was significantly greater in the samples taken through the end-wall. Thus, further testing was performed using the simultaneous sampling technique to determine when a nearly uniform distribution of products existed within the sample zone. The conclusion derived from such experimentation was that one hour was sufficient.

This experimentation proved that a product rich zone was no longer being sampled. Nevertheless, one additional question concerning the sampling technique merits discussion. Is there any movement of the product gases out of the sample zone and into the test section before the ball valve is closed? This question was resolved by sampling the gases trapped within the closed ball valve during a typical experimental run in addition to those in the sample zone. Gas chromatographic analysis of these samples revealed that the quantity of products in the ball valve was less than 1.0% of the quantity observed in the sample zone of uniform composition.

The calibration procedure necessary to determine the mass of an injected gaseous compound closely follows earlier work in this laboratory. Peak identification was accomplished by injecting pure samples of carbon monoxide and carbon dioxide into the thermal conductivity chromatograph operating at the specified conditions. A similar procedure was used to

identify the retention times of the species detected using the flame ionization gas chromatograph.

Inherent in all quantitative gas chromatographic analysis is the assumption that the detector response is proportional to the mass (or alternately moles) of the injected compound. Therefore, the response is also proportional to the concentration of the species if uniform volumes of sample are injected. Data presented in terms of concentration, however, are not meaningful since they are specific to the experimental apparatus from which they are extracted. Therefore, it is more desirable to express the amount of all compounds in terms of a more generic quantity such as grams of gas per gram of sample or as a percentage of the initial mass of the charged sample.

This value can be calculated in a straightforward manner if the concentration (g/g-mol) of each species in the injected sample is equal to the concentration of the component in the nearly homogeneous sample zone. Mathematically this is expressed as:

$$\frac{M_i}{N_i} = \frac{M_s}{N_s} , \qquad (6)$$

where M_i and M_s are the grams at component injected and in the sample zone, respectively, and N_i and N_s are the number of gram-moles injected and in the sample zone, respectively. The quanity N_i is calculated from the ideal gas law as,

$$N_i = \frac{PV_i}{RT} , \qquad (7)$$

where,

P = Pressure of injected sample = 1 atm,

V_i = Volume of gas injected = 2×10^{-4} ℓ,

R = Universal gas constant = 0.0821 $\frac{\text{atm } \ell}{\text{g-mol K}}$,

T = Temperature of injected sample - 300 K.

Evaluation of this equation yields that $N_i = 8.17 \times 10^{-6}$ g-moles. Similarly, the total number of gram-moles in the sample zone,

$$N_s = \frac{P_s V_s}{RT} , \tag{8}$$

where, P_s is the pressure in the shock tube after completion of the experiment and V_s is the volume of the sample zone, 1.01 ℓ. Substitution of the appropriate numerical values gives the following formula for the number of gram-moles in the sample zone,

$$N_s = 4.13 \times 10^{-2} P_s . \tag{9}$$

The method of calculating M_i depends upon the chromatograph used. For the oxides of carbon, detected using the thermal conductivity chromatograph, the expression for M_i is given by,

$$M_i = (CF)(M_p) , \tag{10}$$

where CF is a calibration factor. It relates the grams of carbon oxide to the mass of the strip chart recorder paper and is determined by injecting a known mass of an oxide of carbon into the gas chromatograph. M_p is the mass in grams of the strip chart recorder paper under the peak

of interest resulting from a 2×10^{-4} ℓ injection of the sample gas.

The calculation of the quantity of hydrocarbons present makes use of a response weighing factor, F. This technique is discussed in detail by McNair and Bonelli[53]. These weighing factors are based upon the assumption that the ratio of the responses produced by the injection of two equal masses of any two ionizable species is equal to a constant for all flame ionization detectors. The values of the response weighing factors used in this study are given in Table 10.

The species independent calibration factor was determined daily to account for normal variations in the chromatographic equipment. This was accomplished by injecting 2.00×10^{-4} ℓ of 100 ppm ethyne (acetylene) calibration gas into the system and dividing the corresponding mass of ethyne by the integrated number of counts under the ethyne peak. The use of both the standard calibration factor, CF', having units of g/counts and the unitless weighing factor, F, permitted calculation of the mass (g) of compound of interest in the injected sample from the equation

$$M_i = (CF')(F)(C) , \qquad (11)$$

where C is the integrated number of counts under the peak of interest. Similar to the carbon oxides, the mass, in grams, of an individual hydrocarbon produced is

$$M_s = 5.05 \times 10^{-3} (P_a)(CF')(FC) . \qquad (12)$$

Table 10. Flame ionization detector response weighing factors used in this investigation (From (53)).

Component	Response Weighing Factor
CH_4	0.97
C_2H_2	1.09
C_2H_2	1.02
C_2H_6	.97
C_3H_4	1.00 (a)
C_3H_6	1.00 (a)
C_4H_x	1.09 (a)

(a) Assumed values.

Division of M_s by the sample size, 20 mg, and multiplication by 100 gives the percentage of the original sample present in each species of pyrolyzate.

3.0 EXPERIMENTAL RESULTS AND DISCUSSION

The goal of this study was to probe into the mechanics of ignition in agricultural dusts. Inasmuch as the optical data recorded on the oscilloscope played an essential role in the interpretation of phenomena occurring in a heated dust suspension in both inert and oxidizing environments, the first section of this chapter addresses the interpretation of these data. In the second section the ignition delay data are presented. The third section contains a quantitative and qualitative description of the production of stable gaseous products during devolatilization. In the final section, the results are discussed with a view towards coupling the ignition and devolatilization processes.

3.1 Interpretation of Optical Data

The optical diagnostics associated with the SPST play a vital role in characterizing the phenomena occurring in the heated dust/test gas suspension. The continuum emission from the incandescent dust particles served as a means of defining ignition, and the transmission behavior of the helium-neon laser beam passing through the reaction zone permitted estimation of the time needed for nearly complete devolatilization. The use of these optical probes in shock tube experimentation was developed initially by Seeker[7].

The optical system was described in Section 2.2. A helium-neon laser beam was passed through the test section and the output was detected with a photomultiplier tube. The transmitted intensity of the laser beam

through the particle suspension is related to the total extinction cross-section of the particles through Beer's law,

$$T = \frac{I}{I_o} = \exp\left(-\sum_{i=1}^{n} N_i \sigma_i L\right) \quad , \tag{13}$$

where I_o and I are the beam intensity incident upon the suspension and emerging from the suspension, respectively, T is the fractional laser transmission, N_i is the number density of the particles in the i-th size class, σ_i is the extinction cross section, and L is the optical path length of the laser beam through the suspension.

In general, the extinction cross section is a complicated function of particle size and complex refractive index. The analysis is greatly simplified in the present case because the extinction cross section is a well-behaved function of particle size for diameters greater than 1 μm and may be adequately approximated as 2.1 times the geometric cross-sectional area[7], $\pi D^2/4$. The importance of this cannot be overstated, for if the extinction coefficient were not simply related to the geometrical cross-sectional area of the particle, mere transmission measurements would be insufficient to deduce any information about the particle size as a function of time during the pyrolysis or combustion of dust. Therefore, for the purposes of this investigation, it is sufficient to realize that only changes in the total surface area, and thus in the volume fraction, of the particles will cause changes in the observed transmission.

A qualitative appreciation for the kind of information which can be deduced from the laser transmission behavior can be obtained by considering the laser transmission traces represented in Fig. 10-A, B, and C. In these figures time is the horizontal axis and the passage of the incident and reflected shocks are identified by the two step-changes in the pressure trace. The gradual decrease in the pressure trace marks the beginning of very rapid cooling by the rarefaction wave. Figure 11-A[50] shows the behavior recorded when benzene in the gas phase is shock heated in an inert environment. As benzene reacts to form soot, thereby increasing the total volume fraction in the path of the laser beam, the laser transmission decreases. Figure 11-B illustrates the behavior when soybean dust is pyrolyzed under similar conditions. The laser transmission is seen to drop dramatically when the dust/test gas suspension is swept into the path of laser beam. The subsequent rapid increase in the transmission trace indicates that the total cross-section in the beam is decreasing, presumably due to particle disappearance through devolatilization or particle coagulation. Particle coagulation changes the surface area but not the volume fraction of the suspension. Therefore, it has the same destructive influence on interpretation of the transmission data as the aforementioned complex behavior of extinction cross-section with particle refractive index. The possible effect of turbulent coagulation on the transmitted beam intensity was shown to be insignificant to such an extent that it would not produce the observed changes in laser transmission[54]. Thus,

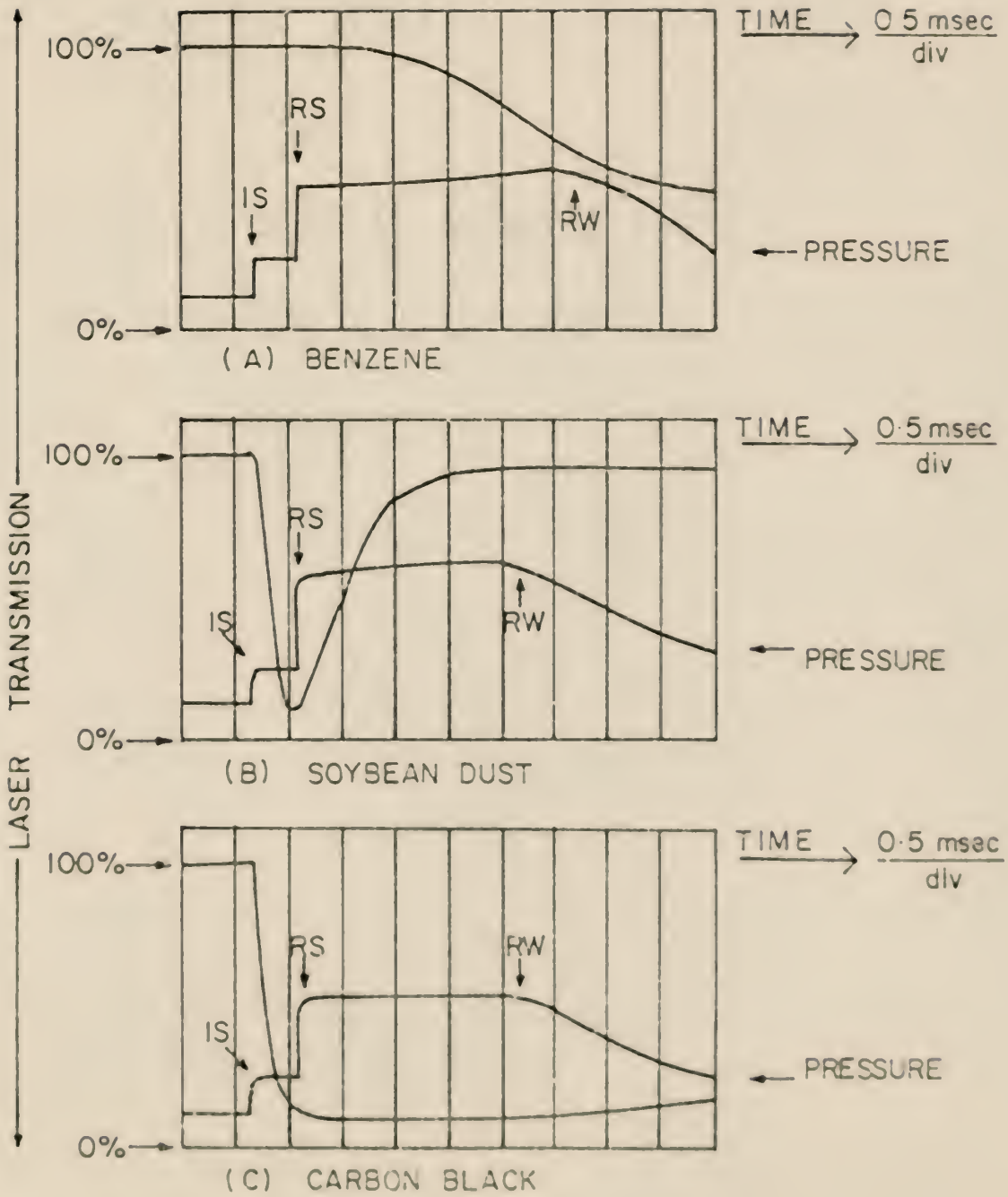

Fig. 11. Behavior of transmission and pressure traces during pyrolysis of (A) Benzene in the gas phase, (B) soybean dust, (C) carbon black. (IS-incident shock, RS-reflected shock, and RW-rarefaction wave).

the increase in the laser transmission after the initial decrease due to the movement of the dust cloud into the laser beam is attributed to devolitilization of the dust particles to the gas phase. The chromatographically determined presence of massive devolatilization in short periods of time, as shown later in this chapter, adds additional credence to this supposition.

The laser transmission trace shown in Fig. 11-C, resulting from the pyrolysis of very low volatile carbon black particles, reveals a constant level of laser transmission after the initial decrease caused by the movement of the particle dispersion into the path of the laser beam. Thus, the carbon black particles are observed to remain in a relatively unchanging suspension throughout the duration of the reaction period. Transmission traces similar to those obtained from carbon black have also been observed during pulverized coal devolatilization. The coal's volatile content is at least a factor of 2.5 less than that found in the agricultural dusts. These three cases, produced from pyrolyzing a gaseous sample, a sample composed primarily of volatile constituents, and a sample with very little volatile matter, reveal how the laser transmission can be employed to give estimates of the particle behavior during an experimental run.

Laser transmission was employed to estimate the duration of devolatilization, i.e., the reaction time for nearly complete pyrolysis. This parameter was necessary in the calculation of the energy of activation of pyrolysis as detailed in the next section. The reaction time was

estimated from the oscillograms as the period between the passage of the reflected shock and the point at which the transmission trace had stabilized at a nearly constant level following the increase due to devolatilization. This time period was very sensitive to temperature, and it was initially hoped that some useful kinetic information about the devolatilization process might be gathered totally from the optical data. This proved impossible due to the sensitivity of the analysis to small uncertainties in the photomultiplier current output. Digitalization of the output might give the required accuracy; however, the necessary equipment were not available during this study.

As previously described, the continuum emission from the incandescent dust particles passed through a narrow band pass filter (589.3 nm) and was detected by a photomultiplier tube. The wavelength was chosen so there would be a minimum of interference from the banded radiation of gas phase species. This optical system was designed originally by Seeker[7] to record the data necessary to the calculation of the particle temperature as a function of time. However, in this study the emission was employed primarily to determine the occurrence of exothermic reactions in the heated dust/air suspension which were manifest by an increase in the particle temperature above the temperature of the gas.

Emission at any wavelength is related to the blackbody temperature through Planck's law,

$$E_{b\lambda} = \frac{C_1 \lambda^{-5}}{e^{C_2/\lambda T} - 1} \qquad (14)$$

where $E_{b\lambda}$ is the monochromatic emissive power of a black body at λ, the wavelength of the emission, T is the temperature, and both C_1 and C_2 are radiation constants. Thus, the output current from the photomultiplier tube is proportional to the particle temperature through the observed intensity of emission from the incandescent dust suspension.

Following the procedure outlined by Seeker, a few preliminary runs in air were conducted to insure that the agricultural dust cloud temperature exceeded the gas temperature as predicted by the frozen gas equations. As expected, the particle cloud temperature was greater than the calculated gas temperature, indicating that exothermic chemical reactions occurred, combustion of the heated dust particles. Throughout the remainder of the ignition studies, the emission was used to define the onset of ignition. Comparable runs in nitrogen yielded emission intensities at 5893 Å several orders of magnitude less than those observed in air.

Theoretical considerations of a nonadiabatic oxidation process dictate that ignition can be defined as the lowest temperature at which the rate of heat loss is less than the rate of heat generation[26]. Thus, the ignition delay is the time required for the combustibles to heat to such a temperature as to satisfy this criterion. The experimental determination of the ignition delay was made by locating the intersection of the emission voltage baseline and the line representing its maximum rate of increase, a procedure depicted in Fig. 12. The ignition delay is then measured from the oscillogram as the time between the passage

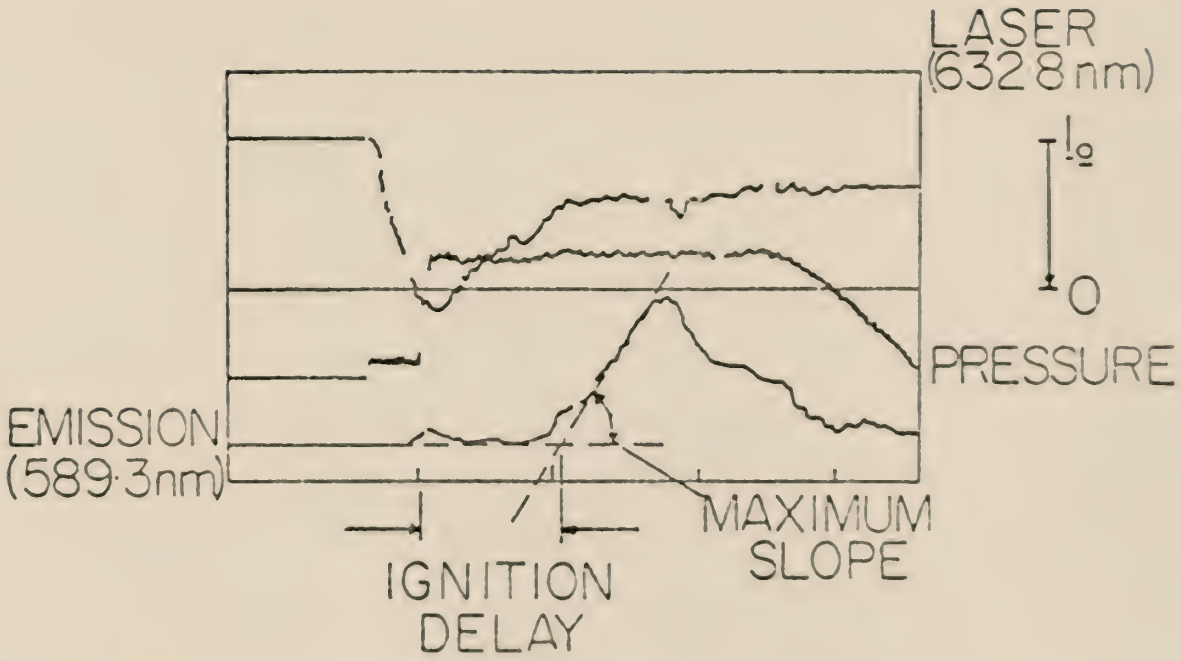

Fig. 12. Schematic of oscillogram illustrating definition of ignition delay.

of the reflected shock and point of intersection of these two lines.

The use of optical techniques to define ignition is by no means unique to this study. Fox, et al.[55], reported that optical techniques are favorite experimental methods of determining the onset of ignition in metal powders by a 5:2 margin. Furthermore, the authors observed that spectrally selective measurements, as employed in this study, gave the most definitive results.

3.2 Particle Ignition Delay

The objective of this portion of the study was to examine the temperature dependence of the onset of ignition in agricultural dust samples subjected to shock heating in moisture free air. The oscillograms, recording the behavior of the dust suspension through the extinction of a helium-neon laser beam, and the rate of emission increase in the dispersion from the onset of exothermic reactions, provided the data with which to partially characterize the ignition process.

A commonly used measure of ignition sensitivity of a combustible substance is the time required for the material to ignite, once exposed to the appropriate conditions. The behavior of the experimentally observed ignition delays for milo dust is shown in Fig. 13 as a function of the temperature behind the reflected shock. This behavior is typical of all the dusts studied, i.e., the ignition delay decreases with increasing temperature in an approximately exponential manner. The line connecting the datam points is the best fit to the data using an Arrhenius

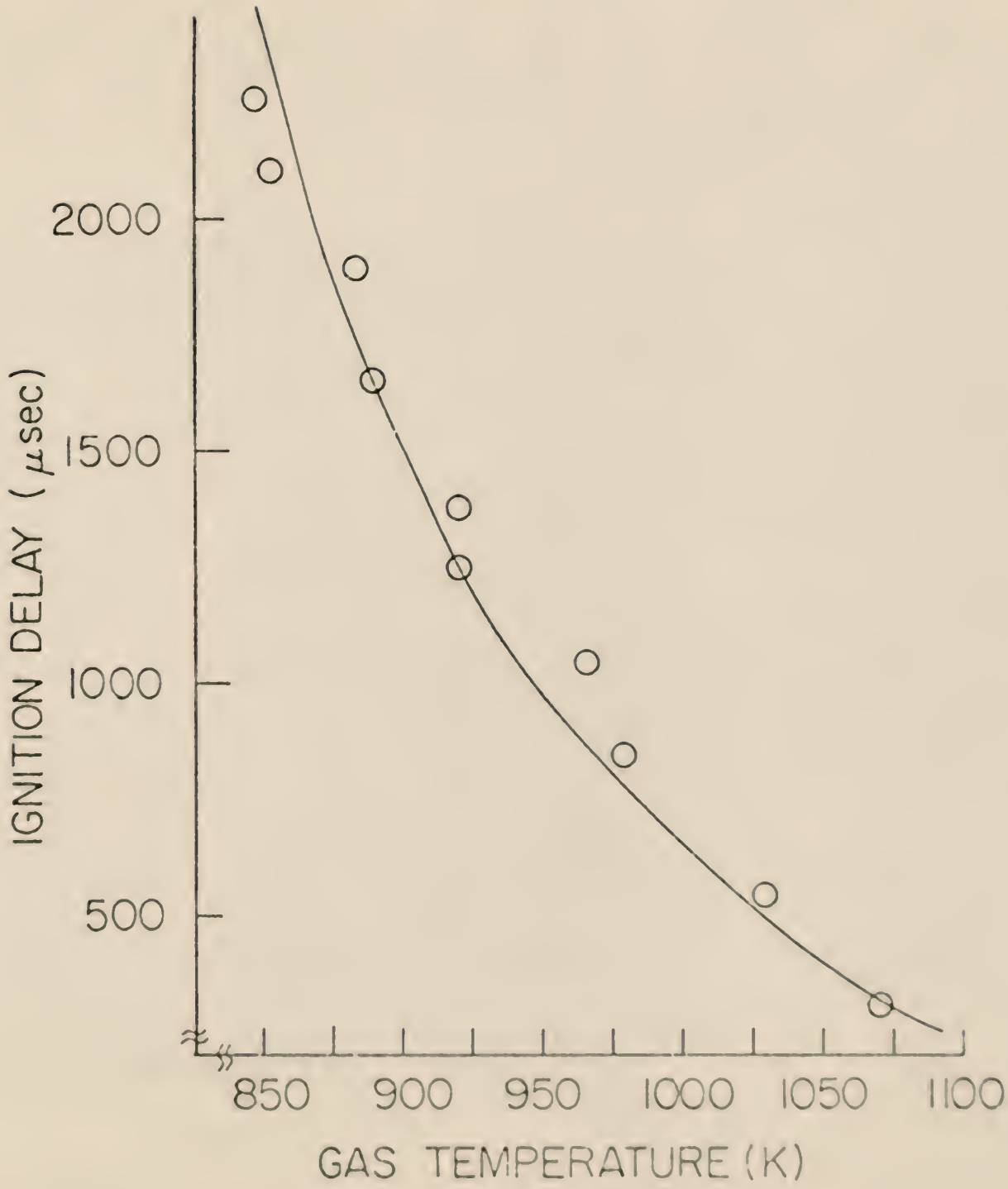

Fig. 13. Observed ignition delays versus gas temperatures obtained using milo dust.

type temperature dependence. The measured ignition delays and the temperatures at which they were obtained are given for each of the dusts in Table 11.

It was assumed that the rate of reaction leading to ignition of these dusts obeyed an Arrhenius relationship of the form

$$k = A_I \exp^{-E_I/RT} , \qquad (15)$$

where k is the pseudo first order reaction rate constant (sec^{-1}), A_I is the empirical pre-exponential factor, E_I is the empiricial activation energy of ignition, R is the universal gas constant, and T is the gas temperature as represented by T_5. With the additional assumption that the observed ignition delay, τ, is inversely proportional to the reaction rate, Eq. (15) can be manipulated into the form

$$\ln(1/\tau) = \frac{-E_I}{R} \left(\frac{1}{T}\right) + \ln A' , \qquad (16)$$

in which A' represents the new empirical pre-exponential factor arising from the assumed proportionality. Plots of the quantity $\ln(1/\tau)$ versus $10^4/T_5$ obtained using corn, milo, soybean, and wheat dust samples are presented in Figs. 14 through 16. A least squares fit of the ignition delay data as represented in their linear form permits determination of the activation energies. A tabular representation of the resulting quantities of interest with the statistically determined uncertainties are given in Table 12. The derivation of the uncertainty in each activation energy is given in Appendix C.

Table 11. Ignition delay data obtained from oxidation of agricultural dusts in 0% moisture air.

Run	Dust	P_5 (atm)	T_5 (K)	$10^4/T_5$ (K^{-1})	τ Ig. Delay (μsec)	$\ln(1/\tau)$
Y11	Wheat	6.71	856	11.69	2000	6.21
Y85	Wheat	6.89	877	11.40	1925	6.25
W13	Wheat	7.00	917	10.90	1300	6.65
Y12	Wheat	7.43	921	10.86	1250	6.68
W87	Wheat	7.48	961	10.41	1050	6.86
W86	Wheat	7.81	1026	9.75	800	7.13
W1	Wheat	7.50	1037	9.64	750	7.20
W14	Wheat	8.29	1042	9.54	550	7.60
Y18	Milo	6.55	847	11.80	2250	6.10
W21	Milo	7.11	852	11.74	2100	6.17
W19	Milo	6.82	883	11.32	1900	6.27
W23	Milo	6.77	890	11.23	1650	6.41
W22	Milo	7.39	919	10.88	1375	6.59
W20	Milo	7.24	920	10.87	1250	6.68
Y22	Milo	7.77	966	10.34	1050	6.86
Y19	Milo	7.95	978	10.22	850	7.07
Y20	Milo	7.87	1030	9.71	550	7.51
Y21	Milo	7.46	1070	9.34	300	8.11
Y35	Soybean	7.74	917	10.91	2150	6.14
Y36	Soybean	7.99	955	10.47	1775	6.33
W30	Soybean	7.14	965	10.36	1175	6.74
W36	Soybean	8.44	1000	10.00	1300	6.65
W37	Soybean	8.13	1032	9.69	925	6.99
W35	Soybean	8.18	1036	9.65	550	7.50
W38	Soybean	8.96	1122	8.91	250	8.29
W33	Soybean	8.87	1177	8.49	200	8.52
W39	Soybean	8.49	1193	8.38	100	9.21
W50	Corn	7.41	942	10.62	1450	6.54
Y50	Corn	7.09	949	10.54	1450	6.54
W51	Corn	6.85	959	10.43	1400	6.57
Y51	Corn	7.09	1007	9.93	850	7.07
Y47	Corn	7.10	1042	9.60	600	7.42
W52	Corn	7.72	1090	9.17	625	7.38
Y53	Corn	8.09	1187	8.43	300	8.11
Y52	Corn	8.03	1263	7.92	525	8.03

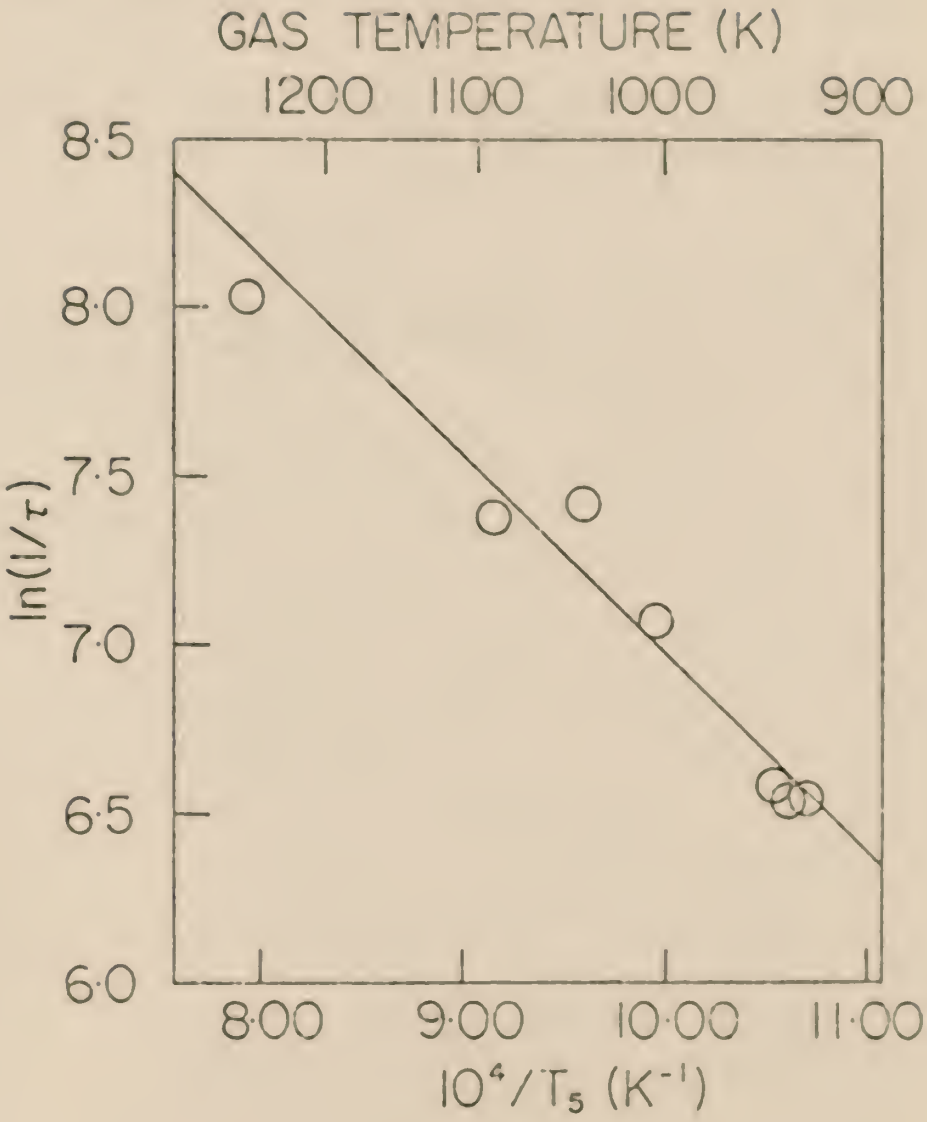

Fig. 14. Plot of $\ln(1/\tau)$ vs. $10^4/T_5$ for ignition delays obtained using corn dust.

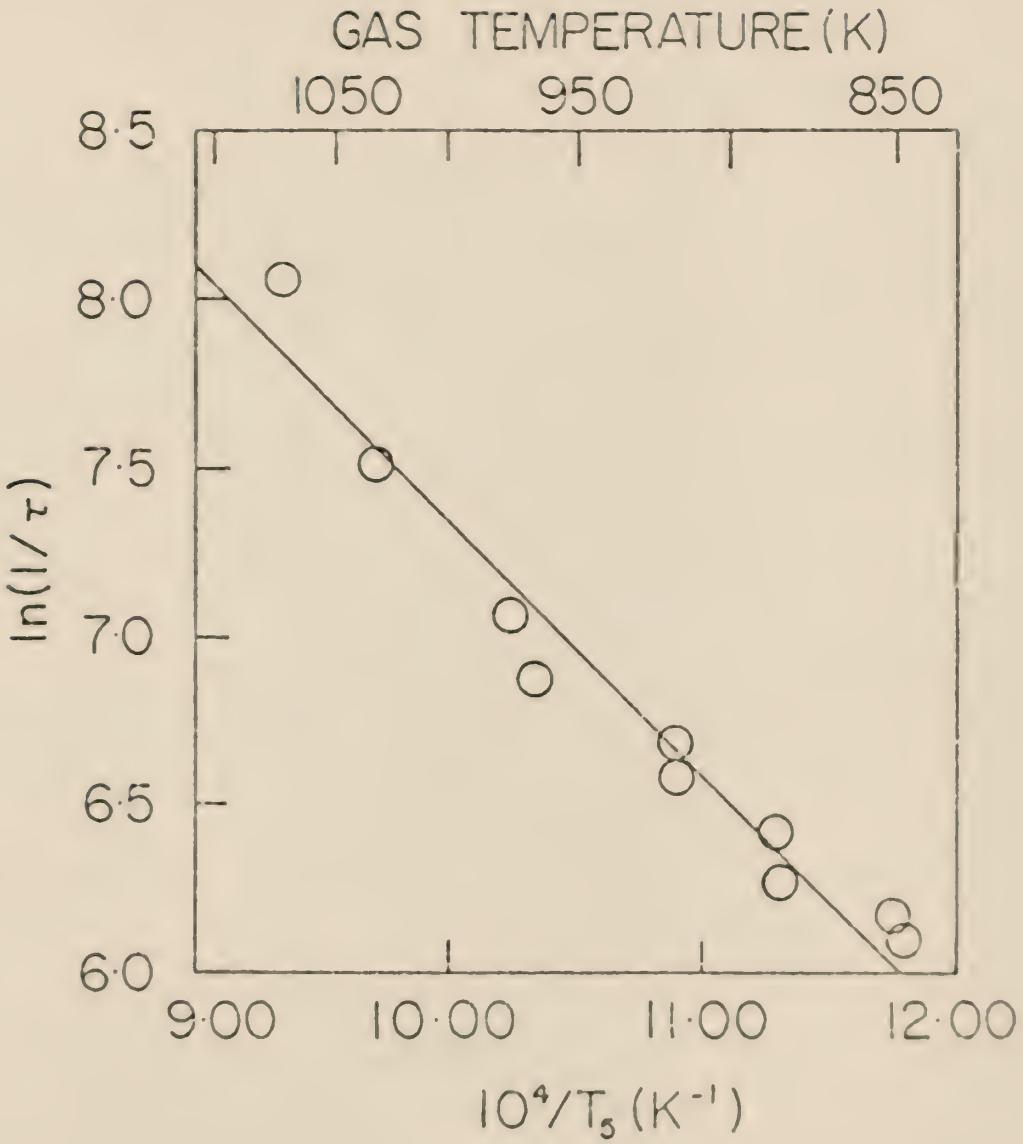

Fig. 15. Plot of $\ln(1/\tau)$ vs. $10^4/T_5$ for ignition delays obtained using milo dust.

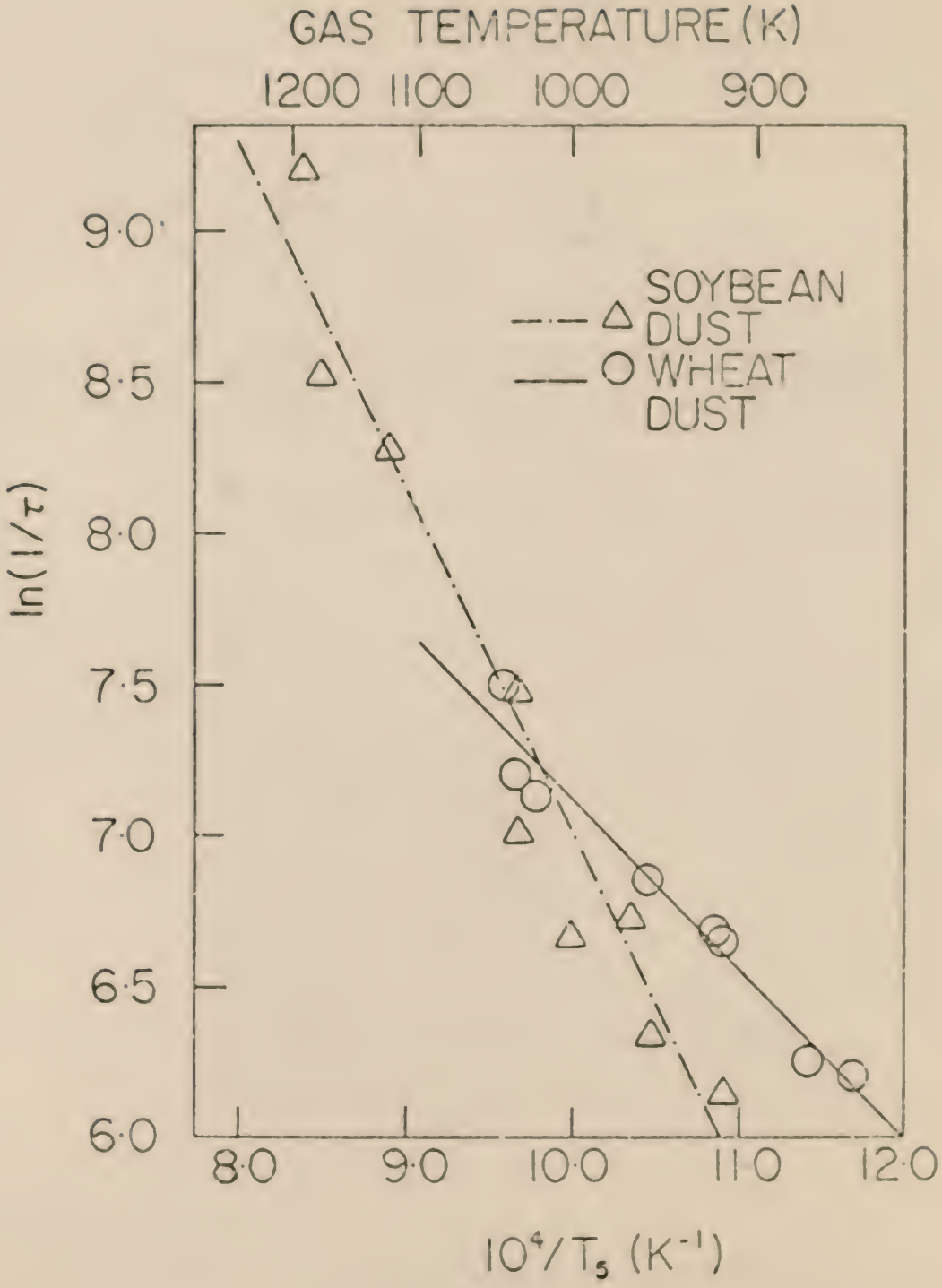

Fig. 16. Plot of $\ln(1/\tau)$ vs. $10^4/T_5$ for ignition delay data obtained using soybean and wheat dust.

Table 12. The activation energies of ignition for agricultural dusts. Results of Aldis, et al[56]. are presented for comparison.

Dust Type	E_I (kJ/g-mol)	Temp. Range (K)	Apparatus	Investigator
Wheat	46.8 ± 5.5	850-1040	Shock tube	Breipohl
Corn	51.4 ± 6.3	940-1265	Shock tube	Breipohl
Milo	62.4 ± 7.1	850-1070	Shock tube	Breipohl
Soybean	97.2 ±10.2	920-1195	Shock tube	Breipohl
Cow Cockle Starch	59.9	725- 940	Furnace	Aldis, et al.[56]
Corn Starch	71.8	725- 940	Furnace	Aldis, et al.[56]

Inasmuch as the activation energies of ignition for agricultural dust have not been addressed in the literature, direct comparisons are impossible. However, the work of Aldis, et al.[56] in which activation energies were obtained from ignition delays merits comparison since starch is the major component of all the dusts investigated in this study. The results, which are also shown in Table 12, compare impressively; particularly when one considers that these data were obtained at lower temperatures (723 to 940 K) with ignition delays varying from 0.1 to 4.5 seconds.

In the present case, soybean dust was determined to have a significantly higher activation energy than the other grain dusts investigated. Similarly, the minimum ignition temperature of soybean dust is also reported to be significantly higher than that observed for other grain dusts (see Table 5).

Some pertinent observations about the mode of ignition can be made from the behavior of the laser transmission and continuum emission traces with temperature. In light of the ensuing discussions, a series of oscillograms, recording the behavior of these traces when agricultural dusts are heated in air are presented in Fig. 17 A-F. The experimental conditions for these runs are given in Table 13. The sequence illustrated was obtained by heating individual 5 mg samples of desiccated soybean dust in 0% moisture air at temperatures ranging from 917 to 1195 K. The following trends are apparent. First, from the laser transmission trace, reflecting the effective cross-sectional area of the particle cloud, it may be inferred that the percentage of the laser beam intensity

Table 13. Parameters from soybean oxidation runs in 0% moisture air. The oscillograms from these experimental runs are given in Fig. 17.

Figure No.	Gas Temperature (K)	Ignition Delay (μsec)
17A	917	2150
17B	955	1775
17C	996	1300
17D	1035	550
17E	1123	250
17F	1195	100

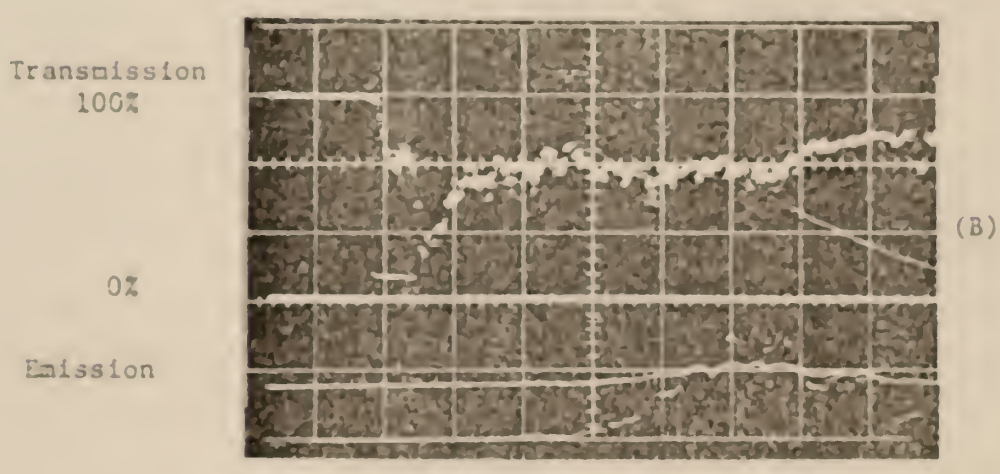

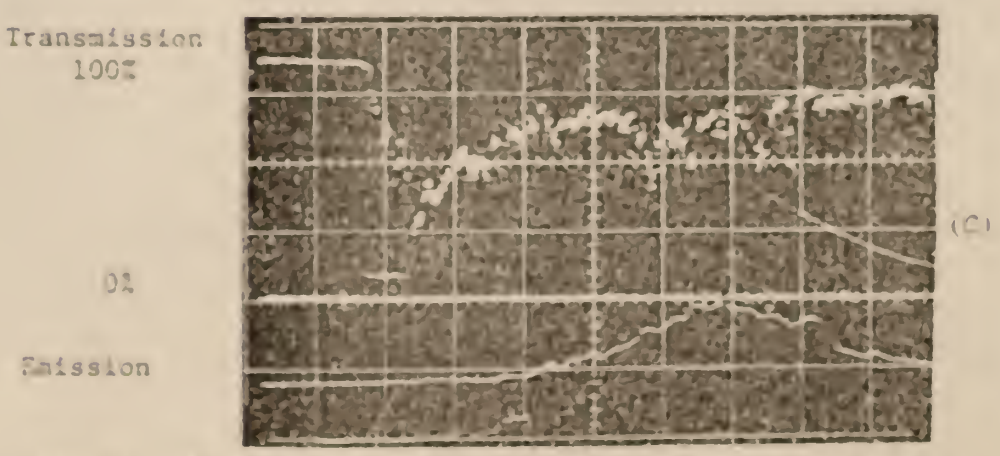

Fig. 17. Oscillograms of soybean dust ignition. Time is to the right at 500 usec per major division.

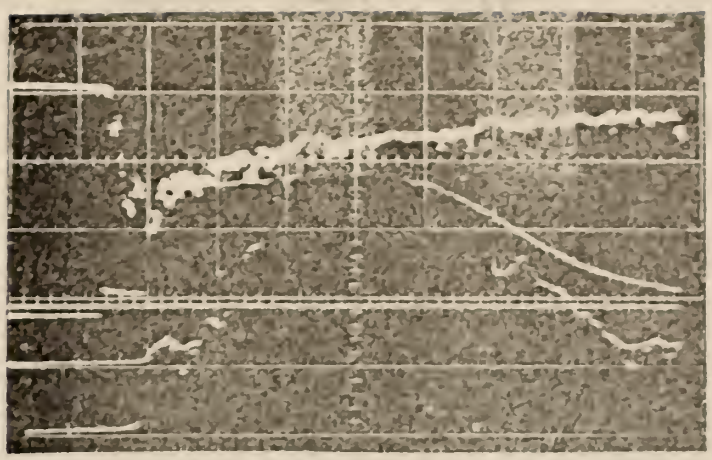

(D)

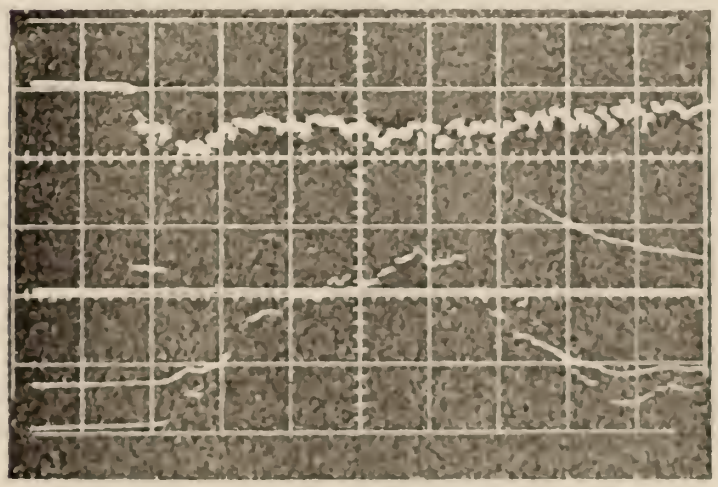

(E)

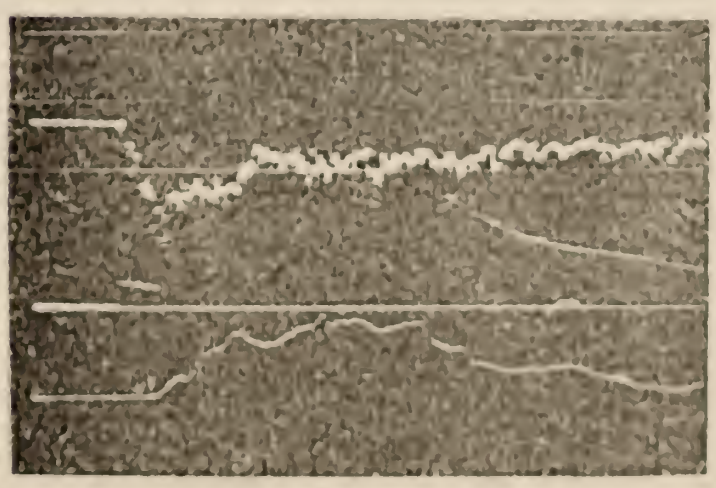

(F)

Fig. 17. (Continued)

that passes through the suspension at its maximum density increases with increasing temperature behind the reflected shock. Second, the time required for the transmission trace to stabilize at a relatively constant level decreases with increasing gas temperature . In all cases, an immediate increase in the transmission from the minimum behind the reflected shock is observed. In other words, no delay, such as an ignition delay is observed in the transmission traces. Devolatilization ensues at relatively low temperatures as compared to those characteristic of ignition. Hence, it is not surprising that the transmission trace mirrors the rapid inception of devolatilization.

These observations have plausible explanations that bear upon the ignition mechanism. The disappearance of much of the originally solid matter from suspension occurs presumably as the result of rapid conversion of the dust particles to the gaseous phase, or rapid devolatilization. The more rapid stabilization of the transmission trace indicates that devolatilization occurs more rapidly at higher temperatures. It must be noted, again, that such observations must remain largely qualitative. An attempt to fit the rate of transmission increase behind the reflected shock with a kinetic interpretation was unsuccessful.

Nevertheless, the phenomenological significance, in general, of these transmission data may be gleaned from the lower temperature oxidation runs. The oscillograms recorded from experiments at these temperatures indicate the transmission increases to nearly one hundred percent prior to any evidence of ignition (as deduced from the emission

traces). Therefore, devolitilization is possibly complete before the onset of ignition. This behavior is consistent with the "Faraday" mechanism of ignition which envisions ignition occurring first in the gas phase volatiles rather than on the particle surface.

It should be emphasized that these oscillograms displayed were acquired from the oxidation of soybean dust. The three other grain dusts exhibited similar behavior. That the change in the suspension cross-section (and probably devolatilization) is complete prior to ignition is witnessed by the three oscillograms shown in Fig. 18.

Inasmuch as volatiles appear to play an important role in the ignition process, the second, and complimentary, portion of this study was directed at quantitatively identifying the gaseous products released upon thermal decomposition in an inert environment. If homogeneous ignition is actually occurring in the released gaseous species, then one would expect that some aspect of the soybean pyrolysis might mirror the differences of the soybean ignition vis-a-vis the ignition of the other dusts.

3.3 Pyrolysis Behavior

The objective of this portion of the investigation was to quantitatively identify the pyrolytically produced products from several dusts and determine the temperature dependence of their evolution. Before these subjects are addressed, the structural changes occurring in the dust particles during pyrolysis as observed by a scanning electron microscope, S.E.M., are examined. A scanning electron

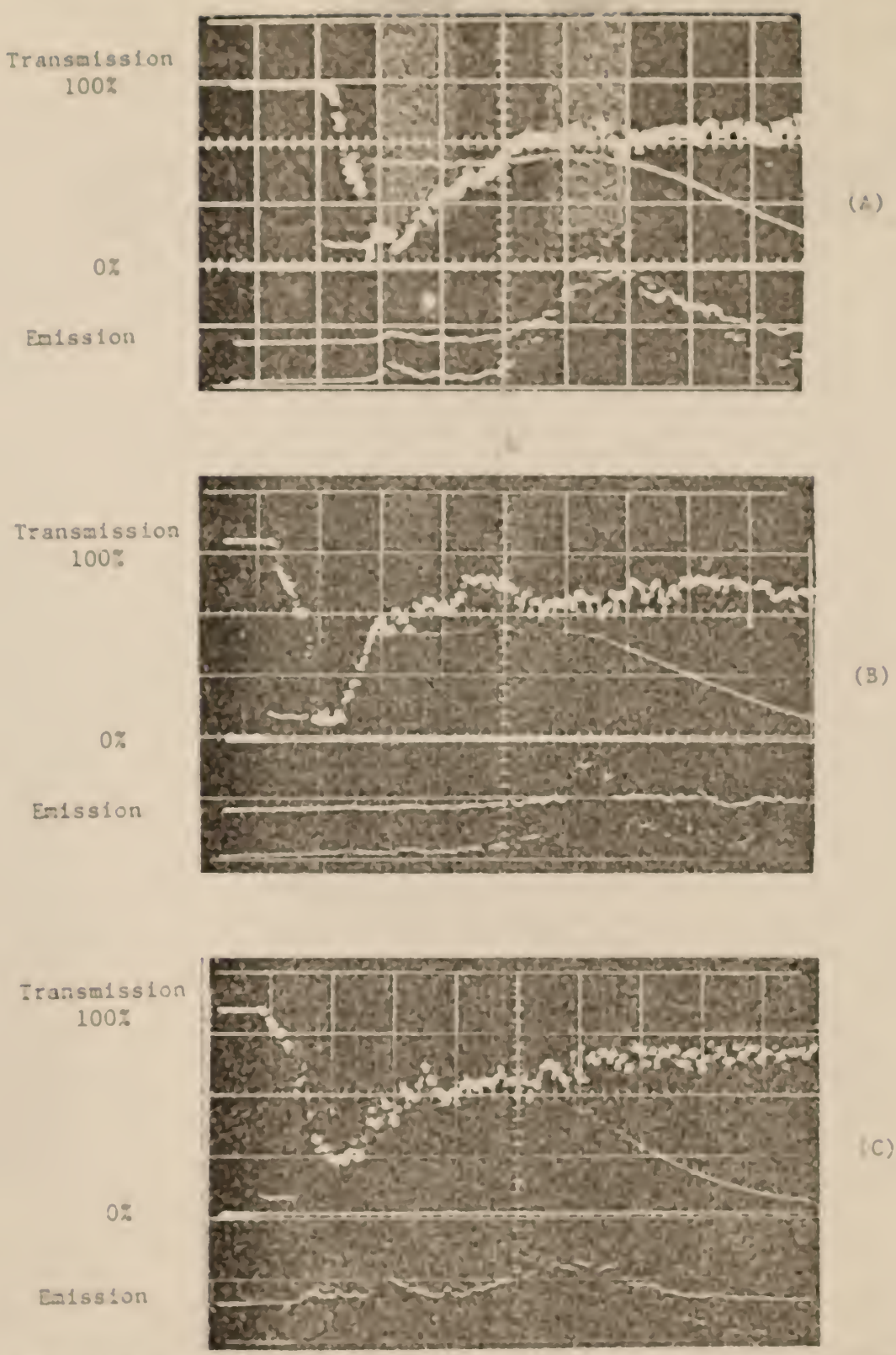

Fig. 18. Oscillograms from low temperature runs of agricultural dusts. Time is to the right at 500 μsec per division. (A-wheat dust oxidation at 964K. B-milo dust oxidation at 851K, and C-corn dust oxidation at 943K).

microscope explores the microscopic structure by bombarding the prepared sample with electrons and translating the output into a visual display from which photographs may be obtained. The unshocked dust samples were prepared by sprinkling the desiccated dust onto two-sided adhesive tape attached to a S.E.M. stub. Shock heated samples were obtained from the optical port directly above the reaction zone in the shock tube using two sided adhesive tape.

From S.E.M. photographs similar to those shown in Fig. 19 A-G and described in Table 14, the following general trends were observed in all four dusts. First, when shock heated, the dusts tend to proceed from a more organized structure (crystalline-like) to an amorphous form. Additionally, with increasing gas temperature, the average diameter of the pores observed increases and more excessive particle fragmentation becomes apparent. Micrographs 19E and F support the hypothesis that dust pyrolysis may proceed similarly to the devolitilization of coal dust (Refer to Fig. 1 and associated discussion).

For large particles it appears from the S.E.M. photographs that substantial erosion of the outer surface occurs concurrently with the escape of volatile constituents from the particle interior. So dynamic is this process, that vestiges of "blow holes" are evident on some particles. The outgassing volatiles apparently void the particle interior, leaving a cenosphere, the shell of which continuously thins until fragmentation occurs. The above scenario, deduced from the pyrolyzed dust remnants, must be viewed with some caution insofar as

Table 14. Identification of Experimental parameters associated with the scanning electron micrographs shown in Fig. 19.

Figure	Dust	Conditions	Magnification
19(A)	Wheat	Unshocked	x 400
19(B)	Wheat	Unshocked	x 4000
19(C)	Wheat	Shocked, N_2 T_5 = 1200 K	x 7000
19(D)	Wheat	Shocked, N_2 T_5 = 1300 K	x 3000
19(E)	Wheat	Shocked, N_2 T_5 = 1870 K	x 3500
19(F)	Wheat	Shocked, A T_5 = 2100 K	x 8000
19G)	Wheat	Shocked, A T_5 = 2100 K	x 1500

(A)

(B)

Fig. 19. Scanning electron micrographs of wheat dust.

(C)

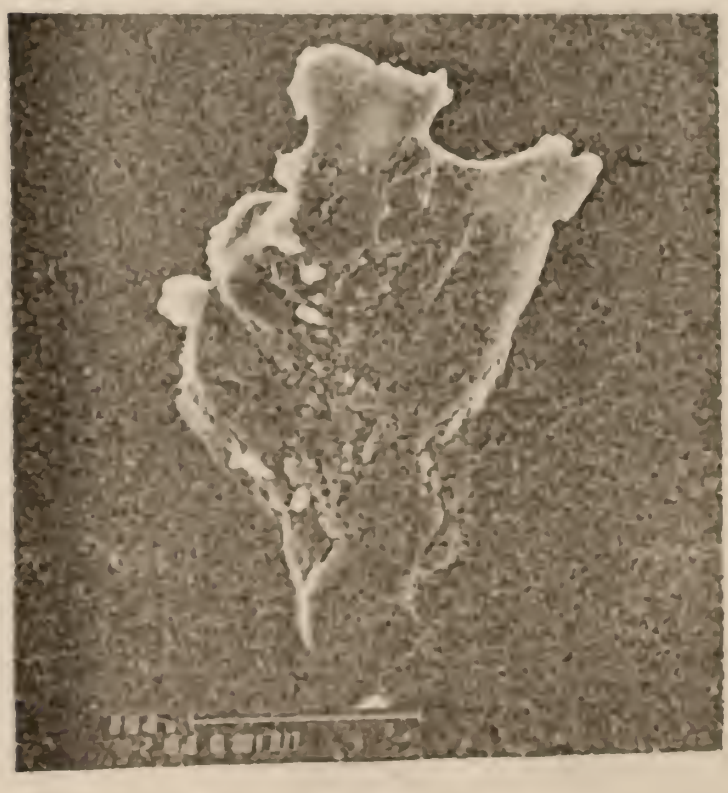

(D)

Fig. 19. (Continued)

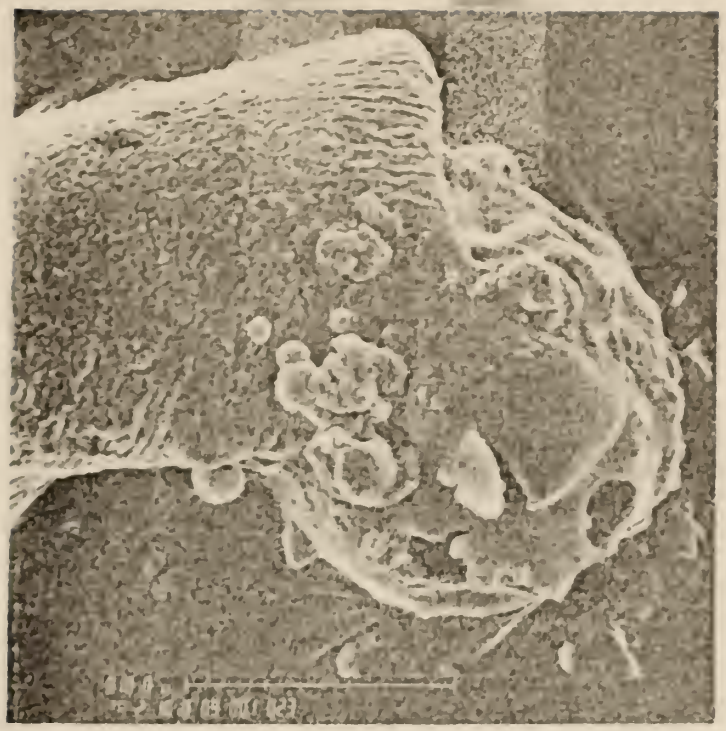

(E)

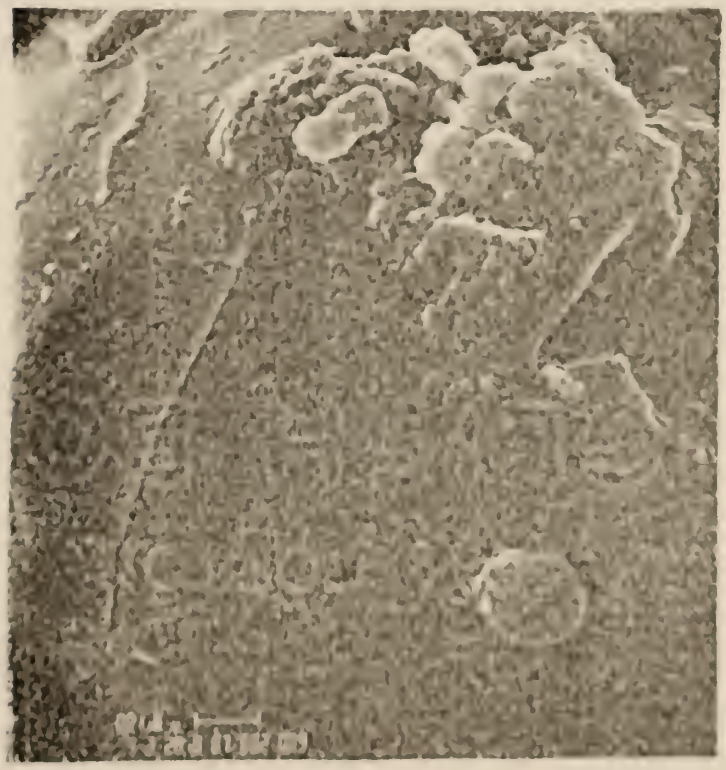

(F)

Fig. 19. (Continued)

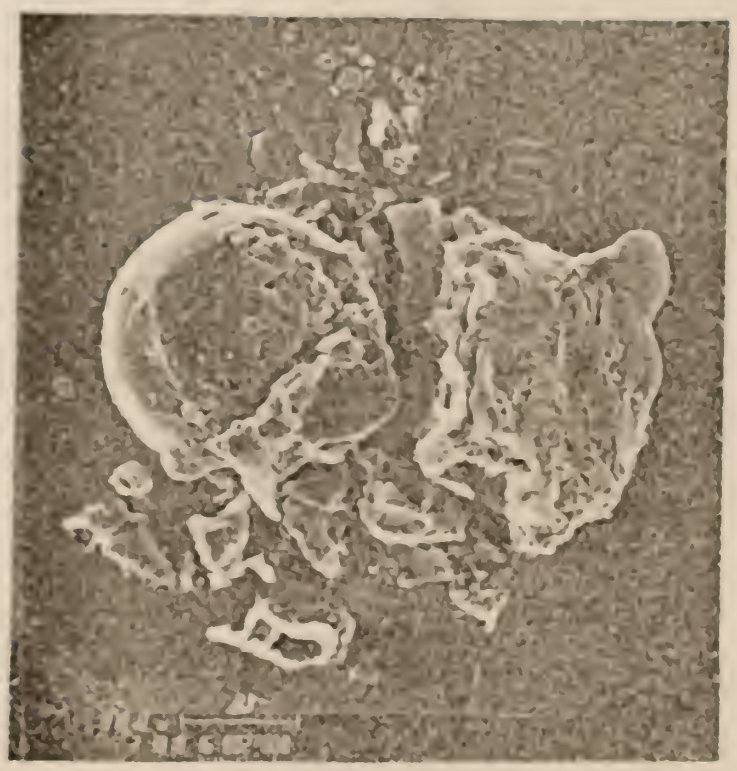

(G)

Fig. 19. (Continued)

the particles collected from the optical port may not be wholly indicative of the behavior occurring within the central core flow of the shock tube. Specifically, they may be more representative of the behavior in the cooler (and more turbulent) boundary layer adjacent to the wall.

Devolatilization experiments were performed on soybean and corn dusts. Additionally, starch obtained from cow cockle plants was used as a standard of comparison. The soybean dust was selected because of its distinctly high ignition activation energy, with respect to the other dusts, and corn dust studied because it contained the highest starch content of the three dusts which had similar ignition activation energies. The temperature range (900-1400 K), the reaction pressure (7.5 $\pm$ 1 atm), and the reaction time as dictated by a fully extended driver section were commensurate with the conditions employed during the ignition study. Thus, it has been assumed that volatile yields are only a function of temperature and time. As previously noted, Martin[15] heated cellulose samples in both oxidizing and reducing atmospheres using carbon arc radiation. The author reported that the volatile yields prior to ignition in an oxidizing environment corresponded quite well with the quantitative yield observed during pyrolysis. If agricultural dust behaves in an analogous manner, then one might expect that the chromatographic analysis of the pyrolyzate would reveal the presence of combustible gases.

The yields of C_1-C_4 hydrocarbons and carbon oxides were determined

from 28 runs. These yields were converted to a fraction of the mass of the charged sample and were expressed as a function of the gas temperature behind the reflected shock. The C_1-C_4 hydrocarbon yields resulting from the pyrolysis of starch, corn dust, and soybean dust samples in each of the experimental runs are presented in Tables 15 and 16. For the sake of comparison, the totals of the C_1-C_4 hydrocarbon yields obtained for each of the three sample types are also plotted against temperature as shown in Fig. 20. The more abundant hydrocarbon species, CH_4, C_2H_2, C_2H_4, and C_2H_6 have been plotted as a function of temperature in Figs. 21-23. It should be noted that the line connecting the data in these figures is drawn only to aide in the visual interpretation of the data. Error bars, equivalent to approximately $\pm$ 10% of the determined yield, were omitted from these plots for the sake of clarity.

The pyrolytic yields of carbon monoxide and carbon dioxide are given in Table 17. The gas samples collected after the pyrolysis of cow cockle starch were found to contain quantities of CO and CO_2 below the detection limit, equivalent to approximately 2.6 weight percentage of the charged sample, of the thermal conductivity gas chromatograph. The carbon oxide yields (expressed as a weight percentage from the corn and soybean samples) are plotted against temperature in Fig. 24.

The experimental activation energies of pyrolysis were calculated assuming that devolatilization proceeded in a manner which could be described accurately by first order kinetics, i.e., the rate of volatile

Table 15. C_1-C_4 hydrocarbons yields (g/g dust) from the pyrolysis of soybean dust.

Run	Temp (K)	CH_4	C_2H_2	C_2H_4	C_2H_6	C_3H_6	C_3H_4	C_4H_x	Total
Y62	888	0.0000	0.0000	0.0053	0.0000	0.0000	0.0000	0.0000	0.0053
W64	949	0.0015	0.0000	0.0042	0.0000	0.0007	0.0000	0.0052	0.0116
W67	1034	0.0040	0.0018	0.0152	0.0000	0.0000	0.0000	0.0000	0.0197
W60	1081	0.0062	0.0012	0.0232	0.0000	0.0066	0.0000	0.0067	0.0439
Y63	1115	0.0098	0.0084	0.0336	0.0058	0.0087	0.0000	0.0069	0.0732
W65	1154	0.0114	0.0089	0.0354	0.0075	0.0087	0.0000	0.0100	0.0923
Y67	1159	0.0129	0.0101	0.0384	0.0142	0.0060	0.0012	0.0069	0.0890
W61	1245	0.0163	0.0128	0.0533	0.0094	0.0063	0.0000	0.0142	0.1123
Y61	1289	0.0180	0.0168	0.0411	0.0056	0.0042	0.0025	0.0122	0.1004
Y65	1309	0.0109	0.0141	0.0337	0.0065	0.0056	0.0042	0.0091	0.0841
W66	1341	0.0158	0.0146	0.0345	0.0020	0.0073	0.0000	0.0022	0.0763
W63	1347	0.0132	0.0168	0.0248	0.0013	0.0015	0.0023	0.0127	0.0727
Y66	1426	0.0260	0.0404	0.0467	0.0000	0.0000	0.0000	0.0000	0.1123
Y64	1486	0.0329	0.0561	0.0520	0.0000	0.0016	0.0062	0.0062	0.1488

Table 16. C_1-C_4 hydrocarbons yields (g/g dust) from the pyrolysis of corn dust and starch samples.

Corn Dust Pyrolysis

Run	T_5 (K)	CH_4	C_2H_2	C_2H_4	C_2H_6	C_3H_6	C_3H_4	C_4H_x	Total
W50	954	0.005	0.0000	0.0011	0.0000	0.0000	0.0000	0.0117	0.0133
Y50	1002	0.0018	0.0000	0.0041	0.0000	0.0013	0.0000	0.0116	0.0188
W53	1063	0.0061	0.0056	0.0181	0.0008	0.0064	0.0000	0.0139	0.0509
Y51	1129	0.0127	0.0146	0.0376	0.0041	0.0110	0.0000	0.0059	0.0860
W51	1136	0.0078	0.0093	0.0224	0.0016	0.0091	0.0000	0.0133	0.0640
W52	1249	0.0209	0.0198	0.0485	0.0065	0.0094	0.0000	0.0068	0.1120
Y53	1405	0.0407	0.0630	0.0748	0.0053	0.0031	0.0055	0.0084	0.2008

Starch Dust Pyrolysis

Run	T_5 (K)	CH_4	C_2H_2	C_2H_4	C_2H_6	C_3H_6	C_3H_4	C_4H_x	Total
Y53	1006	0.0018	0.0000	0.0027	0.0000	0.0000	0.0000	0.0042	0.0098
Y34	1022	0.0026	0.0000	0.0043	0.0000	0.0000	0.0000	0.0046	0.0115
W34	1067	0.0069	0.0047	0.0067	0.0000	0.0000	0.0000	0.0032	0.0215
Y36	1091	0.0096	0.0100	0.0208	0.0034	0.0024	0.0000	0.0114	0.0592
Y33	1161	0.0157	0.0128	0.0257	0.0035	0.0041	0.0000	0.0147	0.0766
W35	1262	0.0266	0.0237	0.0437	0.0096	0.0047	0.0001	0.0126	0 1210
W37	1323	0.0290	0.0380	0.0549	0.0066	0.0016	0.0000	0.0092	0.1393

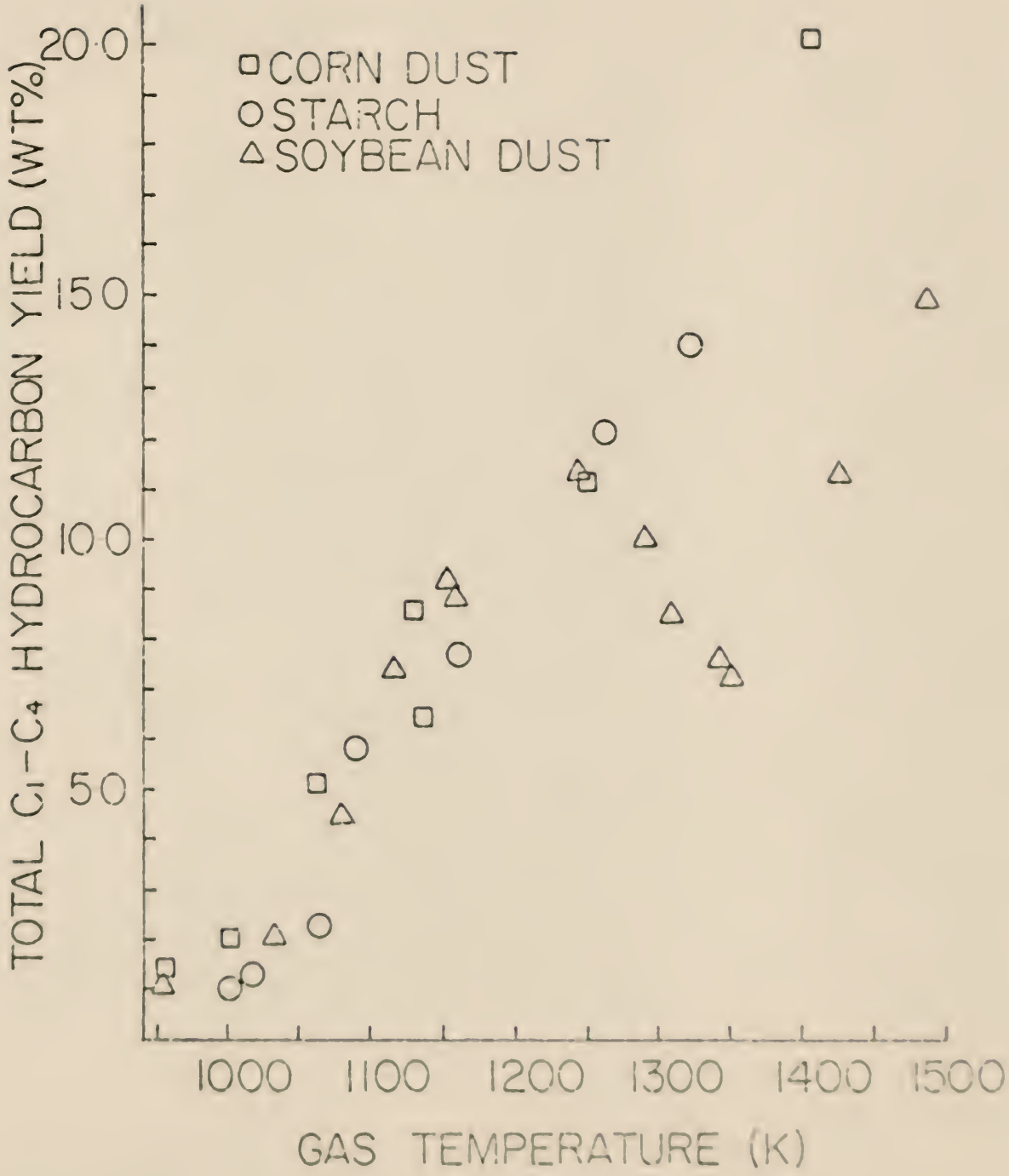

Fig. 20. Pyrolytic C_1 - C_4 hydrocarbon yields from agricultural dusts plotted against gas temperature.

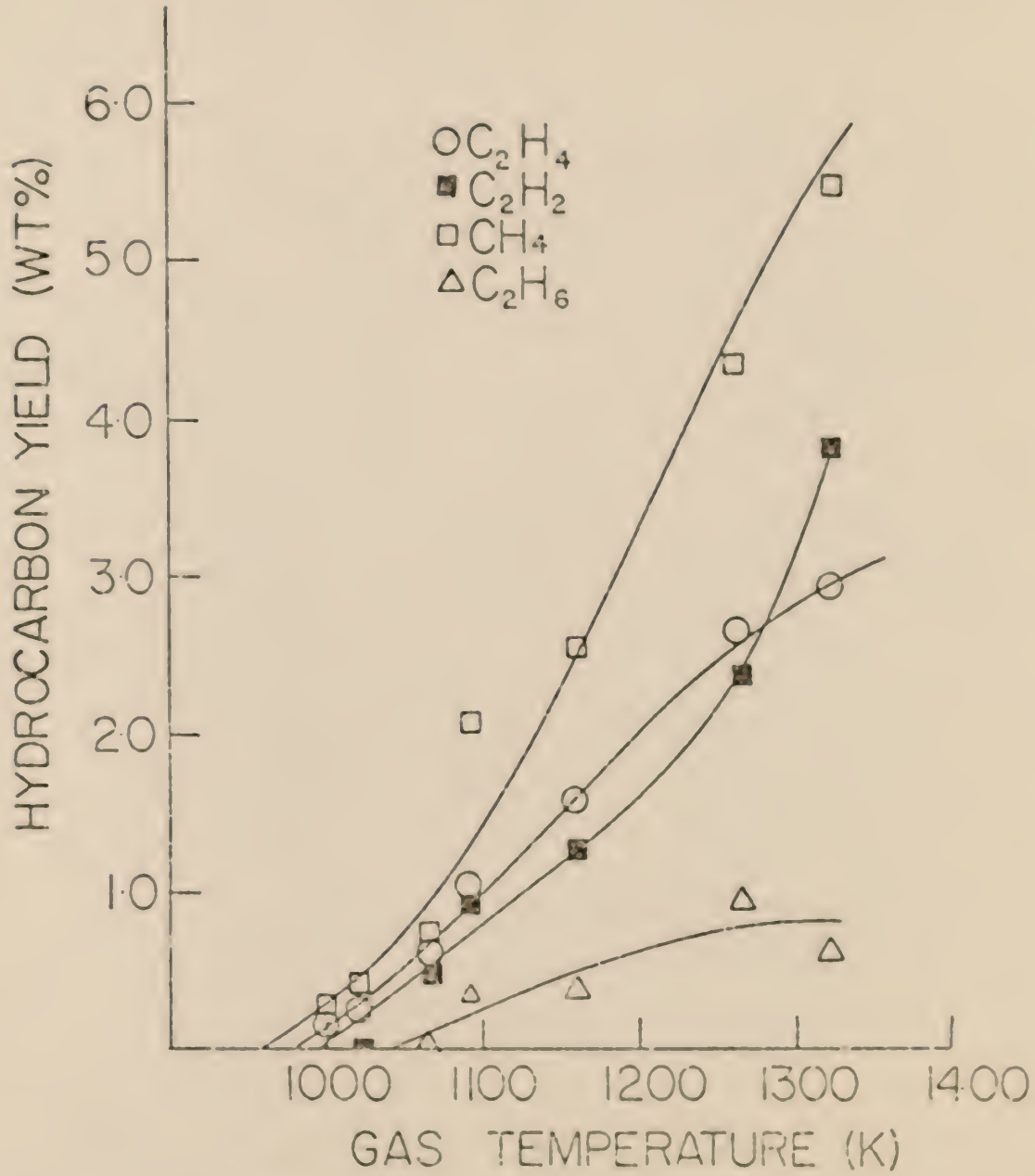

Fig. 21. Pyrolytic yields of the more abundant individual C_1 - C_4 hydrocarbons evolved from starch plotted against temperature.

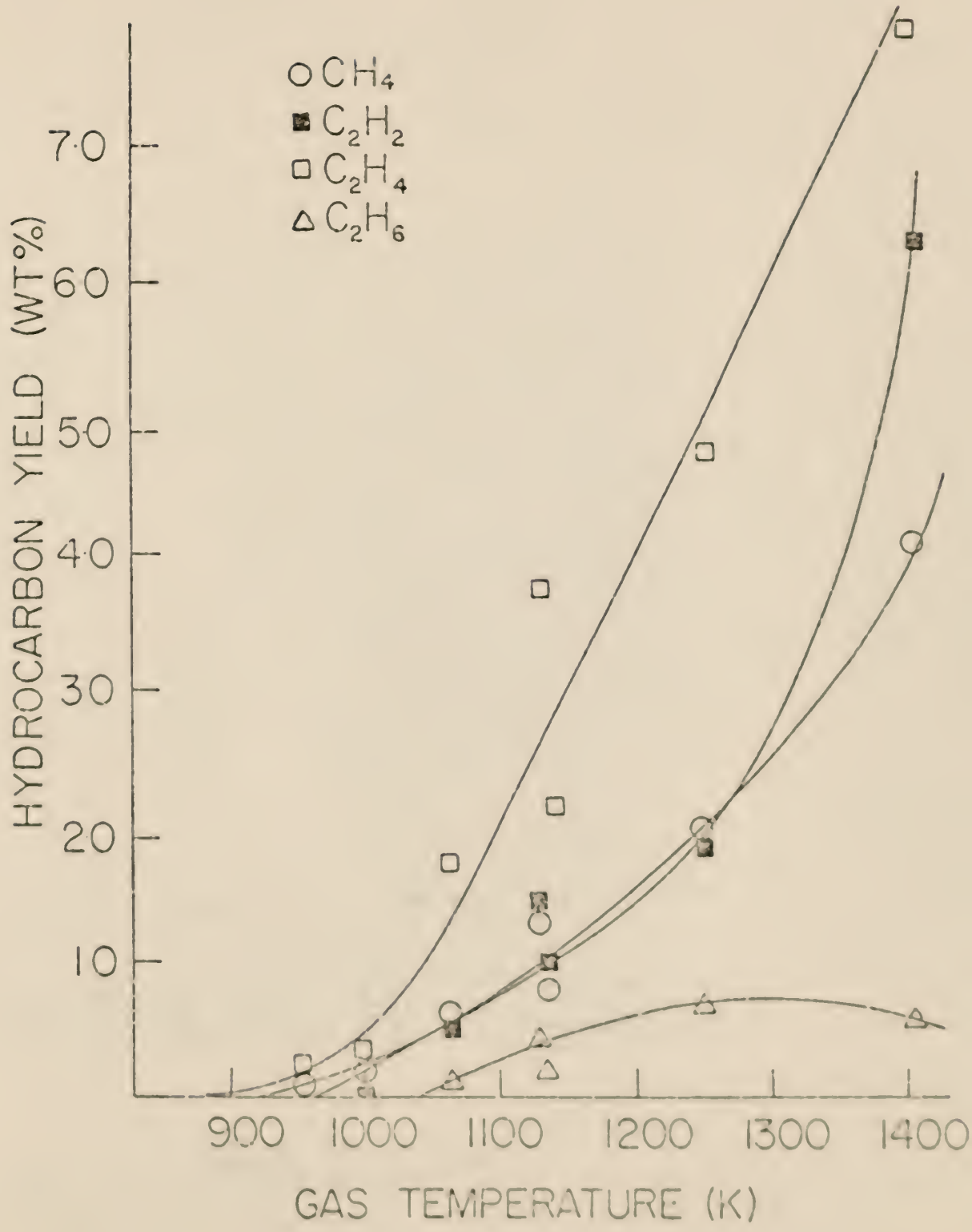

Fig. 22. Pyrolytic yields of the more abundant individual C_1 - C_2 hydrocarbons evolved from corn dust plotted against temperature.

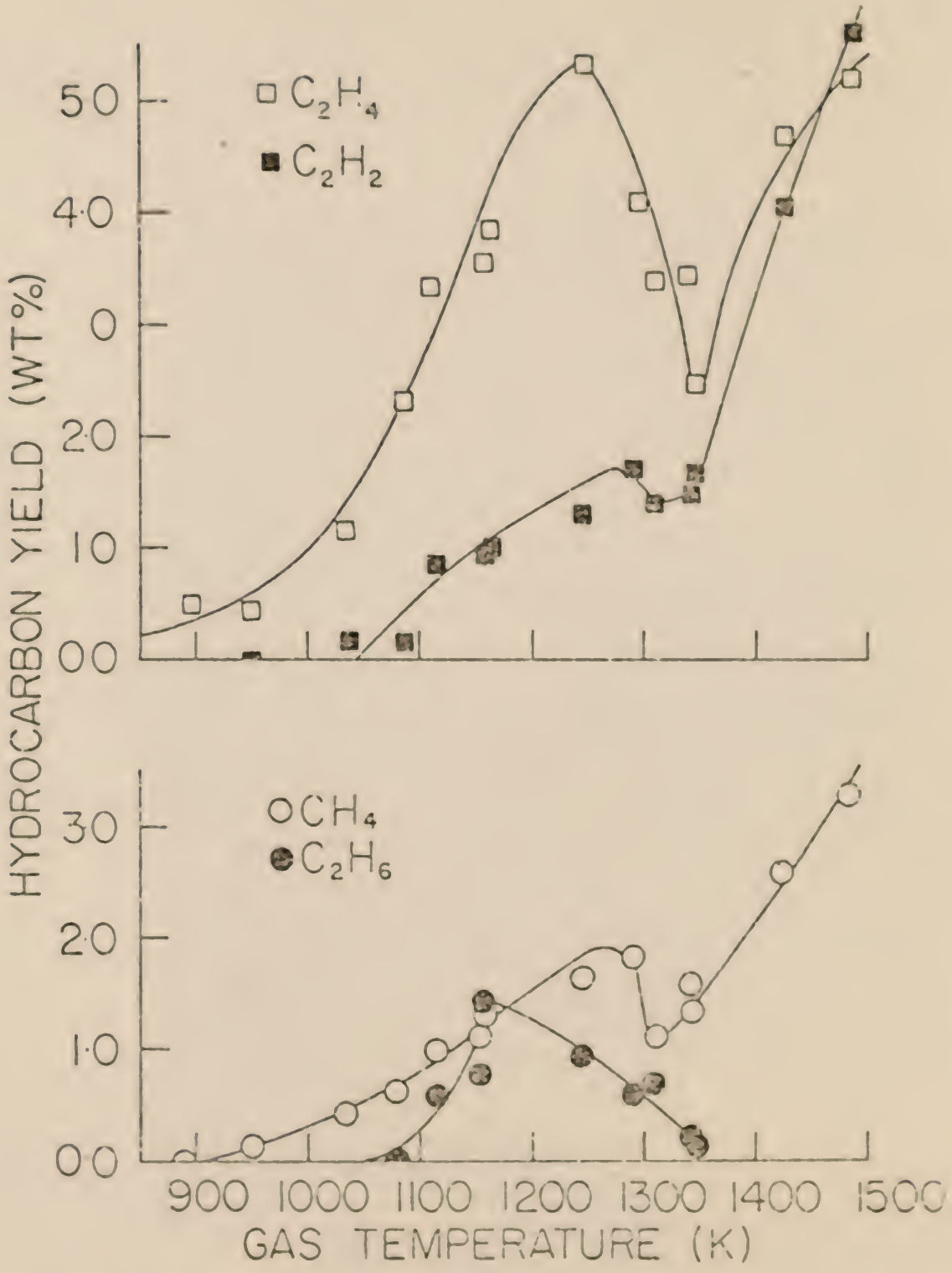

Fig. 13. Pyrolytic yields from the more abundant individual C_1 - C_4 hydrocarbons evolved from soybean dust plotted against temperature.

Table 17. Carbon oxide yields (g/g dust) from pyrolysis of corn and soybean dust.

Dust	Run	T_5 (K)	CO yield (g/g dust)	CO_2 yield (g/g dust)
Corn	W50	954	< 2.6	< 2.6
Corn	Y50	1002	< 2.6	< 2.6
Corn	W53	1063	9.2	< 2.6
Corn	Y51	1129	16.8	5.7
Corn	W51	1136	22.6	NA[2]
Corn	W52	1249	NA[1]	8.7
Corn	Y52	1362	31.2	14.8
Corn	Y53	1405	36.8	17.9
Soybean	Y62	888	< 2.6	< 2.6
Soybean	W64	949	< 2.6	< 2.6
Soybean	W67	1034	4.8	< 2.6
Soybean	W65	1081	NA[1]	6.2
Soybean	W61	1245	15.9	NA
Soybean	W62	1268	11.3	8.1
Soybean	Y61	1289	20.5	9.5
Soybean	Y65	1309	NA[1]	19.1
Soybean	W66	1341	NA[1]	12.3
Soybean	W63	1347	14.5	NA[2]
Soybean	Y66	1426	13.9	8.8
Soybean	Y64	1486	21.1	18.7

NA[1] - sample not analyzed.
NA[2] - invalid calibration factor.

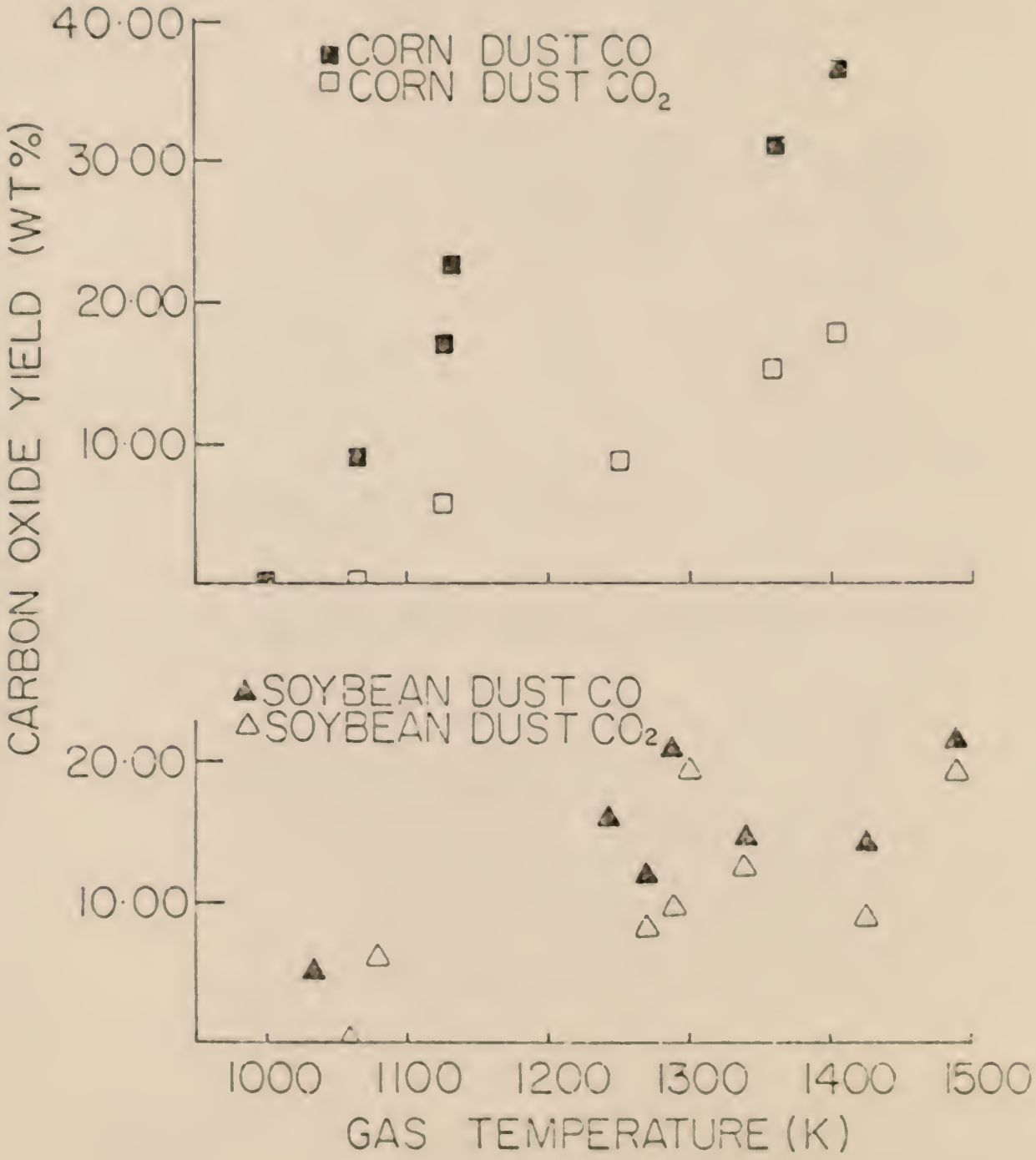

Fig. 24. Yield (g/g dust) of carbon oxides from pyrolysis of agricultural dusts as a function of temperature.

components in the unreacted portion of the sample. Mathematically, this is expressed as:

$$\frac{dV}{dt} = k\ (V^*-V) \qquad (17)$$

where k is the first order rate constant (sec^{-1}) in the unreacted volatile matter, V* is the initial quantity of sample, V is the quantity of the sample already volatilized, t is the reaction time, and the derivative dV/dt represents the instantaneous rate of volatile evolution. Integration of the differential equation and substitution of the initial conditions (v=0 @ t=0) and subsequent substitution of the assumed Arrhenius behavior of the rate constant yields

$$\ln(k) = \ln\left[\frac{-\ln(\frac{V^*-V}{V^*})}{t}\right] = \frac{-E_p}{R}\ (\frac{1}{T}) + \ln A \qquad (18)$$

in which, E_p is the energy of activation of pyrolysis and the parameters R, T and A are defined as in Eq. (15).

From each experimental run, the quantity V was specified as the total quantity in grams of hydrocarbons detected using chromatographic analysis, the time t as the period between the passage of the reflected shock and stabilization of the transmission trace as recorded on the oscillogram, and T_5 the gas temperature calculated in the usual manner. Estimation of the total volatile hydrocarbon content of the dusts, V*, was accomplished by calculating the hydrocarbon fraction of the released volatiles (hydrocarbons plus carbon oxides) from the chromatographic analyses and multiplying this fraction by the total

volatile content as specified by the proximate analysis performed on these dusts. The total quantity of C_1-C_4 hydrocarbons in the starch was assumed to be 70 $\pm$ 30 weight percent in lieu of any estimation of the purity of the starch or chromatographic detection of any species other than hydrocarbons. The high level of uncertainty of this assumption is taken to account in the error analysis presented in Appendix 1. A similar procedure was employed to estimate the maximum volatile content of CO and CO_2 from the corn and soybean dusts.

A least squares fit of the plot of ln (k) versus $10^4/T_5$ permits calculation of the activation energy of pyrolysis. Such plots are shown for the hydrocarbon pyrolysis data from the starch, corn dust, and soybean dusts in Figs. 25, 26, and 27, respectively. Similar plots of carbon oxide data for corn and soybean dusts are illustrated in Figs. 28 and 29. From the slopes of the best fit lines experimental activation energies of pyrolysis were obtained. The calculation of the pyrolysis activation energy of soybean dust was performed using only those points at which pyrolytic yields increased with increasing temperature. The raw data from which activation energies were obtained are given in Tables 18 and 19. The results are presented in Table 20. The experimental activation energy of the overall pyrolysis for cellulose as obtained by Lewellen[17], is also given in this table.

Table 18. Listing of hydrocarbon data used to calculate experimental activation energies of pyrolysis in agricultural dusts.

Run	Dust	T_5 (K)	$10^4/T_5$ (K^{-1})	V (g/g dust)	t (msec)	ln(k)
W50	Corn	954	10.48	0.0133	3.0	2.96
Y50	Corn	1002	9.98	0.0188	2.8	3.39
W53	Corn	1063	9.41	0.0509	2.3	4.66
Y51	Corn	1129	8.86	0.0860	2.1	5.37
W51	Corn	1136	8.80	0.0640	2.3	4.92
W52	Corn	1299	8.01	0.1120	1.8	5.88
Y53	Corn	1405	7.11	0.2008	1.5	7.15
Y35	Starch	1000	10.00	0.0098	2.3	1.81
Y34	Starch	1022	9.78	0.0115	2.3	1.97
W34	Starch	1067	9.37	0.0215	2.2	2.65
Y36	Starch	1091	9.17	0.0592	2.1	3.70
Y33	Starch	1161	8.61	0.0766	2.0	4.06
W35	Starch	1262	7.92	0.1210	1.9	4.60
W37	Starch	1323	7.56	0.1393	1.4	5.07
Y62	Soybean	883	11.26	0.0053	2.8	2.16
W64	Soybean	949	10.54	0.0116	2.7	3.00
W67	Soybean	1034	9.67	0.0197	2.7	3.55
W60	Soybean	1081	9.25	0.0439	2.6	4.45
Y63	Soybean	1115	8.97	0.0732	2.3	5.17
W65	Soybean	1154	8.66	0.0923	2.4	5.42
Y67	Soybean	1159	8.63	0.0890	2.3	5.42
W61	Soybean	1245	8.03	0.1123	2.2	5.78

Table 19. Listing of carbon oxide data used to calculate experimental activation energies of pyrolysis in agricultural dusts.

Run	Gas	Dust	T_5 (K)	$10^4/T_5$ (K^{-1})	v (g/g dust)	t (msec)	ln(k)
W53	CO	Corn	1063	9.41	0.092	2.3	4.65
Y51	CO	Corn	1129	8.86	0.168	2.1	5.46
W51	CO	Corn	1136	8.80	0.226	2.3	5.76
Y52	CO	Corn	1362	7.34	0.312	1.9	6.52
Y53	CO	Corn	1405	7.12	0.368	1.5	7.16
Y51	CO_2	Corn	1129	8.86	0.057	2.1	5.05
W52	CO_2	Corn	1249	8.01	0.087	1.8	5.73
Y52	CO_2	Corn	1362	7.34	0.148	1.9	6.80
Y53	CO_2	Corn	1405	7.12	0.179	1.5	7.24
W67	CO	Soybean	1034	9.67	0.048	2.7	4.20
W61	CO	Soybean	1245	8.03	0.159	2.2	5.89
W62	CO	Soybean	1268	7.89	0.113	1.4	5.87
Y61	CO	Soybean	1289	7.76	0.205	1.5	6.70
W65	CO_2	Soybean	1081	9.25	0.062	2.6	4.86
W62	CO_2	Soybean	1268	7.89	0.081	1.3	5.88
Y61	CO_2	Soybean	1289	7.76	0.095	1.4	6.01
W65	CO_2	Soybean	1309	7.64	0.191	1.5	7.24

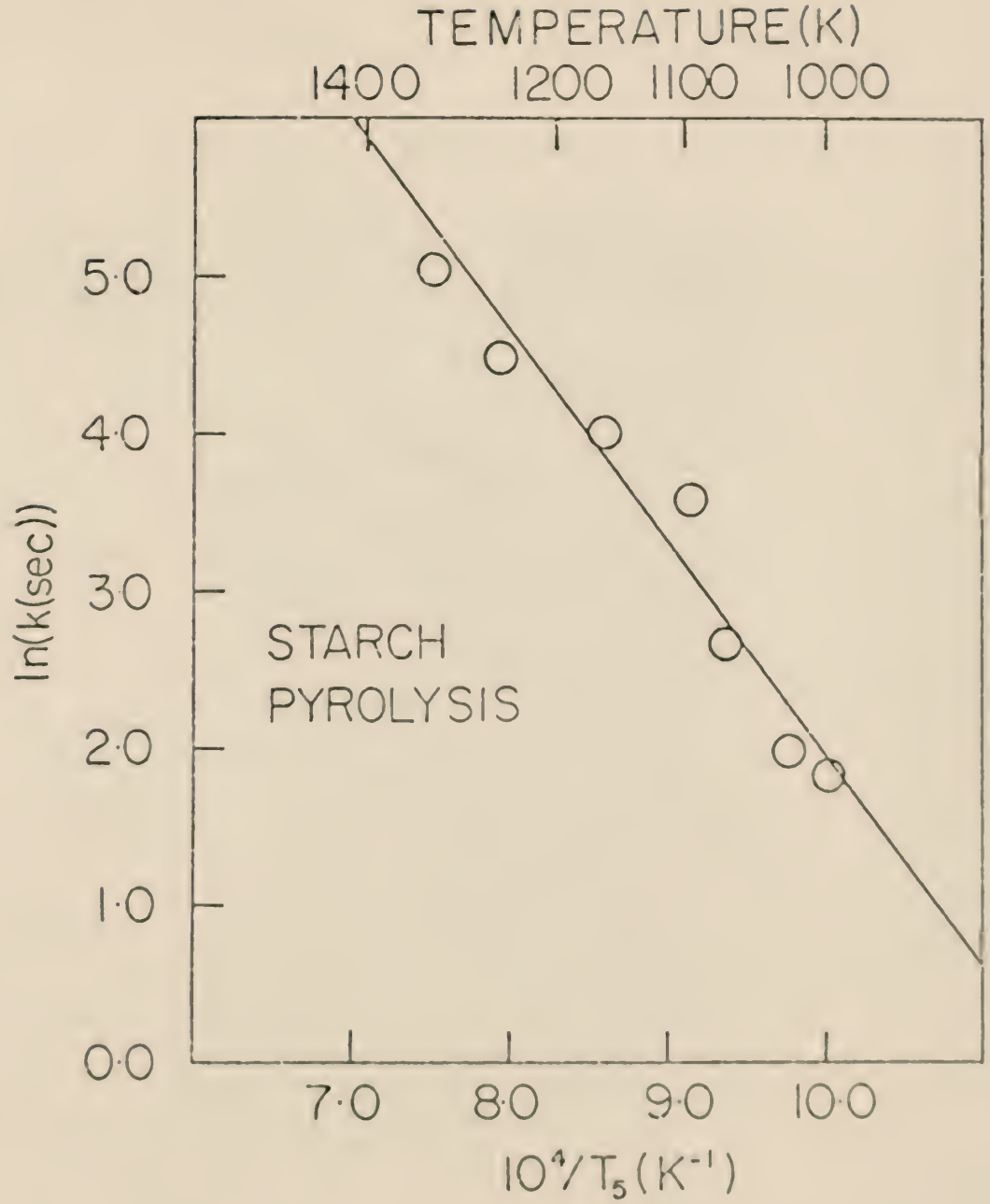

Fig. 25. Arrhenius graph of first order rate constant for hydrocarbon production from starch.

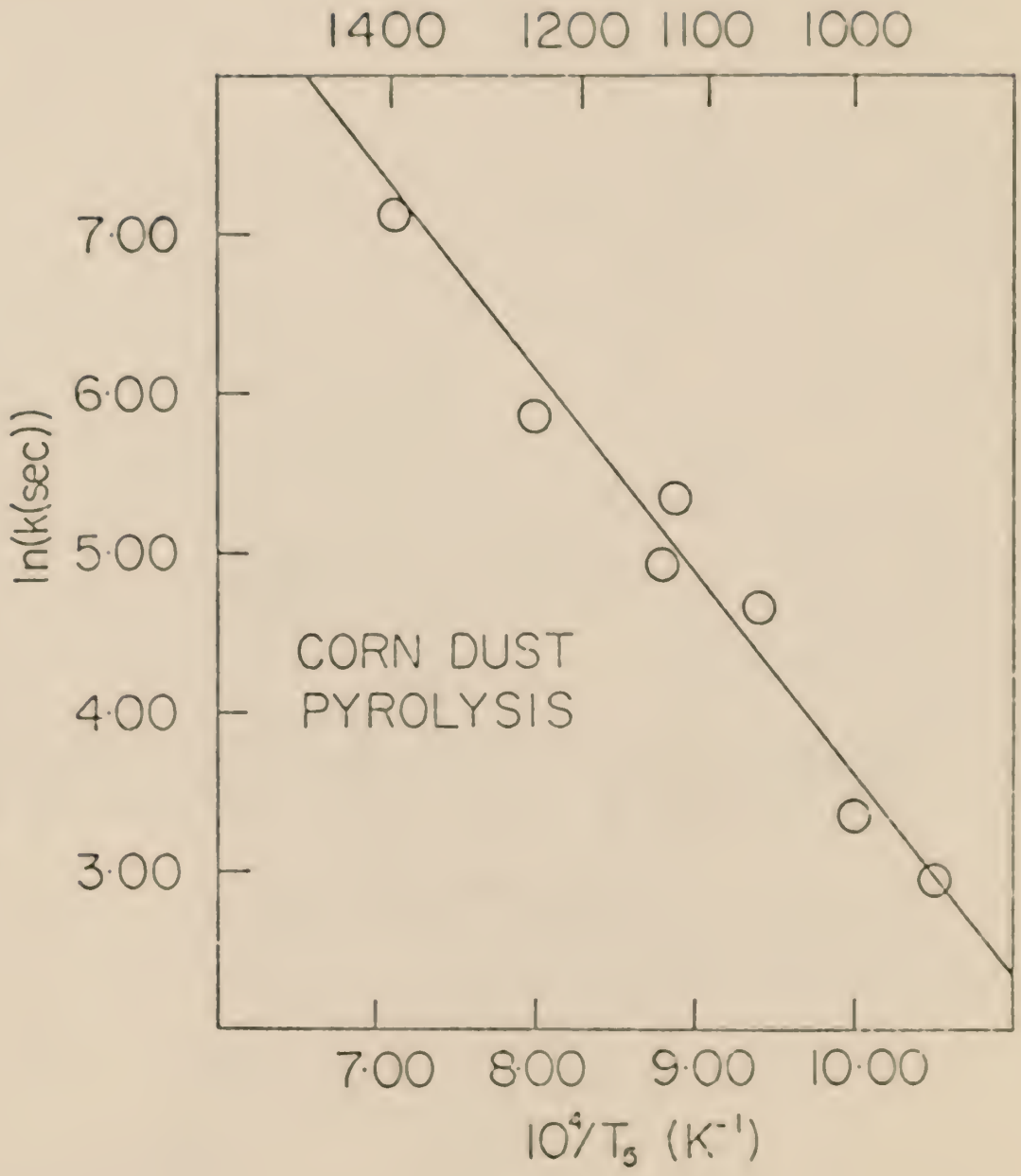

Fig. 26. Arrhenius graph of first order rate constant for hydrocarbon production from corn dust.

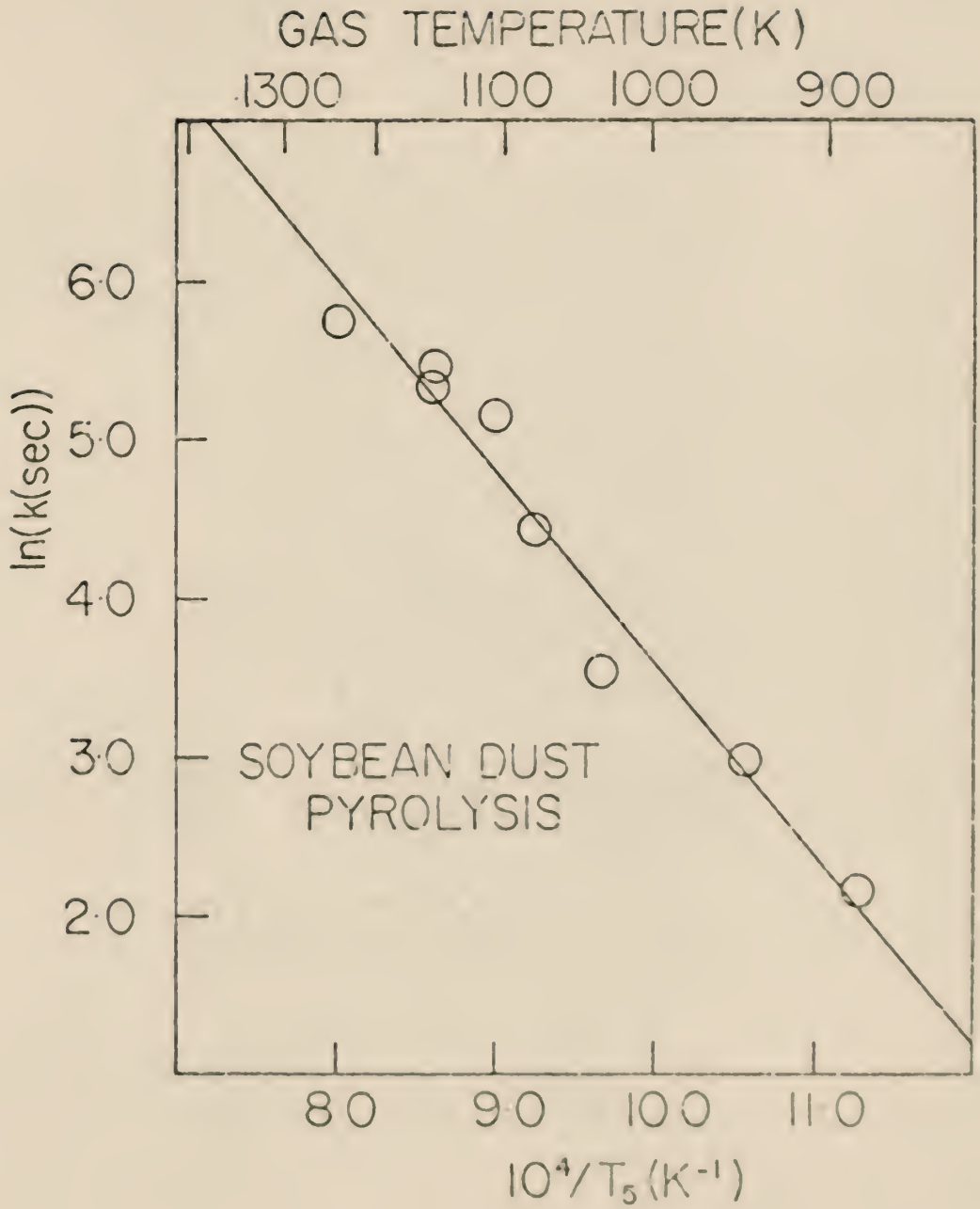

Fig. 27. Arrhenius graph of first order rate constant for hydrocarbon production from soybean dust.

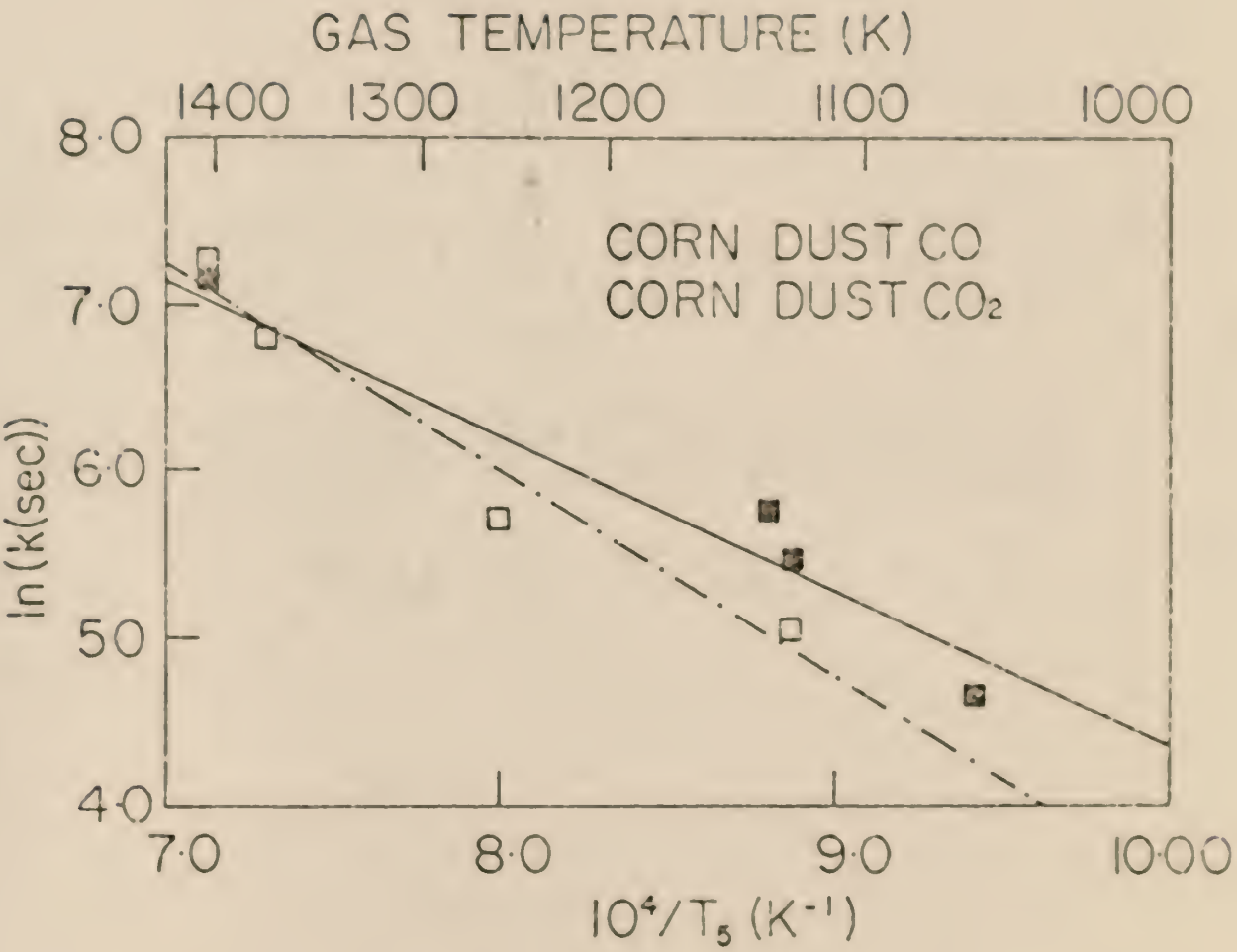

Fig. 28. Arrhenius graph of first order rate constant for carbon oxide production from corn dust.

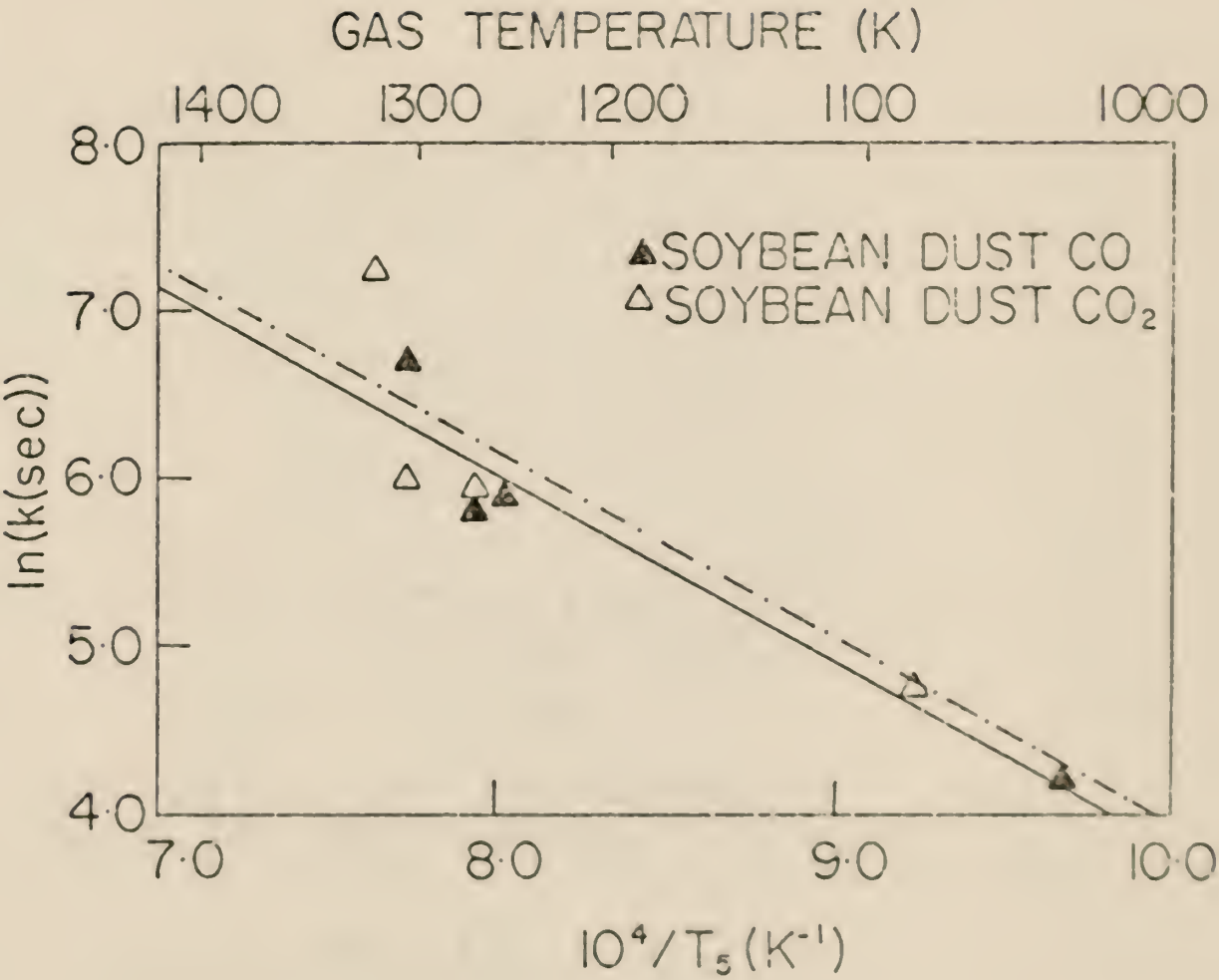

Fig. 29. Arrhenius graph of first order rate constant for carbon oxide production from soybean dust.

Table 20. Experimentally determined energies of activation of pyrolysis for agricultural dusts.

Dust	E_p (kJ/g-mol)			Investigator
	HC	CO	CO_2	
Starch	111.8 ± 10.6	-	-	Breipohl
Corn	102.4 ± 11.6	76.4 ± 9.4	104.1 ± 16.5	Breipohl
Soybean	100.9 ± 10.0	94.0 ± 13.1	91.5 ± 15.4	Breipohl
Cellulose		139.8†		Lewellen[17]

†Obtained from overall weight loss data.

3.4 Discussion of Results

The most prominent feacure of the devolatilization data is the unusual decrease in the amount of C_1-C_4 hydrocarbons produced from soybean dust with increasing temperature in the range from 1250 to 1350 K as shown in Fig. 20. A similar decrease in the yields of carbon monoxide and carbon dioxide is apparent in Fig. 24 over a temperature range of approximately 1300-1380 K. This behavior is obviously contrary to the assumed Arrhenius rate constant which predicts a continuous increase in the reaction rate with temperature until reactant depletion. This behavior cannot be dismissed as an artifact of the experimental system because of the number of points involved, the reproducibility of these runs, and the strictly increasing behavior exhibited by the corn dust yields over the same temperature interval for both C_1-C_4 hydrocarbon and carbon oxide yields. The effect is real, occurring in the production of carbon monoxide, carbon dioxide, as well as C_1-C_4 hydrocarbons, and will be discussed later in this section. However, this behavior is not germane to the mechanism of ignition because it occurs at temperatures considerably above those at which ignition occurs.

The other salient observation from Fig. 20 is the similarity in the temperature dependent yields of C_1-C_4 hydrocarbons from all three of the pyrolyzed samples at temperatures below 1250 K. This observation is quantitatively verified by the similarity of the experimentally determined activation energies for these species.

Additional similarity between the corn dust and the starch is evident from a comparison of the temperature dependant production of the more abundant hydrocarbon species (Fig. 21 and 22). Likewise, the same plot

of the production of CH_4, C_2H_2, C_2H_4, and C_2H_6 from soybean dust is very similar at temperatures below 1250 K.

The production of C_1-C_4 hydrocarbons from starch is an interesting process. If one examines the structure of starch (shown in Fig. 1-D and 1-E), it is obvious that a single oxygen atom must be removed from each carbon atom detected as a hydrocarbon species. This implies that since the pyrolysis of starch at 1323 K resulted in the formation of approximately 14 weight percentage of C_1-C_4 hydrocarbons, then approximately 16 weight percentage oxygen must have been removed from the carbon atoms forming the hydrocarbons. What happens to the oxygen liberated in this process? Gas chromatographic analysis reveals that less than 5.2 weight percentage of it was converted into either CO or CO_2 (less than 2.6 weight percentage of each). Based on the classical combustion reaction depicted by the combination of a hydrocarbon fuel with oxygen to produce H_2O and CO or CO_2 (depending upon the degree of completion), the chromatographically determined absence of CO and CO_2 would indicate that cow cockle starch did not undergo self-ignition during pyrolysis runs. Presumably a major portion of the released oxygen was converted into pyrolytically formed water. Additionally, it is conceivable that a portion of this oxygen was incorporated into oxygen containing compounds such as alcohols, ethers, aldehydes, and ketones which were not detectable using the chromatographic apparatus employed in this study.

This argument leads to the question of the origin of the carbon monoxide and carbon dioxide generated in copious quantities during the

pyrolysis of corn dust and, to a lesser extent, in soybean dust. Inasmuch as 35 weight percentage of the corn dust was pyrolytically converted into carbon monoxide and 18 weight percentage to carbon dioxide at a gas temperature of 1405 K, it is apparent the decomposition products of starch must play an integral role in the production of CO and CO_2 if the proximate analysis given in Table 1 is accurate. One possible explanation for the seemingly contradictory role which starch plays in the formation of CO and CO_2 stems from the effect which impurities have on the pyrolysis activation energies of cellulose. As previously explained (see discussion referenced to Roberts[19] and Tang[20]), the presence of trace impurities may catalyze alternate reaction pathways which lower the pyrolysis activation energy of cellulose. In an analogous manner, the cow cockle starch of presumably high purity, does not devolatilize through a pathway in which carbon oxides are produced. Conversely, the starch in corn dust may undergo an alternate reaction sequence leading to the production of CO and CO_2. These alternate pathways could result in an exothermic reaction sequence leading to self-ignition as well as the large quantities of CO and CO_2 observed in the pyrolysis runs.

It is interesting to note that dust explosions in commercial grain elevators were determined to occur during or immediately after handling corn dust in a recent report by the U.S. Department of Agriculture[58]. This is the same type of dust from which large quantities of CO and CO_2 were produced during pyrolysis. The elemental analysis of agricultural

dusts (see Table 7) reveals that oxygen comprises roughly 40 weight percentage of the total mass of the corn dust. It is likely that as a result of thermal decomposition, oxygenated free radicals will be formed. Recombination of these free radicals with hydrocarbon radicals either in the gas phase or on the surface of the remaining dust particles could lead to an exothermic reaction that would in turn increase the dust cloud temperature above the initial gas temperature. A behavior similar to this has been reported in the thermogravimetric analysis of wood waste by Braunstein[59]. Due to the large amount of oxygen present, a significant increase in temperature might accompany pyrolysis and could result in self-ignition. It is uncertain as to whether these oxidative reactions could induce self-ignition in an oxygen deficient environment; but it is conceivable that they would be exothermic enough to promote flame propagation even in atmospheres with depleted oxygen concentrations.

The fact that the temperature dependent production of C_1-C_4 hydrocarbons from pyrolyzed corn dust so closely follows the behavior exhibited by starch suggests that the mechanism leading to CO and CO_2 production may be different than the mechanism leading to hydrocarbon production. In the case of CO production, the experimentally determined activation energies of pyrolysis (76.4 kJ/g-mol for CO production and 102.4 kJ/g-mol for C_1-C_4 hydrocarbon production) tend to substantiate this supposition.

In both the ignition and pyrolysis studies (above 1250K) soybean dust exhibited strikingly different behavior than was observed for the other agricultural dusts. Based on the limited product analysis performed in this

study, the exact reason for the significantly higher activation energy of ignition of soybeans cannot be explained. However, the relatively higher activation energy of ignition of soybean dust is consistent with the activation energies of pyrolysis for the release of CO; indicating that CO might play a major role in the ignition process. The relative ignition activation energies are consistent with the trends observed for minimum ignition temperatures and minimum explosive concentrations of agricultural dusts. Specifically, not only soybeans exhibit the highest activation energy, but its minimum ignition temperature and minimum explosive concentration as determined by the Grain Marketing Research Center[60] were substantially greater than those obtained for corn, wheat, or milo dusts.

Obviously, in the temperature interval where decreased pyrolytic yields are observed from soybeans, the precursors of hydrocarbons and carbon oxides must participate in a different reaction sequence than at lower temperatures. From the mechanistic point of view, a large quantity of descriptive data was obtained from the pyrolysis runs. The question in attempting to analyze this data is; what chemical or physical characteristics of the soybean dust could produce the observed behavior. Based on the individual species profiles, a strictly physical mechanism, for instance, plasticity of particles, can probably be ruled out.

The difficulty of the chemical analysis arises from the diversity and complexity of the components present in agricultural dusts. For

example, if it is assumed that fat, cellulose, and starch components in soybean dust and their decomposition products do not cause the decreasing yields with increasing temperature over the range in question, then only the protein and ash fractions remain as possible contributors. The only thing known about the ash fraction is it is not combustible; however, it may contain compounds which catalyze a yet unknown reaction sequence. The role of impurities as catalysts is witnessed in the behavior of the higher ignition activation energies of pure starch as compared with the ignition activation energies of corn dust which contains starch in a contaminated form. Consideration of the protein portion begins with investigating the bonds in the linear protein chain and proceeds to an examination of the remainder of the amino acids attached to the linear chain (denoted by R groups in Fig. 1). This becomes very complicated, since the organic R groups in amino acids can be characterized on the basis of acidity, aromaticity, degree of unsaturation, and nitrogen content to name a few. Therefore, some recommendations are presented in the next chapter which should help to expose the reason for the observed behavior in soybean dust.

Throughout this chapter there has been a signel unifying concept; namely that ignition proceeds via a homogeneous mechanism. The experimental evidence supporting this statement is delineated below. First, the laser transmission behavior during pyrolysis is consistent with a significant portion of the agricultural dust being converted to the gas phase during pyrolysis. Second, the S.E.M. photographs provided

supportive evidence as to the occurrence of substantial devolatilization. Third, the laser transmission behavior in the low temperature runs in air indicated that agricultural dusts devolatilize prior to ignition, and finally, chromatographic analysis of the stable gas phase devolatilization products revealed significant quantities of combustible C_1-C_4 hydrocarbons in the temperature range studied. A definitive statement of whether ignition proceeds via a homogeneous or heterogeneous mechanism is often difficult as evidenced by the controversy in the literature concerning the mechanism with regard to coal. However, the above experimental finding provide strong evidence that ignition occurs in agricultural dusts via a homogeneous mechanism even at heating rates in excess of 10^6 K/sec and for particle sizes of less than 10μm diameter.

4.0 Conclusions and Recommendations For Further Study

Ignition and devolatilization studies employing a single pulse shock tube and its associated diagnostics revealed that corn, wheat, milo, and soybean dusts probably ignite in the gas phase after devolalitilization via a homogeneous mechanism. Additionally, a new gas sampling technique was developed and its validity confirmed. The results of chromatographic analysis indicated that the evolution of carbon monoxide may play an important role in the ignition process. Furthermore, the role that starch plays in the devolatilization process is a complicated one as evidenced by the lack of agreement of carbon oxide yields from starch and corn dusts. The activation energies of ignition and pyrolysis were experimentally determined. Soybean dust displayed an ignition activation energy nearly double that of the other grain dusts investigated. Furthermore the soybean dust also exhibited an unexplained decrease in devolatilization yields with increasing temperatures over a narrow temperature interval. Such behavior is probably caused by a combination of transport and chemical mechanisms. It is believed that a more comprehensive identification of the released volatiles would provide an explanation consistent with the pyrolytic behavior observed for soybean dust in this study.

Three methods are proposed to explore more adequately the devolatilization process in soybean dust and agricultural dusts in general. First, mass spectrometry coupled with gas chromatography and wet chemical analyses should be employed to more completely characterize the stable

gas phase products of pyrolysis. Second, the use of techniques, recently developed in this laboratory[51] by which the solid products remaining after a devolitilization run can be characterized, could further illuminate the devolatilization process occurring in agricultural dusts. Finally, an examination of the temporal behavior of the pyrolytic process, both physically by S.E.M. analysis and chemically by mass spectrometry and gas chromatography is necessary.

The following procedure is recommended to determine if agricultural dusts heated in an inert atmosphere can undergo self-ignition. Instead of monitoring one wavelength of continuum emission, the emission from the incandescent dust particles should be monitored at three wavelengths. From these measurements, the temperature of the heated dust suspension can be determined accurately as a function of time and a more definitive statement to the likelihood of ignition can be obtained.

With respect to the practical problem of grain dust explosions in commercial grain handling facilities, it is recommended that the effect of biologically safe gas phase inhibitors upon both ignition and flame propagation in grain dust suspensions be thoroughly investigated.

1. Chiotti, P., International Symposium on Grain Dust Explosions, p. 13, Grain Elevator and Processing Society, Minneapolis, Minn. (1977).

2. Aldis, D. F. and Lai, F. S., Review of Literature Related to Technical Aspects of Grain Dust Explosions, United States Department of Agriculture, Miscellaneous Publication 1375 (1978).

3. Martin, C. R., Characterization of Grain Dust Properties, Paper No. 78-3020, American Society of Agricultural Engineers (1978).

4. American Association of Cereal Chemists, Approved Methods of the AACC, 12th edition, The Association, St. Paul, Minn. (1975).

5. Association of Official Analytical Chemists, Official Methods of Analysis, 12th edition, The Association, Washington, DC (1975).

6. Conn, E. and Stumpf, P., Outlines of Biochemistry, Wiley and Sons, New York, NY (1976).

7. Seeker, W. R., "The Kinetics of Ignition and Particle Burnout of Coal Dust Suspensions Under Rapid Heating Conditions," Ph.D. Thesis, Kansas State University, 1979.

8. Lowenstein, H. I. and vonRosenberg, C.W., Jr., Proceedings of the Eleventh International Symposium on Shock Tubes and Waves. p. 366, University of Washington Press, Seattle, Wash. (1977).

9. Woodburn, E., Everson, R., and Kirk, A., Fuel 53, 38 (1974).

10. Lightman, P., and Street, D., Fuel 47, 7 (1968).

11. American Society of Testing Materials, Designation ASTM-D-388-64T.

12. Anthony, D., and Howard, J., AIChE Journal, 22, 625 (1976).

13. Suuberg, E., Peters, W., and Howard, J., Seventeenth Symposium (International) on Combustion, The Combustion Institute, Pittsburgh, Pa., in press (1979).

14. Min, K., Combustion and Flame, 30, 285 (1977).

15. Martin, S., Tenth Symposium (International) on Combustion, p. 877, The Combustion Institute, Pittsburgh, Pa. (1965).

16. Shafizadeh, F., Advances in Carbohydrate Chemistry, Academic Press, London, p. 419 (1968).

17. Lewellen, P. C., Peters, W. A., and Howard, J. B., Sixteenth Symposium (International) Symposium on Combustion, p. 1471, The Combustion Institute, Pittsburgh, Pa. (1976).

18. Franklin, W. E., Analytical Chemistry, 51, 992 (1979).

19. Roberts, A. F., Combustion and Flame, 14, 261 (1970).

20. Tang, W. K., Journal of Polymer Science, Part C, No. 6, 65 (1964).

21. Lakshmanan, C., Galon, B., and Hoelscher, H., Stärke, 22, 221 (1970).

22. Wolff, I., Olds, D., and Hilbert, G., Die Stärke, 20, 150 (1968).

23. Puddington, I.E., "The Thermal Decomposition of Carbohydrates," Division of Chemistry, Canadian National Research Laboratories, Issued as NRC No. 1736 (1948).

24. Bryce, D. and Greenwood, C., Die Stärke, 15, 166 (1973).

25. Chiotti, P. and Morris, V., Cereal Foods World, 32, 314 (1977).

26. Glassman, I., Combustion, Academic Press, New York (1977).

27. Palmer, K., Dust Explosions and Fire, Chapman and Hall, London (1970).

28. Eckhoff, R., "A Study of Selected Problems Related to the Assessment of Ignitability and Explosibility of Dust Clouds," A.S. John Greigs, Boktrykkeri (1976).

29. Enomoto, H., International Symposium on Grain Dust Explosions, Grain Elevator and Processing Society, Minneapolis, Minn. (1977).

30. Jacobson, M., Nagy, J., Ball, F., "Explosibility of Agricultural Dusts," U.S. Bureau of Mines Report of Investigations 5753 (1961).

31. Mulcahy, M. F., and Smith, I. W., Rev. Pure and Appl. Chem., 19, 81 (1969).

32. Essenhigh, R., International Symposium on Grain Dust Explosions, p. 276, Grain Elevator and Processing Society, Minneapolis (1977).

33. DeGrey, A., Rev. Metall. 19, 645 (1922).

34. Anson, D., Moles, F., and Street, P., Combustion and Flame, 16, 265 (1978).

35. Nettleton, M. and Sterling, R., Combustion and Flame, 22, 407, (1974).

36. Thomas, G. R., Harris, J. J., and Evans, D. G., Combustion and Flame, 12, 391 (1968).

37. Annalamalai, K., and Durbetaki, P., Combustion and Flame, 29, 193 (1977).

38. Anthony, D. B., Palmer, J. B., Hottel, H. C., and Meissner, H. D., Fifteenth Symposium (International) on Combustion, p. 1303, The Combustion Institute, Pittsburgh, Pa. (1975).

39. Bandyopadhyay, S., and Bhaduri, D., Combustion and Flame, 18, 411 (1972).

40. Welker, J. R., Fire and Flammability, 1, 12 (1970).

41. Weatherford, W. D., and Sheppard, D. M., Tenth Symposium (International) on Combustion, p. 897, The Combustion Institute, Pittsburgh, Pa. (1965).

42. Kuwata, M., Stumbar, J., and Essenhigh, R., Twelfth Symposium (International) on Combustion, p. 663, The Combustion Institute, Pittsburgh, Pa (1969).

43. Nagy, J., and Surincik, D., Bureau of Mines, Department of Agriculture, Report of Investigations 6811 (1966).

44. Seeker, W. R., "The Design, Assembly and Testing of a Shock Tube for the Study of Coal Combustion Kinetics," M.S. Thesis Kansas State University, 1977.

45. Zucrow, M. J. and Hoffman, J. D., Gas Dynamics, Wiley, New York, NY (1976).

46. Gaydon, A. G. and Hurle, I. R., The Shock Tube in High-Temperature Chemical Physics, Reinhold, NY (1963).

47. Martin, C., Private communication (1979).

48. Particle Data Laboratories, Ltd., Elmhurst, Ill. (1978).

49. Chang, C. S., Lai, F. S., and Miller, B. S., Joint Meeting of American Society of Agricultural Engineers and Canadian Society of Agricultural Engineering, Paper No. 79-3012, Societies, Winnipeg, Canada (1979).

50. Vaughn, S., Private communication (1979).

51. Lester, T. W., Merklin, J. F., and Szydlowski, S., "Single Pulse Shock Tube Investigation of the Kinetics and Mechanism of Hydroliquefaction," Quarterly Report, January 1 - March 31 to AMOCO Oil Co. (1979).

52. Wegener, D. C., "The Production of Lower Molecular Weight Hydrocarbons During The Thermal Decomposition of Pulverized Coal in Air and Nitrogen," M.S. Thesis, Kansas State University, 1978.

53. McNair, H. M. and Bonelli, E. J., Basic Gas Chromatography, Varian Aerograph, Palo Alto, CA (1968).

54. Breipohl, G., Lester, T. W., and Merklin, J. F., "Chemical Shock Tube Studies of Mechanisms of Grain Dust Explosions," Grain Dust Report 5 to United States Department of Agriculture, U. S. Grain Marketing Research Laboratory, (1979).

55. Fox, T. W., TeVelde, J. A., and Nicholls, J. A., Proceedings of the 1976 Heat Transfer and Fluid Mechanics Institute, Stanford University Press, (1976).

56. Aldis, D. F., Lai, F. S., Lee, R. S., and Fan, L. T., 1979 Summer Meeting of American Society Agriculture Engineers and Canadian Society of Agricultural Engineers, Paper No. 79-3091, The Societies, (1979).

57. Howell, J., Private Communication (1979).

58. Kiewet, F., "Corn Dust is Main Suspect in Grain Elevator Blasts," Kansas City Star, p. 5J, August 5, 1979.

59. Braunstein, H., Oak Ridge National Laboratory, Private Communication (1979).

60. Lai, F. S., Private Communication (1979).

61. Kennedy, I. B. and Neville, A. M., Basic Statistics Methods for Engineers and Scientists, IEP A Dun-Donnelley, New York, NY (1976).

Acknowledgements

The author wishes to express his appreciation to the U.S. Grain Marketing Research Laboratory, Department of Agriculture for the grant which provided personal financial income in addition to the funds necessary to conduct this research.

A most sincere expression of gratitude is extended to Dr. T. W. Lester for his guidance, encouragement, assistance, understanding, and friendship. The knowledge imparted by Dr. J. F. Merklin under the broad classification of chemistry was indispensible and greatly appreciated. The value of having Mr. Bill Starr available to speed-up the trouble-shooting process of malfunctioning equipment cannot be overstated. Special notes of thanks are warranted to Mr. Galen King, who provided seemingly undeserved assistance during chromatographic analysis, and to Ms. Shelly Kemnitz who typed this manuscript, and to Ms. Terry Gleue, who drafted the figures. The typing assistance provided by Merna "Mom" Brisbin was definitely above and beyond the call of duty and was most sincerely appreciated.

The friendship provided by Ms. Deb Foster and Mr. Chris Southwick demands recognition.

Finally, a very special note of thanks is due to Mr. Steve Vaughn, a most deserving Ph.D. candidate. Steve taught me how to operate the shock tube, provided me with invaluable assistance throughout the course of this research, and most (?) importantly, provided me with a partner with whom I could attempt to win my final intramural championship.

APPENDIX A

Experimental Procedure

Appendix A

Experimental Procedure

The procedure employed to obtain gas samples for post-shock analysis is summarized in the following checklist.

____ 1) Remove test section end wall and dispersion plate. Also pull the pressure transducer back 0.5 cm from the observation prot.

____ 2) Separate the test section from the driver section and blow compressed air through test section.

____ 3) Insert 10 mil mylar diaphragm into position.

____ 4) Clean the inside of the test section up to the ball valve using acetone and paper towels.

____ 5) Remove and clean 15 micron filter with acetone.

____ 6) Replace all parts.

____ 7) Open valves to vacuum pumps and evacuate both sections of the tube.

____ 8) When test section is evacuated to less than 10^{-3} torr, close valves to both vacuum pumps.

____ 9) Fill test section to 40 torr with air.

____ 10) Close the valve to the sub-atmospheric gauge of the test section.

____ 11) Fill the driver section to 200 psia helium.

____ 12) Burst the diaphragm (this shock is used to clean the tube) and vent the tube.

____ 13) Remove ruptured diaphragm and insert the appropriate mylar diaphragm into position.

____ 14) Remove grain dust from desiccator, place 20 mg of sample on dispersion plate, and return dust to desiccator.

____ 15) Place sample containing dispersion plate in shock tube.

____ 16) Repeat step 7.

____ 17) Align the laser beam and position oscilloscope traces (pressure, emission, and transmission) on screen.

____ 18) Repeat step 8.

____ 19) Fill the test section to the appropriate pressure with the desired test gas.

____ 20) Repeat step 10.

____ 21) Fill the driver section to the appropriate pressure with helium.

____ 22) Turn off overhead lights, recheck oscilloscope traces, and return function switch to single sweep mode.

____ 23) Reset time interval counter and oscilloscope trigger.

____ 24) Open camera shutter.

____ 25) Rupture diaphragm.

____ 26) Close test section ball valve.

____ 27) Close camera shutter.

____ 28) Turn on lights and record the time of diaphragm rupture, time indicated by time interval counter, and gauge pressure after the shock.

____ 29) Connect a sample bottle to sample system and open the valve to vacuum pump and evacuate.

____ 30) One hour after rupturing diaphragm close valve to vacuum pump, open the valve to the gas sampling system, and fill the gas bottle to a positive pressure.

____ 31) When a positive pressure is attained, close the valve on sample bottle, open the ball valve, and vent the tube through the hood.

The procedure employed to obtain ignition delay data is somewhat simplier in that checklist steps 3, 7 through 12, 26, and 29 through 31 can be omitted.

APPENDIX B

Raw data of particle size analysis by
Particle Data Laboratory.

Particle Size Analysis by Particle Data Labs. - Elzone Method
115 Hahn Street, Elmhurst, IL 60126
Telephone: 312/832-5658

For: USDA
On Sample: Colo. Corn
Date: 12 Feb 78

Tabulation

Data ID 5672 Date 12 Feb
Size-Normalized Area Distribution
Total = 347231

Chnl	Size	Area	Chnl	Size	Area	Chnl	Size	Area
1	.72	8	40	2.79	756	79	10.79	6051
2	.75	21	41	2.89	777	80	11.17	6859
3	.77	26	42	2.99	806	81	11.56	7753
4	.80	426	43	3.10	835	82	11.97	8596
5	.83	871	44	3.21	833	83	12.39	9520
6	.86	1198	45	3.32	805	84	12.83	10532
7	.89	1334	46	3.44	756	85	13.28	11288
8	.92	1308	47	3.56	722	86	13.75	12098
9	.95	1193	48	3.68	692	87	14.23	12764
10	.99	1057	49	3.81	713	88	14.74	13246
11	1.02	944	50	3.95	748	89	15.26	13266
12	1.06	861	51	4.09	785	90	15.79	13220
13	1.10	801	52	4.23	824	91	16/35	12832
14	1.13	760	53	4.38	864	92	16.93	12321
15	1.17	730	54	4.54	905	93	17.52	11977
16	1.22	715	55	4.70	1080	94	18.14	11190
17	1.26	708	56	4.86	1181	95	18.78	10130
18	1.30	706	57	5.03	1241	96	19.44	9452
19	1.35	709	58	5.21	1303	97	20.13	8509
20	1.40	713	59	5.39	1338	98	20.84	7383
21	1.45	714	60	5.58	1372	99	21.57	6516
22	1.50	714	61	5.78	1370	100	22.34	5488
23	1.55	715	62	5.98	1397	101	23.12	4812
24	1.60	720	63	6.20	1459	102	23.94	4011
25	1.66	730	64	6.41	1522	103	24.78	3685
26	1.72	750	65	6.64	1587	104	25.66	2633
27	1.78	769	66	6.87	1701	105	26.56	2117
28	1.84	774	67	7.12	1823	106	27.50	1512
29	1.91	760	68	7.37	1954	107	28.47	1621
30	1.97	741	69	7.63	2095	108	29.47	1737
31	2.04	731	70	7.90	2307	109	30.51	931
32	2.12	734	71	8.18	2540	110	31.59	998
33	2.19	749	72	8.46	2865	111	32.70	1069
34	2.27	771	73	8.76	3148	112	33.85	1146
35	2.35	799	74	9.07	3456	113	35.05	1228
36	2.43	815	75	9.39	3792	114	36.28	1317

Chnl	Size	Area	Chnl	Size	Area	Chnl	Size	Area
37	2.52	810	76	9.72	4159	115	37.56	1411
38	2.60	780	77	10.06	4660			
39	2.70	756	78	10.42	5320			

Particle Size Analysis by Particle Data Labs. - Elzone Method
115 Hahn Street, Elmhurst, IL 60126
Telephone: 312/832-5658

For: USDA
On Sample: 784 05 Milo Dust
Date: 29 Nov 78

Tabulation

Data ID 5626 Date 29 Nov
Size-Normalized Count Distribution
Total = 301999

Chnl	Size	Count	Chnl	Size	Count	Chnl	Size	Count
			36	5.58	5873	70	18.14	1177
			37	5.78	5760	71	18.78	1029
4	1.84	3224	38	5.98	5577	72	19.44	878
5	1.91	3945	39	6.20	5369	73	20.13	733
6	1.97	4676	40	6.41	5193	74	20.84	603
7	2.04	4960	41	6.64	5058	75	21.57	491
8	2.12	5171	42	6.87	4942	76	22.34	393
9	2.19	5256	43	7.12	4811	77	23.12	304
10	2.27	5236	44	7.37	4641	78	23.94	229
11	2.35	5233	45	7.63	4435	79	24.78	170
12	2.43	5346	46	7.90	4226	80	25.66	125
13	2.52	5537	47	8.18	4018	81	26.56	90
14	2.60	5725	48	8.46	3810	82	27.50	65
15	2.70	5884	49	8.76	3588	83	28.47	46
16	2.79	6003	50	9.07	3376	84	29.47	33
17	2.89	6051	51	9.39	3203	85	30.51	24
18	2.99	6029	52	9.72	3060	86	31.59	18
19	3.10	6050	53	10.06	2931	87	32.70	14
20	3.21	6181	54	10.42	2851	88	33.85	12
21	3.32	6326	55	10.79	2762	89	35.05	11
22	6346	6346	56	11.17	2677	90	36.28	10
23	3.56	6252	57	11.56	2595	91	37.56	10
24	3.68	6182	58	11.97	2496	92	38.89	10
25	3.81	6194	59	12.39	2375	93	40.26	8
26	3.95	6248	60	12.83	2245	94	41.68	6
27	4.09	6255	61	13.28	2130	95	43.15	4
28	4.23	6153	62	13.75	2045	96	44.67	3
29	4.38	5975	63	14.23	1974	97	46.25	3
30	4.54	5831	64	14.74	1886	98	47.88	3
31	4.70	5797	65	15.26	1765	99	49.57	3
32	4.86	5853	66	15.79	1623	100	51.31	3
33	5.03	5924	67	16.35	1499	101	53.12	1
34	5.21	5937	68	16.93	1405			
35	5.39	5918	69	17.52	1306			

Particle Size Analysis by Particle Data Labs. - Elzone Method
115 Hahn Street, Elmhurst, IL 60126
Telephone: 312/832-5658

For: USDA
On Sample: Colo Beans
Date: 12 Feb 78

Tabulation

Data ID 5684 Date No Date
Size-Normalized Area Distribution
Total = 996012

Chnl	Size	Area	Chnl	Size	Area	Chnl	Size	Area
2	.74	30773	41	5.11	9354	80	35.22	2536
3	.78	30162	42	5.37	9313	81	37.01	2306
4	.82	29525	43	5.64	9223	82	38.89	2182
5	.86	28574	44	5.93	9090	83	40.86	2008
6	.90	27689	45	6.23	8917	84	42.94	1995
7	.95	26802	46	6.54	8708	85	45.12	1958
8	1.00	26213	47	6.87	8484	86	47.41	1816
9	1.05	24879	48	7.22	8269	87	49.81	1803
10	1.10	24274	49	7.59	8084	88	52.34	1793
11	1.16	23544	50	7.98	7947	89	55.00	1802
12	1.22	22855	51	8.38	7844	90	57.79	1874
13	1.28	22267	52	8.81	7784	91	60.72	1988
14	1.34	21556	53	9.25	7709	92	63.80	2113
15	1.41	20644	54	9.72	7626	93	67.04	2214
16	1.48	19873	55	10.22	7503	94	70.44	2328
17	1.56	19113	56	10.73	7370	95	74.02	2459
18	1.64	18273	57	11.28	7235	96	77.78	2622
19	1.72	17447	58	11.85	7093	97	81.72	2784
20	1.81	16676	59	12.45	6973	98	85.87	2956
21	1.90	15974	60	13.08	6855	99	90.23	3149
22	1.99	15324	61	13.75	6728	100	94.81	3370
23	2.10	14689	62	14.45	6550	101	99.62	3544
24	2.20	14061	63	15.18	6318	102	104.68	3639
25	2.31	13400	64	15.95	6089	103	109.99	3654
26	2.43	12698	65	16.76	5809	104	115.58	3599
27	2.55	11936	66	17.61	5519	105	121.44	3433
28	2.68	11137	67	18.50	5270	106	127.61	3136
29	2.82	10353	68	19.44	5000	107	134.08	2705
30	2.96	9647	69	20.43	4768	108	140.89	2132
31	3.11	9070	70	21.47	4544	109	148.04	1515
32	3.27	8666	71	22.56	4344	110	155.55	974
33	3.44	8469	72	23.70	4121	111	163.45	570
34	3.61	8451	73	24.91	3878	112	171.74	302
35	3.80	8560	74	26.17	3705	113	180.46	142
36	3.99	8745	75	27.50	3455	114	189.62	57
37	4.19	8946	76	28.89	3313	115	199.25	17

Chnl	Size	Area	Chnl	Size	Area	Chnl	Size	Area
38	4.40	9132	77	30.36	3103	116	209.36	2
39	4.63	9264	78	31.90	2937			
40	4.86	9339	79	33.52	2702			

Particle Size Analysis by Particle Data Labs. - Elzone Method
115 Hahn Street, Elmhurst, IL 60126
Telephone: 312/832-5658

For: USDA
On Sample: 784 02 Extrap. Below 1.66, Microns, Wheat Dust
Date: 29 Nov 78

Tabulation

Data ID 5626 Date 29 Nov
Size-Normalized Count Distribution
Total = 2599469

Chnl	Size	Count	Chnl	Size	Count	Chnl	Size	Count
1	.77	16189	34	3.52	53205	67	16.16	980
2	.80	19012	35	3.68	48299	68	16.93	871
3	.84	22152	36	3.86	43726	69	17.73	766
4	.88	25609	37	4.04	39574	70	18.57	674
5	.92	29378	38	4.23	35742	71	19.44	599
6	.96	33438	39	4.43	31386	72	20.36	531
7	1.01	37765	40	4.64	26818	73	21.33	459
8	1.06	42322	41	4.86	23070	74	22.34	375
9	1.11	47060	42	5.09	20720	75	23.39	296
10	1.16	51922	43	5.33	18641	76	24.50	237
11	1.22	56843	44	5.58	16293	77	25.66	188
12	1.27	61748	45	5.85	14177	78	26.87	146
13	1.33	66555	46	6.12	12505	79	28.14	111
14	1.40	71181	47	6.41	10801	80	29.47	82
15	1.46	75537	48	6.72	9102	81	30.87	64
16	1.53	79539	49	7.04	7884	82	32.33	56
17	1.60	83106	50	7.37	7064	83	33.85	49
18	1.68	86159	51	7.72	6294	84	35.46	38
19	1.76	88636	52	8.08	5549	85	37.13	28
20	1.84	90482	53	8.46	4977	86	38.89	21
21	1.93	91661	54	8.86	4452	87	40.73	17
22	2.02	92061	55	9.28	3751	88	42.65	15
23	2.12	91796	56	9.72	3026	89	44.67	12
24	2.22	90922	57	10.18	2570	90	46.78	10
25	2.32	89161	58	10.66	2267	91	49.00	6
26	2.43	86852	59	11.17	1931	92	51.51	4
27	2.55	83947	60	11.70	1683	93	53.74	4
28	2.67	80509	61	12.25	1549	94	56.28	4
29	2.79	76613	62	12.83	1462	95	58.94	4
30	2.92	72341	63	13.44	1390	96	61.73	3
31	3.06	67777	64	14.07	1301	97	64.65	2
32	3.21	63010	65	14.74	1203	98	67.71	1
33	3.36	58125	66	15.43	1094	99	70.91	1

APPENDIX C

Error Analysis

Appendix C

Error Analysis

Because of the many uncertainties associated with research on a system in which heat and mass transfer and chemical kinetics are concurrently involved, a concise error statement is seldom made. Although the shock tube minimizes some of these errors, it also introduces others. The error analysis contained herein is aimed at finding the approximate range of the error associated with the activation energies and to identify the major sources of error in the calculation of the activation energies at ignition and pyrolysis. The method of propagating error utilized in this analysis is discussed in detail by Kennedy and Nevelle.[61]

The expression for the activation energy of ignition was given in Eq. (16) as

$$\ln(1/\tau) = \frac{-E_I}{R}\left(\frac{1}{T}\right) + \ln A'. \qquad (C1)$$

The independent variables in this equation are τ, the ignition delay, and T the temperature. Solving this expression for E_I and taking the partial derivatives with respect to each of these variables yields,

$$\frac{\partial E_I}{\partial T} = R\,[\ln A' - \ln(1/\tau)] \qquad (C2)$$

and

$$\frac{\partial E_I}{\partial \tau} = \frac{-RT}{\tau}\,. \qquad (C3)$$

These expressions are evaluated at the mean values of T and τ using

the lnA' obtained from the least squares fit. If these partial derivatives for T and τ are set equal to the new variables a and b respectively, then the approximate expression for the standard deviation of the ignition activation energy, σ_{E_I}, becomes

$$\sigma_{E_I} = [a^2\sigma_T^2 + b^2\sigma_\tau^2]^{1/2} \qquad (C4)$$

where, σ_T and σ_τ are the standard deviations of temperature and ignition delay, respectively. The value of σ_T was assumed to be 50 K based on the reported uncertainties in Gaydon and Hurle.[46] The measurement of the ignition delay was assumed to have a standard deviation of 2×10^{-4} seconds. Evaluation of Eq. (C4) yielded the values of σ_{E_I} presented in Table C1. If E_I were a random variable with a normal distribution and with a mean value given by that obtained from the least squares fit, then the probability is 0.95 that E_I lies between $E_I - 1.96\ \sigma$ and $E_I + 1.96\ \sigma$.

Similarly, the energy of activation of pyrolysis is obtained from Eq. (18),

$$\ln\left[\frac{-\ln\left[\frac{V^*-V}{V^*}\right]}{\tau}\right] = \frac{E_p}{R}\left(\frac{1}{T}\right) + \ln A. \qquad (C5)$$

The independent variables in this expression are T, τ, V, and V*. Solving this expression for E_p and taking the partial derivative with respect to each independent variable yields

$$\frac{\partial E_p}{\partial T} = R\left[\ln A - \ln\left[\frac{-\ln\left(\frac{V^*-V}{V^*}\right)}{\tau}\right]\right], \qquad (C6)$$

Table C1. Important parameters in the analysis at the error associated with activation energies of pyrolysis and ignition.

Error Analysis of Ignition Activation Energies

Variable	dust	σ_{T_I} (K)	σ_{t_I} (sec)	ln A	σ_{E_I} (kJ/g-mol)	1.96-σ_{E_I} (kJ/g-mol)	$\frac{\sigma_{E_I}}{E_I}$
E_I	Corn	50	2×10^4	13.14	3.2	6.3	0.06
E_I	Milo	50	2×10^4	14.18	3.6	7.1	0.06
E_I	Soybean	50	2×10^4	18.65	5.2	10.2	0.05
E_I	Wheat	50	2×10^4	12.78	2.8	5.5	0.06

Error Analysis of Pyrolysis Activation Energies

Variable	Dust	V^* (g)	σ_{V^*}	σ_V	ln A	σ_{E_p} (kJ/g-mol)	1.96-σ_{E_p} (kJ/g-mol)	$\frac{\sigma_{E_p}}{E_p}$
E_p (HC)	Starch	1.4×10^{-2}	1.4×10^{-3}	1.3×10^{-4}	15.39	5.41	10.6	0.09
E_p (HC)	Corn	4.7×10^{-3}	4.7×10^{-4}	1.6×10^{-4}	15.29	5.94	11.6	0.11
E_p (HC)	Soybean	4.4×10^{-3}	4.4×10^{-4}	1.1×10^{-3}	15.74	5.10	10.0	0.10
E_p (HC)	Corn	8.6×10^{-3}	8.6×10^{-4}	1.0×10^{-3}	13.55	4.78	9.4	0.06
E_p (HC)	Corn	4.4×10^{-3}	4.4×10^{-4}	1.0×10^{-3}	16.02	8.41	16.5	0.08
E_p (HC)	Soybean	5.8×10^{-3}	5.8×10^{-4}	1.0×10^{-3}	15.07	6.66	13.1	0.07
E_p (HC)	Soybean	4.4×10^{-3}	4.4×10^{-4}	1.0×10^{-3}	14.95	7.89	15.4	0.09

$$\frac{\partial E_p}{\partial t} = \frac{RT}{t} \quad , \tag{C7}$$

$$\frac{\partial E_p}{\partial V} = \frac{-RT}{(V^*-V)\ \ln\left(\frac{V^*-V}{V^*}\right)} \quad , \tag{C8}$$

and

$$\frac{\partial E_p}{\partial V^*} = -RT\ \frac{V^2}{(V^*-V)\ \ln\left(\frac{V^*-V}{V^*}\right)\ V^{*2}} \quad . \tag{C9}$$

By letting the new variables w, x, y, and z represent the values of these partial derivatives of E_p with respect to T, t, V and V* evaluated at the mean values of these quantities, respectively, the following expression for the standard deviation of E_p is obtained;

$$\sigma_{E_p} = [\ w^2\sigma_T^{\ 2} + x^2\sigma_t^{\ 2} + y^2\sigma_V^{\ 2} + z^2\sigma_{V^*}^{\ 2}]^{1/2} \quad , \tag{C10}$$

where σ_{E_p}, σ_r, σ_t, σ_V, and σ_{V^*} are the standard deviations of the subscripted variables.

The analysis for the error associated with E_p proved to be rather independent of the assumed values for standard deviations with the exception of the σ_T and σ_V in the case of $E_p(CO)$ and $E_p(CO_2)$. For the sake of completeness, the rational for assuming values for σ_V and σ_{V^*} as shown in Table C1 are delineated below. The standard deviations of T and t were assumed to be 50 K and 4×10^{-4} sec. The standard deviation in the chromatographically determined hydrocarbon content, V_{HC} was assumed to be 10% of the mean value of V_{HC} for each dust. The standard deviation of the total hydrocarbon content was assumed to be 10%

of the respective value for each of the dusts. Inasmuch as the thermal conductivity gas chromatograph was less sensitive than the flame ionization gas chromatograph and significantly larger error was introduced in determining the concentration of CO and CO_2. Therefore, the standard deviation in V, was assumed to be 5% of the initial mass of dust in the analysis of the error associated with the activation energies of carbon oxide formation. The standard deviation associated with the maximum carbon oxide content was assumed to be 10% of the respective volatile content of each dust.

Evaluation of Eq. (C10) yielded the values of σ_{E_p} given in Table C1. If E_p is a random variable with a normal distribution and a mean value given by the value of E_p as determined from a least squares fit of Eq. (18), then the probability is 0.95 that E_p lies between $E_p - 1.96\ \sigma_{E_p}$ and $E_p + 1.96\ \sigma_{E_p}$.

Obviously, there are a number of assumptions involved in obtaining a bound on the error associated with the activation energies of ignition and pyrolysis. The analysis reveals that, even with the use of these presumably conservative estimates, reasonably small uncertainties are obtained. Additionally, the majority of the error usually results from the term containing the uncertainty in temperature. Intuitively, this is expected since the instantaneous rate of volatile release is related exponentially to the gas temperature. Inasmuch as this is the first attempt at a quantitative error analysis on the data obtained using the S.P.S.T. at Kansas State University, it is recommended that work aimed

at reducing the number of assumptions inherent in this analysis be undertaken, particularly with respect to temperature measurements.

Chemical Shock Tube Studies of Mechanisms of Grain Dust Ignition

by

Gary Walter Breipohl

B.S., Kansas State University, 1978

AN ABSTRACT OF A MASTER'S THESIS

submitted in partial fulfillment of the
requirements for the degree

MASTER OF SCIENCE

Department of Nuclear Engineering
KANSAS STATE UNIVERSITY
Manhattan, Kansas

1979

Abstract

The chemical and physical mechanisms of grain dust ignition have been studied for the first time under temperatures, heating rates, and pressures characteristic of those found in explosions. A single pulse shock tube with optical diagnostics was used to study the relative ease of ignition of sized samples of corn, wheat, milo, and soybean dusts. Whereas the corn, wheat, and milo dusts all had activation energies of ignition in the range of 46.8 to 62.4 kJ/g-mol, soybean dust exhibited an activation energy nearly twice as large at 97.2 kJ/g-mol.

Laser transmission measurements through the reacting dust cloud in both oxidation and pyrolysis runs coupled with the line emission from the incandescent dust particles indicated that corn, milo, soybean, and wheat dusts underwent substantial devolatilization prior to ignition. Scanning electron microscopy of the solid residue after pyrolysis indicated massive voiding of the particle volume and erosion of the particle surface.

Gas chromatographic analysis of the pyrolyzate revealed that up to one half of the sample mass devolatilized within two milliseconds. Lower order hydrocarbon yields were comparable from starch, soybean, and corn dust; however, carbon monoxide yields from corn were nearly a factor of two greater than from soybean dust, and no CO or CO_2 were detected from starch. From the above data, ignition is postulated to occur first in the gas phase and both carbon monoxide and lower hydrocarbons are thought to be important participants in the ignition process.